Deposit characteristics and dynamic processes of large volume pyroclastic density currents of the Taupo Volcanic Zone approaching and entering the sea

A thesis

submitted in partial fulfilment

of the requirements for the degree

of

Master of Science (Research) in ***Earth Sciences***

at

The University of Waikato

by

Mia Ani Richmond

THE UNIVERSITY OF
WAIKATO
Te Whare Wānanga o Waikato

2022

Abstract

Pyroclastic density currents (PDCs) entering the sea are a rare but dynamic phenomenon that cause significant change to the topography and bathymetry of coastal and island arc settings. Very little is known about their complex behaviour and depositional processes, as observation of such an event is uncommon and conducting experiments that simulate PDCs is challenging. A better understanding of this phenomena can aid in future volcanic monitoring and hazard management around coastal and oceanic settings.

This study combines both field observations and laboratory experiments of PDCs entering the sea. Case studies around North Island, New Zealand of pre-historic pyroclastic deposits found near the coast focused on, the Rotoiti Ignimbrite that originated from the Okataina Volcanic Centre (Pacific Coast Highway between Matata and Maketu; Mimiha Road near Matata), and the Ongatiti Ignimbrite (Glenbrook Beach, Waiuku; Kihi Road, inland of Kawhia Harbour) from the Mangakino Volcanic Centre. At each location, field observations were recorded, and samples collected, followed by grainsize and texture analysis in the laboratory (scanning electron microscopy, laser diffraction particle size analysis, dry sieving). Laboratory experiments that simulated small-scale PDCs generated by a column collapse mechanism and a dam-break mechanism into a flume were conducted.

The Ongatiti Ignimbrite at Glenbrook Beach presented flow-water interaction features through soft sediment deformations such as dewatering structures, flame structures, and thin beds of convoluted laminae. The Rotoiti Ignimbrite at Mimiha Road showed distinctive crossbedding. Both examples highlighted PDC processes after entry into the water. The Rotoiti and Ongatiti ignimbrites along the Pacific Coast Highway and Kihi Road, respectively presented typical subaerial ignimbrites that had travelled long distance overland and were still undergoing significant deposition near the coastline. The flume experiment demonstrated that PDCs segregate into two parts when entering the water, (1) a dilute overflow cloud, and (2) a dense underwater current. The entrance of pyroclastic ash material into water also generated a wave. Underwater obstructions will affect a submergent current by significantly decreasing its height and runout distance.

Acknowledgements

Firstly, a very big thank you to my supervisor Dr Adrian Pittari who has been a great help in several ways. For being my right-hand man in the field through rain, wind, sun, and the sticky mud, for navigating me around bumps in the road, and for helping proofread and edit all my work. I am very grateful for Adrian's time and guidance through this all.

Secondly, a thank you to laboratory technician Annette Rodgers who has assisted me and all my needs in the laboratory. Anette's here-to-help attitude never went unnoticed. I am very grateful for her door always being open.

A massive thank you to my family, especially my parents, for always being there when I needed them. For always listening and understanding and providing never ending support. I couldn't have done this without their contributions and encouragement.

This research has been partially funded by The University of Waikato Masters Research Scholarship and the Terry Healy Memorial Scholarship.

Lastly, a warm thank you to my partner Ethan. I well and truly couldn't have made it to the finish line without his comfort and cheering me on every step of the way. I am very lucky to have Ethan's kindness and intellect by my side.

Table of Contents

Abstract ..... **i**

Acknowledgements ..... **ii**

Table of Contents ..... **iii**

List of Figures ..... **vi**

List of Tables ..... **ix**

Chapter 1 - Introduction **1**

1.1 Background 1

1.2 Aim and Objectives 2

1.3 Methods 2

1.4 Outline 2

Chapter 2 – Literature Review **4**

2.1 Introduction 4

2.2 Pyroclastic Flows and Ignimbrites 4

2.3 Plumes & Turbidity Currents 5

2.4 New Zealand Volcanism 6

2.4.1 Ongatiti Ignimbrite 7

2.4.2 Volcaniclastic Turbidities at Mahia Peninsula 9

2.4.3 Rotoiti Ignimbrite 10

2.5 Global Examples of Pyroclastic Flows Entering the Sea 11

2.5.1 Green Tuff of the Pantelleria Trough 11

2.5.2 Krakatau 12

2.5.3 Kikai Caldera 14

2.5.4 Pyroclastic deltas in Montserrat 15

2.6 Modelling Pyroclastic Flows 16
2.6.1 Flume Experiments 17
2.6.2 PDC simulator at Massey University 18
2.6.3 Simulating the Mount Peleé Eruption of 1902 19
2.6.4 Simulating tsunamis generated by PDCs 20
2.7 Conclusion 22
Chapter 3 – NZ Case Studies 23
3.1 Introduction 23
3.2 Methods 23
3.2.1 Site Investigation 24
3.2.2 SEM Imaging 25
3.2.3 Grainsize by Laser Diffraction Particle Size Analysis 25
3.2.4 Grainsize by Dry Sieving 26
3.3 Rotoiti Ignimbrite along the Bay of Plenty Coast 26
3.3.1 Site 1A: Pacific Coast Highway 28
3.3.2 Site 1B: Mimiha Road 32
3.3.3 Grainsize and Textural Analysis 33
3.4 Ongatiti Ignimbrite in the Waiuku Inlet 34
3.4.1 Site 2: Glenbrook Beach 35
3.4.2 Grainsize and Textural Analysis 40
3.5 Ongatiti Ignimbrite in Kawhia 42
3.6 Conclusion 45
Chapter 4 – Experimental Studies 46
4.1 Introduction 46
4.2 Methods 46
4.2.1 Flume 47
4.3 Desktop Analysis of the Bay of Plenty Coastline 49

4.4 Column Collapse Experiment....50
4.4.1 Column Collapse Results....50
4.5 Dam Break Experiment....54
4.5.1 Dam Break Results....55
4.6 Obstruction Run....57
4.7 Conclusion....59
Chapter 5 - Discussion....61
5.1 Introduction....61
5.2 Case Studies....61
5.2.1 Flows Approaching the Sea....61
5.2.2 Flows Entering the Sea....63
5.3 Experimental Studies....65
5.4 Connecting Field Observations to Experimental Studies....67
5.5 Cascading Hazards....68
5.6 Limitations....69
5.7 Further Research....69
Chapter 6 - Conclusion....71
References....73
Appendices....80
Appendix 1 – Dry Sieving....81
Appendix 2 – Laser Particle Diffraction Analysis....85
Appendix 3 – Desktop Analysis for Slope....86
Appendix 4 – Experimental Raw Data....88

List of Figures

Figure 2.1 – Volcanic centres of North Island, New Zealand (GNS Science, n.d.). 6
Figure 2.2 – Map showing extent of Ongatiti from the MVC (Cooper & Wilson, 2014). 8
Figure 2.3 - Sketch of primary monomagmatic volcaniclastic turbidite (Schneider et al., 2001).10
Figure 2.4 - Map showing extent of the Rotoehu ash and Rotoiti ignimbrite sourced from OVC (Hopkins et al., 2021).....11
Figure 2.5 - Sketch of the emplacement process of pyroclastic flows transitioning into the sea and into turbidity currents (Mandeville et al., 1996).....13
Figure 2.6 – Map showing location of the Tar River and White River deltas in Montserrat (Google, n.d.-a) 16
Figure 2.7 – Diagram of flume tank used for turbidity current experiments (Khavasi et al., 2012). 17
Figure 2.8 – Schematic diagram of the PELE facility used for pyroclastic flow simulations (Lube et al., 2015).....18
Figure 2.9 – Results of the 1902 Mount Peleé pyroclastic flow simulation produced (Gueugneau et al., 2020).....20
Figure 2.10 – A schematic diagram of the different mechanisms associated with pyroclastic flows entering the sea (Watts & Waythomas, 2003).....21
Figure 3.1 - Map showing locations of case studies observed in the field *(Google, n.d.-d).*.....24
Figure 3.2 – Composite stratigraphic column of the Rotoiti Breccia (Burt et al., 1998).....27
Figure 3.3 – Map showing locations of Site 1A and Site 1B visited for this field study *(Google, n.d.-e).* 28
Figure 3.4 – Photographic image of a large-scale deposit of Rotoiti Ignimbrite observed from Pikowai Campground along the Pacific Coast Highway [37°51’24.11” S / 176^{0}39’56.78” E]. ...29
Figure 3.5 – Stratigraphic column of the lower unit of the Rotoiti ignimbrite observed at Site 1A. 30
Figure 3.6 – Photograph of the lower portion of the Rotoiti ignimbrite at Site 1A. PCZ = pumice concentration zone. 31

Figure 3.7 – Photograph of the entire outcrop observed at Site 1B (Mimiha Road). 32
Figure 3.8 – Close up image of crossbedding within the Rotoiti Ignimbrite at Site 1B. 33
Figure 3.9 – Scatter plot of the grain size distribution of Sample 1 collected from Site 1A. 33
Figure 3.10 – (a) SEM image of a pumice particle from Sample 1 collected at Site 1A, (b) SEM image of pumice vesicles from Sample 1 collected at Site 1A, (c) SEM image of fine ash particles and blocky crystals from Sample 1 collected at Site 1A, including small pumice fragments and lithics. 34
Figure 3.11 - Map showing location of Site 2 along Glenbrook Beach (Google, n.d.-b). 35
Figure 3.12 - Stratigraphic column of Ongatiti Ignimbrite showing multiple flow units and underlying and overlying sedimentary units at Site 2 36
Figure 3.13 - Sketch of outcrop observed at Site 2. 37
Figure 3.14 – (a) Photograph of load casts observed along the contact of mud Unit 4 and base of ignimbrite Unit 1 at Site 2, (b) Photograph of dewatering structures observed within ignimbrite Unit 1 (lower) at Site 2, (c) Photograph of convoluted laminae observed within ignimbrite Unit 1. 38
Figure 3.15 - Photograph of ignimbrite Unit 1 (upper) showing the contact between very coarse ash and pumice unit. 39
Figure 3.16 - Photograph of ignimbrite Unit 2 (lower) at Site 2. 39
Figure 3.17 - a) SEM image of pumice particles within Sample 3 collected at Site 2, b) SEM image of angular particles (crystals, lithics) within Sample 4 collected at Site 2, c) SEM image of pumice particle within Sample 4 collected at Site 2, d) SEM image of pumice. 40
Figure 3.18 - Scatter plot of the grain size distribution of Sample 13 collected near Site 2, along Glenbrook Beach. 41
Figure 3.19 - Grain size distribution using laser diffraction particle analysis on Samples 3-5 and Samples 10-11 collected from Site 2. 41
Figure 3.20 - Map showing location of Site 3 *(Google, n.d.-c).* 43
Figure 3.21 - a) Photograph of pumice, lithics, and mottle components within the Ongatiti unit observed at Site 3, b) Photograph of large-scale deposits of the Ongatiti Ignimbrite at Site 3. 44
Figure 3.22 - Scatter plot of the grain size distribution of Sample 20 collected near Site 3. 45
Figure 4.1 – Diagram of wavemaker flume tank used for the experiments. 48

Figure 4.2 – Diagram of the flume tank with the dam insert used for the dam-break flow experiments. 48
Figure 4.3 – Diagram of the flume tank with the PVC column used for the ash collapse experiments. 48
Figure 4.4 - Map of approximate cross-section area used for experimental basis (birds eye view) (Bay of Plenty Regional Council, n.d.). 50
Figure 4.5 –Timeseries images of the underwater current produced during experimental Run 1.1. 51
Figure 4.6 - Timeseries images of the cloud produced during experimental Run 1.1. 52
Figure 4.7 –Timeseries images of the underwater current produced during experimental Run 1.2. 53
Figure 4.8 – Timeseries images of the cloud produced during experimental Run 1.2. 53
Figure 4.9 – Graph of current length versus current height for underwater currents from Runs 1.1 to 1.3. 54
Figure 4.10 – Timeseries images of the current produced during experimental Run 2.1. 55
Figure 4.11 – Timeseries images of the cloud produced during experimental Run 2.2 56
Figure 4.12 - Graph of current length versus current height for underwater currents from Runs 2.1-2.2 56
Figure 4.13 – Photograph of ash remaining on slope above the water line during experiment 57
Figure 4.14 – Timeseries images of the underwater moving around an obstruction in experimental Run 3.1 (birds eye view). 58
Figure 4.15 – Timeseries of the underwater current moving past an obstruction in experimental Run 3.1 (side view). 59
Figure 4.16 – Photograph of layers deposited by all six experimental runs 59
Figure 5.1 – Schematic diagram of pyroclastic flows entering the sea at a low angle of incidence (Cas & Wright, 1991). 63
Figure 5.2 – Sketch of load structures described by (Tinterri et al., 2016) 64

List of Tables

Table 2.1 - Characteristics, deposition, and emplacement process descriptions of different flow units associated with the 7.3 Ka Kikai caldera, Japan eruption compiled from (Maeno & Taniguchi, 2007).....14
Table 2.2 - Different eruptions associated with the Tar River delta in Montserrat, notes compiled from (Hart et al., 2004).....15
Table 2.3 - Different eruptions associated with the White River delta in Montserrat, notes compiled from (Hart et al., 2004).....15
Table 2.4 - Parameters of pyroclastic flows from adopted eruptions, notes compiled from (Novikova et al., 2011).....22
Table 3.1 - Median, mean, and sorting values for samples 3-5 and 10-11 collected from Site 2. 42
Table 4.1 - Table displaying the depths, distances, and slopes within the Bay of Plenty Northeast of Mimiha Road using data provided by the Bay of Plenty Regional Council. 49
Table 4.2 - Descriptive statistics of all the three underwater currents from runs 1.1 to 1.3. 54
Table 4.3 - Descriptive statistics of the two underwater currents from runs 2.1 and 2.2.....57

Chapter 1
Introduction

1.1 Background

Pyroclastic density currents (PDCs) are one of the most catastrophic volcanic hazards. PDCs can travel at speeds up to 700 km/h, transporting gas and volcanic material of temperatures at up to 800^{o}C, altering the land they interact with. These violent currents pose great hazards to all that surround their volcanic centre, with many of those volcanic centres being in coastal and island settings. Pyroclastic density currents entering the sea is a rarely observed but impactful phenomenon. Just like PDCs on land, the commonality and destructiveness associated with these currents hinder our full understanding of their dynamics and behaviour. One major gap in knowledge on PDCs entering the sea is whether these submarine currents behave similarly to those in subaerial environments; alongside this, what are the physical characteristics of the PDCs that drive these differences. It is known that subaerial PDCs behave differently based on their particle concentration, flow volume, and surrounding topography. These characteristics can determine how fast or far a flow can travel, which can determine the extent of its destructiveness.

New Zealand resides on the continental setting known as Zealandia which straddles the Indo-Australian Plate and Pacific Plate boundary. With that, the geological evolution of New Zealand is a complex and dynamic product of tectonic and volcanic activity. New Zealand is well-known for its volcanism, from historic accounts of the 25.5 ka Oruanui super-eruption at the Taupo Volcanic Centre (Bemmels et al., 2022) and recent accounts such as the 2019 Whakaari eruption. Many eruption events that have taken place within New Zealand were explosive eruptions generating PDCs, with some of those entering the sea. These instances are pre-historic with no known recent events recorded. Due to this, many of these events only preserve records that stop at the shoreline. The coastal environment is also a complex setting, with many areas experiencing high rates of change due to high energy erosional and depositional conditions.

To better understand New Zealand specific events of PDCs entering the sea, field studies of pre-historic deposits and their potentially unique characteristics are informative, as well as experimental studies on simulations of flows entering the water and their potentially unique behaviour. Engaging in both field and experimental studies will advance our knowledge and aid in future volcanic and coastal hazard assessments.

1.2 Aim and Objectives

The aim of this thesis was to determine specific PDC processes as they pass the coastline and enter the sea in the New Zealand setting by linking field and experimental studies. The objectives developed to achieve the aims of this thesis were:

- Identify and describe the characteristics and components of ignimbrites near the New Zealand coast,
- Observe and describe the characteristics and components of pyroclastic-ash laden PDCs on crossing air-water interface and continuing underwater,
- Determine the physical processes of PDCs entering the sea, by reconciling field and laboratory findings and apply to the New Zealand context.

1.3 Methods

The methods undertaken to achieve the objectives of this thesis include field and laboratory case studies and laboratory experiments. Four sites around North Island, New Zealand with pyroclastic flow outcrops were explored, including outcrop sketching, stratigraphic logging, sample collection, photographic collection, and note taking. Samples collected from the field were brought to the laboratory for analysis. Laboratory analysis methods include grain size through dry sieving, laser diffraction particle size analysis, and scanning electron microscopy (SEM) imaging. Several experiments were undertaken using a flume to simulate pyroclastic ash-laden PDCs underwater. Detailed descriptions of the methodologies used for both the field and laboratory portion of this project can be found within Chapters 3 and 4.

1.4 Outline

Chapter 2 is a literature review that covers PDCs and ignimbrites, turbidity currents, volcanism in New Zealand, and in a global context with several examples or occurrences of

pyroclastic flows entering the sea. Chapter 2 also reviews literature that covers physical and computational modelling of PDCs alone, into the sea, and turbidity currents.

Chapter 3 covers case studies of ignimbrites around New Zealand that are near the coastal environment. Case study areas include the Bay of Plenty coast, Kawhia, and Waiuku. Chapter 3 describes observations made at each site and results from laboratory analysis. Background information relating to the study area and ignimbrite are reviewed, methods used in the field and laboratory are described, and results from both the site investigation and laboratory analysis are presented.

Chapter 4 covers experimental studies carried out in a flume tank using pyroclastic ash material collected from the field. The location basis of the experiment is discussed, methods used to simulate a flow in a flume are described, limitations of the experiment are discussed, and the results of various runs are presented.

Chapter 5 is a discussion on the results from the case studies, experimental studies, and an interpretation on how aspects from both studies may connect. Further discussion is made about associated hazards and potential effects to the coastal environment from pyroclastic flows entering the sea. Recommendations for future research are also given.

Chapter 6 is a conclusion on the key findings from the discussion.

Chapter 2

Literature Review

2.1 Introduction

Chapter 2 is a review on literature relevant to the topic of this thesis. The chapter begins with an overview on volcanism, with attention to PDCs and ignimbrites, and an overview on plumes and turbidity currents. These topics tie into the distinct process of PDCs travelling into the sea. The chapter will then discuss several examples of this process occurring in New Zealand and around the world. Finally, the chapter reviews computational and laboratory studies on the entry of PDCs into sea, or water.

2.2 Pyroclastic Flows and Ignimbrites

Pyroclastic density currents are ground-hugging mixtures of hot ash, gas and pyroclasts produced from explosive volcanic eruptions (e.g., Palladino, 2017). These currents are typically generated from an eruption plume collapse. When an explosive volcanic eruption occurs, a vertical column of volcanic material known as an eruption plume disperses volcanic material into the atmosphere. When the density of the vertical column exceeds the density of the surrounding atmosphere the eruption column will collapse, creating a gravity driven current known as a pyroclastic density current. Other generation mechanisms for PDCs include dome collapse, direct blasts, or boiling over (Palladino, 2017). PDCs are known for their highly destructive behaviour and are considered to be one of the most hazardous natural phenomena, with temperatures reaching up to 800^{o}C and speeds up to 700 km/h. PDCs can be broken into two end member types based on particle concentration: pyroclastic flows and pyroclastic surges. Pyroclastic flows are long-lived steady currents with a high particle concentration. Pyroclastic surges are short-lived turbulent currents with a low particle concentration (Wohletz & Sheridan, 1979). This difference in particle concentration can affect how they transport and deposit material. Pyroclastic surges deposit material through suspended sedimentation across the landscape including along hills and ridges, while pyroclastic flows deposit material as a concentrated dispersion through valleys, rivers, and channels (Browne & Gardner, 2005). The material deposited by pumice-rich pyroclastic

flows is known as an ignimbrite. Ignimbrites can be found as unconsolidated material (non-welded) or consolidated (welded) rock. Welded ignimbrites are produced when the material is hotter than 535^{o}C. High temperatures enable the ash and rock to compact and meld together. Both consolidated and unconsolidated ignimbrites are primarily composed of volcanic ash, pumice, and lithics (USGS, 2019).

2.3 Plumes & Turbidity Currents

A plume, also known as a column, can occur in several geological or environmental settings. Examples of vertical columns include volcanic plumes, hydrothermal plumes, submarine plumes, and lake plumes (Woods, 2009). Examples of horizontal columns include river plumes and turbidity currents. These examples represent the dynamic environmental process of a flow or fluidal body moving through another. Plumes come in a range of shapes and sizes, encompassing different physical phases, but those relevant to this paper are horizontal turbulent columns affected by density differences within dry land and coastal sea environments, i.e., density currents.

Horizontal plumes are classified based on their particle concentration. Dilute river plumes are long-lived density currents that occur at the coastal ocean zone where a river meets the sea (Woods, 2009). River plumes introduce a flux of sediment from the terrestrial environment to the shallow marine. This introduction of particle-laden freshwater into a typically stratified saltwater setting promotes mixing, which can influence coastal dynamic processes and ecosystems. Turbidity currents are seafloor-hugging flows of a high concentration driven by density differences of suspended sediment (Hage et al., 2019). Turbidity currents bring sediment from the terrestrial and shallow marine environment to the deep marine. Generation mechanisms for turbidity currents include slope failures (e.g., slips and slides), or river plumes breaking a sediment concentration threshold, occasionally known as a plunging hyperpycnal flow (Hage et al., 2019).

As mentioned, PDCs are high concentration gas-particulate flows that transport hot pyroclasts (e.g., pumice, glass shards, lithics, crystals) and gas at high speeds over great distances. These significant flows heavily modify the geomorphology and surface features of

their surrounding environment. Similarly, the behaviour of large-scale river plumes and marine turbidity currents permit modification to their surrounding subaqueous environment.

2.4 New Zealand Volcanism

The North Island of New Zealand experiences frequent volcanic activity, and much of North Island geology is of volcanic origin. New Zealand extends over the Australian-Pacific plate boundary. Along the west coast of the South Island is a transform boundary, known as the Alpine Fault. To the east of the North Island is a convergent boundary, known as the Hikurangi-Kermadec Trench, where the Australian plate is subducting under the Pacific plate. This subduction zone is what controls the various volcanic arcs of the North Island, of which the Taupo Volcanic Zone (TVZ) has been the most active in recent times. This zone extends from Mount Ruapehu in the southwest, to Whakaari, also known as White Island in the northeast as shown in Figure 2.1. (GNS Science, n.d.). The TVZ is famously known for producing explosive pyroclastic eruptions, such as the 25.5 ka Oruanui eruption of the Taupo Volcanic Centre (Bemmels et al., 2022). This eruption deposited approximately 320 km^3 of pyroclastic flow deposits and 420 km^3 of fall deposits, reaching many regions of New Zealand and other countries (Manville & Wilson, 2010).

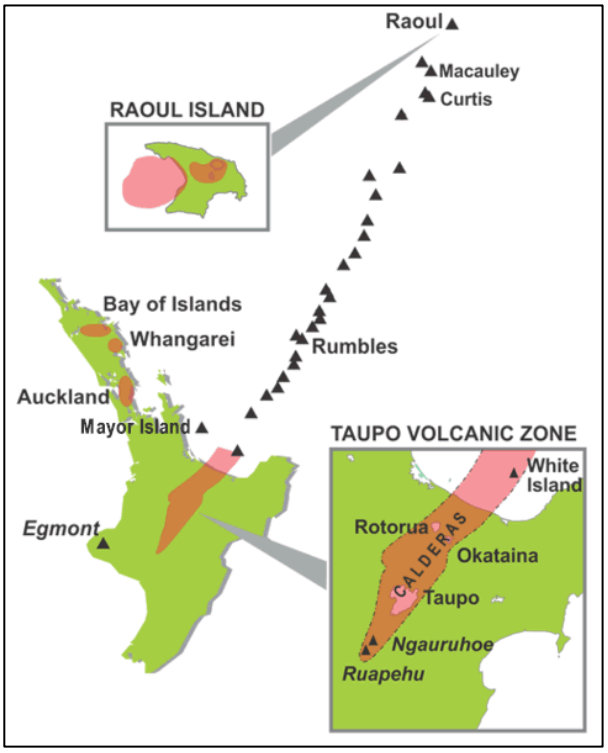

Figure 2.1 – Volcanic centres of North Island, New Zealand (GNS Science, n.d.).

Three examples within New Zealand are reviewed here, 1) the Ongatiti Ignimbrite, 2) volcaniclastic turbidities at Mahia Peninsula, and 3) the Rotoiti Ignimbrite. The Ongatiti Ignimbrite and Rotoiti Ignimbrite are both products of significant historic volcanic eruptions that have spread pyroclastic material across the North Island and coastlines. The case study at Mahia is a unique case of historic PDCs transitioning into subaqueous turbidity currents.

2.4.1 Ongatiti Ignimbrite

The Waiuku Tephra and Ongatiti Ignimbrite are both deposits generated from pyroclastic density currents originating from the Mangakino Volcanic Centre (MVC) of the TVZ. The MVC is the oldest rhyolitic caldera volcano in the TVZ. The largest eruptions generated from the MVC occurred during 1.68 to 1.53 Ma and 1.12 to 0.95 Ma which produced voluminous pyroclastic flows and falls that travelled all around the North Island, New Zealand, and deposited material as far as the east (e.g., Bay of Plenty, Hawkes Bay) and west coast (e.g., Port Waikato), several hundred kilometres away from source (Krippner et al., 2010). Both the Waiuku Tephra and Ongatiti Ignimbrite have been found in the Port Waikato region. The Ongatiti Ignimbrite has also been identified as the Oparau Tephra in the Kawhia region.

The Waiuku Tephra dated 1.00 ± 0.03 Ma (Alloway et al., 2010) is a correlative tephra of the Kidnappers Ignimbrite. The Waiuku Tephra has been identified at several locations, but the focus here is on the three- to nine-metre-thick deposits found at Mission Bush and the southeast region of the Waiuku River inlet. Here the Waiuku Tephra has been described as two units: (1) an upper flow unit and (2) lower surge unit. The upper flow unit presents a transitional material, reflecting the transition of a hot, gas-supported flow into a cooler, water-supported flow (Alloway et al., 2010), described as a hyper-concentrated flow deposit. A hyper-concentrated flow, in this case, is described as an intermediate flow or deposit that typically consists of both water and volcaniclastic material. Moreover, it is a transitional process distinct from debris flows and water-stream flows (Pierson, 2005). The lower surge unit is stratified with three distinct subunits, a basal subunit and two overlying cross-bedded horizons with local dune structures. Between the basal subunit and overlying subunits are flame structures or water escape structures. This suggests that the hot surge travelled over a wet ground which resulted in rapid cooling and transitioning from a degassing process to a

dewatering process (Alloway et al., 2010). Rip-up clasts and charred wood have also been noted within the surge unit.

The Ongatiti Ignimbrite has been dated at 1.21 ± 0.09 Ma (Houghton et al. 1995). It is one of the largest, by volume, ignimbrites from the MVC, therefore it has been identified in many areas of the Waikato and Auckland region. The focus here is the 3.8 m thick deposit found at Glenbrook Beach. Glenbrook Beach is located on the west side of the Waiuku River inlet. The Ongatiti Ignimbrite has also been described as two units: (1) lower volcaniclastic mass flow unit and (2) upper redeposited unit. The lower volcaniclastic mass flow unit includes de-watering structures amongst pinkish grey, poorly sorted, massive, pumice-rich, coarse sandy ash. The Ongatiti Ignimbrite shows no evidence of a surge-like unit, unlike the Waiuku Tephra (Alloway et al., 2010). The Oparau Tephra is a correlative tephra of the Ongatiti Ignimbrite found in the Kawhia district. The Oparau tephra has been described as a massive greyish white unit that is strongly weathered (Kirkman, 2012). The extent of the Ongatiti Ignimbrite across the North of Island can be seen in Figure 2.2 below.

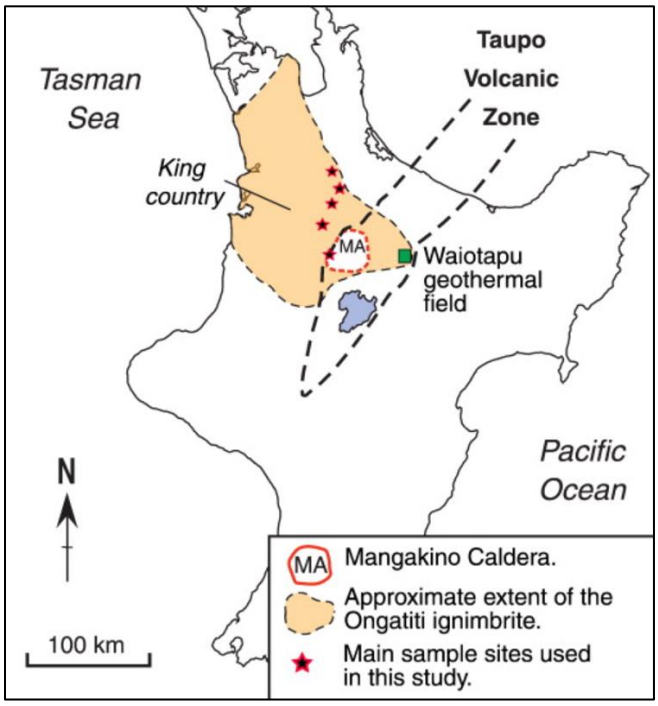

Figure 2.2 – Map showing extent of Ongatiti from the MVC (Cooper & Wilson, 2014).

2.4.2 Volcaniclastic Turbidities at Mahia Peninsula

The Mahia Peninsula is located along the eastern margin of the North Island, extending seaward between Poverty Bay and Hawke Bay. Volcaniclastic turbidities are sea-bottom deposits from turbidity currents composed of volcaniclastic material. Volcaniclastic material includes all clastic or fragmented volcanic particles regardless of their fragmentation process (e.g., pyroclastic, hydroclastic). Several volcanoclastic turbidities from the Miocene Epoch occur in the Mahia Peninsula. Schneider et al. (2001) looked at these different turbidities with the aim to distinguish the deposits and their origin.

The volcaniclastic turbidities found within the marine Miocene deposits at Mahia were broken up into three categories: (1) primary monomagmatic turbidites, (2) secondary monomagmatic turbidites, and (3) secondary multimagmatic turbidites (Schneider et al., 2001). These Miocene volcanic deposits are products from the Coromandel Volcanic Zone (CVZ). Fission-track ages have dated the deposits at 9 to 7.2 Ma which coincides with the beginning of rhyolitic volcanism in the CVZ, around 10 to 7 Ma (Shane et al., 1998). The primary monomagmatic turbidites are a result of subaerial pyroclastic flows entering the sea, transforming the flow into a subaqueous gravity flow. The primary monomagmatic turbidites are composed of magmatic and phreatomagmatic particles. The secondary monomagmatic turbidites are a result of successive eruptions reworking some of the already deposited volcaniclastic material. These are composed of the same magmatic material as the primary turbidites but contain no phreatomagmatic particles. The secondary multimagmatic turbidites are a result of remobilization of volcaniclastic material from multiple eruptions events and differ from the monomagmatic turbidites as they are composed of a heterogenous composition while the monogenetic turbidites are largely homogenous in their vitric and crystal components (Schneider et al., 2001). Moreover, there are no phreatomagmatic particles in the secondary multimagmatic turbidites.

The dynamics of the pyroclastic flows that produced these mono- and multimagmatic turbidites are quite unique. For the primary monomagmatic turbidites, Schneider et al. (2001) have suggested that movement of the pyroclastic flow into the sea would have generated steam explosions from the hot, particle-water interaction prompting secondary hydroclastic quenching. The mix of steam explosions and flows entering the sea leads to the replacement

of gas with water within the flow. This process increases the density of the flow, transforming the subaerial pyroclastic flow into a subaqueous volcaniclastic gravity flow. Figure 2.3 below displays a sketch of a primary monomagmatic volcaniclastic turbidite.

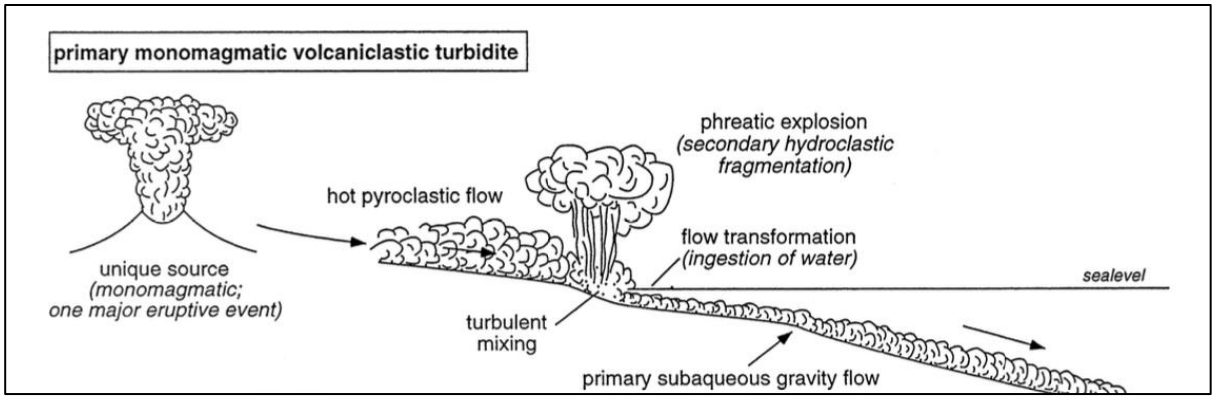

Figure 2.3 - Sketch of primary monomagmatic volcaniclastic turbidite (Schneider et al., 2001).

2.4.3 Rotoiti Ignimbrite

The Rotoiti Ignimbrite, also known as the Rotoiti Breccia, is a non-welded rhyolitic ignimbrite and the most recent major ignimbrite from the Haroharo Caldera complex of the Okataina Volcanic Centre (Walker, 1979). This covers an approximate area of 850 km^2 (Schmitz & Smith, 2004). The estimated, and commonly accepted, age of this deposit is 45.2 ± 8.2 ka (Buhay et al., 1992), but Wilson et al. (2010) have suggested an older age of 64 ± 4 ka. Therefore, the absolute age of this deposit remains controversial. The Rotoiti Ignimbrite is unique as it stretches more than 30 km north from the Haroharo complex towards the Bay of Plenty coast (Walker, 1979). The ignimbrite is comprised of several flow units that total an approximate thickness of 50 to 100 m (Nairn, 1981). The thickness of the ignimbrite varies locally, but generally the deposit is thickest near source and thins towards shore. The deposit extends a 10 km front along the Bay of Plenty coast, between Matata and Maketu townships (Walker, 1979). The ignimbrite has been described as a loosely compacted pumice breccia with interstratified ash bed units, known as the Rotoehu Ash (Nairn, 2012). The Rotoehu Ash is a widely dispersed rhyolitic ash deposit (Hopkins et al., 2021). The extent of these deposits can be found in Figure 2.4.

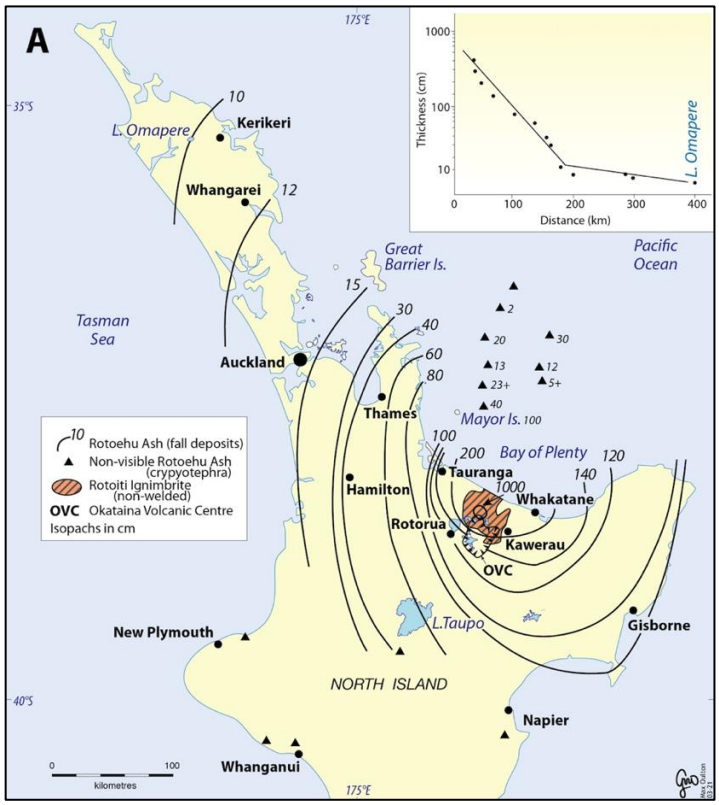

Figure 2.4 - Map showing extent of the Rotoehu ash and Rotoiti ignimbrite sourced from OVC (Hopkins et al., 2021).

2.5 Global Examples of Pyroclastic Flows Entering the Sea

Globally, there have been approximately 1,400 different active volcanoes in the past 10,000 years (Smithsonian Institution, 2022). Volcanoes commonly occur along or near convergent or divergent plate boundaries, and less commonly in hot spot regions, but many volcanoes globally exist in submarine settings. Explosive volcanism producing pyroclastic density currents with the potential to flow into the sea can occur in any of these regions if there is an active volcanic area and a marine basin within reasonable proximity. Four examples are reviewed here, (1) Green Tuff, (2) Krakatau, (3) Kikai Caldera, and (4) Montserrat. These examples present different scenarios of pyroclastic flows entering the sea under different processes.

2.5.1 Green Tuff of the Pantelleria Trough

The Green Tuff is a product of a large explosive eruption from the complex stratovolcano, Pantelleria Island. The Green Tuff has been given a radiocarbon age range of 43 to 47 ± 2 ka, making it the youngest major eruption of Pantelleria, producing a 20 m thick ignimbrite,

and covering almost the entire island and surrounding Ionian Sea. The total estimated area is 85 km^2. Anastasakis and Pe-Piper (2006) focused on a volcaniclastic interval found 12 m below the floor of Pantelleria Trough, located southeast of Pantelleria Island. The study identified this volcaniclastic deposit formed as a result of a pyroclastic flow from the major eruption travelling into the sea which is consistent with the Green Tuff. The volcaniclastic interval is 18 m thick consisting of three major parts: (1) lower massive unit, (2) middle massive unit, and (3) turbidite unit (Anastasakis & Pe-Piper, 2006). The lower and middle units were the result of hyper-concentrated flows, or cool water-saturated flows, transformed from hot-gaseous pyroclastic flows which occurred when the pyroclastic flow entered the sea. Both massive units are fine grained and poorly sorted. These hyper-concentrated flows were high density flows with suppressed turbulence but sufficient energy to travel over 40 km. The lower unit has a low biogenic content suggesting the unit had flowed into the trough from the Pantelleria fault valley. The upper unit has a much higher biogenic content suggesting a different flow path through potentially more varied terrain contributing to the increased biogenic content. The turbidite unit is well sorted with strong grain size gradation suggesting a single turbidity current flow developed from the co-ignimbrite ash cloud (Anastasakis & Pe-Piper, 2006).

2.5.2 Krakatau

Krakatau volcano is a predominately submerged caldera erecting three islands along the rim, located in the Sunda Strait, Indonesia. Krakatau volcano is well-known for its 1883 eruption, which has been considered one of the most violent volcanic eruptions in recorded history (Agustan et al., 2012). This event in its entirety was quite complex and distinct due to different dramatic phases, including the production of several large tsunamis and mud rain. May 20, 1883 was the most explosive eruption phase, which generated several subaqueous pyroclastic flows and surges that flowed over and into the surrounding sea, travelling at speeds >100 km/h and extending distances up to 80 km from the caldera (Carey et al., 1996). This phase formed the present-day caldera and small island group. The flows and surges from this phase affected a total area of 4,000 km^2, including the nearby islands of Sebesi, Sebuku and Legoendi, as well as the south coast of Sumatra and north coast of Java. Most deposits found at these nearby locations are a result of the pyroclastic flows that travelled over the sea. Carey et al. (1996) suggests those flows were able to travel over the sea due to high

temperatures vaporizing the water below, expanding the flow, increasing the turbulence, and decreasing the friction of the flow, allowing them to continue travelling at high speeds and decreased deposition rates. This suggestion is supported by the textural characteristics of the deposits being comparable to flow deposits rather than fall deposits (Carey et al., 1996). The thickest deposits are largely subaqueous, found within a 15 km radius of the caldera from subaerial flows travelling directly into the sea to depths of 40 m below sea level (Mandeville et al., 1996). These deposits have been mostly described as a massive, poorly sorted unit composed of lapilli to block sized pumice and lithics with a silty to sandy ash matrix. Another, less common deposit has been described as a laminated, well sorted unit composed of vitric-enriched silty ash (Mandeville et al., 1996). Both deposits have been described as representing the basal components of the flow. Initially, the subaerial flows travelled over the sea but later sunk due to water-saturation and cooling transitioning into a high-concentration turbidity current which deposited as a poorly sorted massive unit. The laminated facies were deposited from more dilute, low-concentrated density currents generated from the shear stress along the flow boundary. Figure 2.5 below is a sketch that portrays the emplacement process for the described deposits of the Krakatau example.

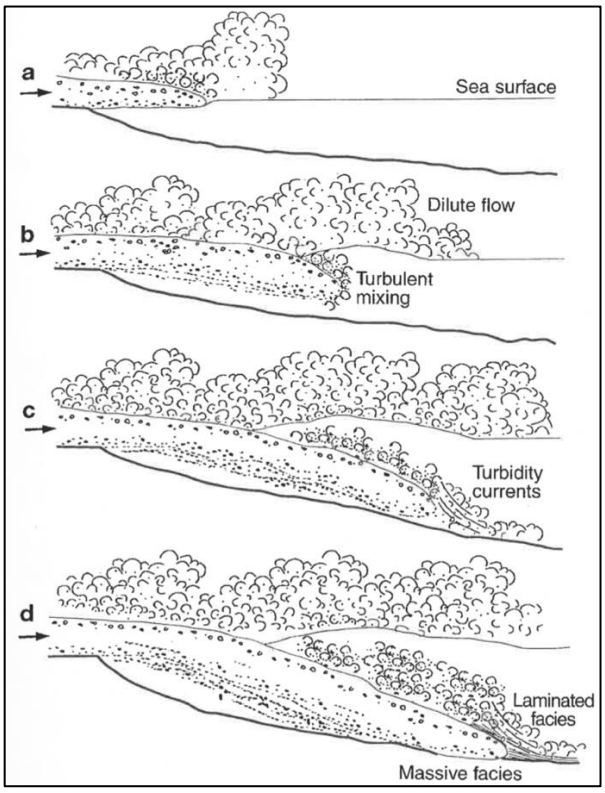

Figure 2.5 - Sketch of the emplacement process of pyroclastic flows transitioning into the sea and into turbidity currents (Mandeville et al., 1996).

2.5.3 Kikai Caldera

Kikai caldera is found on the north end of the Ryuku Islands, Japan. Kikai caldera was formed from one of the largest volcanic eruptions of the Holocene, occurring 7.3 ka, with a volcanic explosivity index (VEI) value of 7 out of 8. This eruption produced four major units (a) plinian fallout, (b) intraplinian pyroclastic flows, (c) climatic pyroclastic flows, and (d) co-ignimbrite fall. Kikai caldera is a mostly submerged caldera approximately 17 km wide and 20 km long exposed subaerially as two islands along the rim. Maeno and Taniguchi (2007) explore deposits on these two islands to interpret the processes of the 7.3 ka eruption. Unit C, representing the climatic pyroclastic flows, marks the start of magma-water interaction. The study suggests that these flows behaved similarly to those at Krakatau, with voluminous pyroclastic flows travelling into and over the sea. Unit C has been broken into three sub-units C1, C2 and C3. Moreover, C3 has been further broken into C3a, C3b and C3c due to lateral variations, marking the start of the caldera collapse. Table 2.1 describes the different characteristics and suggested emplacement processes for Unit C (Maeno & Taniguchi, 2007).

Table 2.1 - Characteristics, deposition, and emplacement process descriptions of different flow units associated with the 7.3 Ka Kikai caldera, Japan eruption compiled from (Maeno & Taniguchi, 2007).

Unit	Description	Depositional Setting	Emplacement Process
C1	Non-welded, mostly stratified facies, lithic-rich, fines-poor, inverse to normal grading (~5 m thick)	Topographic lows, proximal areas	Segregated dense flows
C2	Weakly welded, stratified faces, lithic-rich (>5 m thick)	Topographic lows, proximal areas	Ash and pumice rich flows
C3a	Massive, extremely fines-poor, lithic rich (up to ~10 m thick)	Near-vent area	Flow over sea
C3b	Massive, lithic-rich layer (~a few metres thick)	Near-vent to distal areas	Flow into sea
C3c	Massive, pumice-ash rich layer (up to 30 m thick)	Higher elevations, distal areas	Initial dilute, stratified flow into an expanded, turbulent flow over sea

Crystal content increases, Lithic content decreases ↓

2.5.4 Pyroclastic deltas in Montserrat

Soufriere Hills volcano is a stratovolcano complex that is located on the southern portion of Montserrat Island, West Indies. This volcano has been quite active in recent times, with its most recent eruption occurring in 2013. From November 1995 to July 1998, numerous explosive eruptions of the Soufriere Hills volcano, Montserrat produced pyroclastic flows. Many of these pyroclastic flows reached the coast and flowed into the sea, resulting in the production of two pyroclastic deltas at the Tar and White River deltas. Table 2.2 and Table 2.3 share details of those numerous eruptions and their contribution to the development of the deltas.

Table 2.2 - Different eruptions associated with the Tar River delta in Montserrat, notes compiled from (Hart et al., 2004).

Date	Volume of material deposited in the sea (DRE)	Notes
12-May-96	N/A	Pyroclastic flow entered the sea
28-Jul-96	N/A	Partial dome collapse event
12-Aug-96	N/A	Partial dome collapse event
3-Sep-96	N/A	Partial dome collapse event
17-Sep-96	~$5.2x10^6$ m^3	Large collapse events that entered the sea
16-Jan-97	N/A	Partial dome collapse event with large pyroclastic flows
20-Jan-97	N/A	Partial dome collapse event with large pyroclastic flows
3-Jul-98	$6x10^6$ m^3 to the delta $10x10^6$ m^3 outside the delta	Collapse event

Table 2.3 - Different eruptions associated with the White River delta in Montserrat, notes compiled from (Hart et al., 2004).

Date	Volume of material deposited in the sea (DRE)	Notes
Oct/Sept-97	N/A	Pyroclastic flow entered the sea
4/6-Nov-97	$6x10^6$ m^3 to the delta	Sustained collapses
26-Dec-97	~$60x10^6$ m^3	Major debris avalanche and PDC

Hart et al. (2004) compared historical bathymetry data with newly collected data to estimate the extent and volume of these flows. The main findings were that the influx of pyroclastic material added an extra area of 1 km^2 to the island of Montserrat, with a total volume of $73x10^6 m^3$ DRE (dense rock equivalent). The total areas (and volumes) of the Tar and White River deltas are 0.64 km^2 ($55x10^6$ m^3 DRE) and 0.46 km^2 ($18x10^6$ m^3 DRE) respectively

(Hart et al., 2004). Areas outside of the deltas that contain pyroclastic flow deposits cover an additional area of 6.25 km^2. Although seemingly small, these flow deposits and deltas cover a large portion of the volcano and island. Figure 2.6 below is an aerial image of Montserrat Island from Google Earth, presenting the extent of the deltas (Google, n.d.-a).

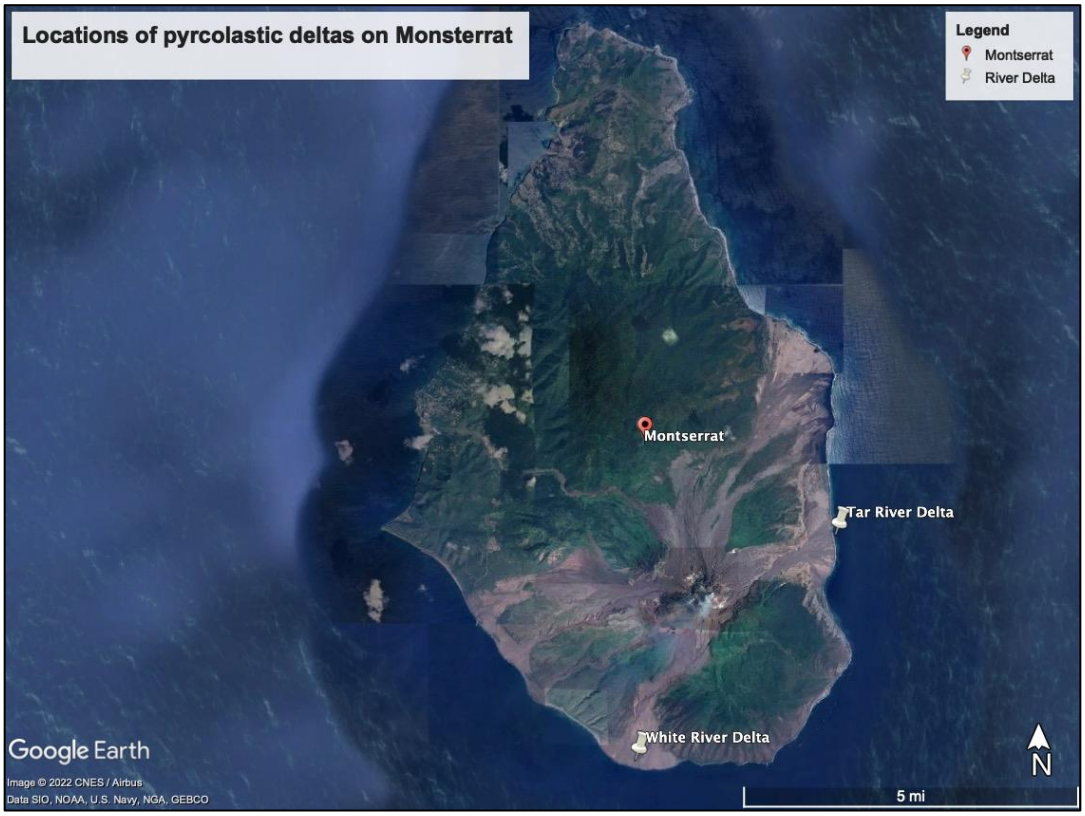

Figure 2.6 – Map showing location of the Tar River and White River deltas in Montserrat (Google, n.d.-a)

Trofimovs et al. (2006) further investigated these pyroclastic deltas through core samples. This study incorporated the more recent and largest 2003 eruption, which generated an additional deposition of $2.15x10^6$ m^3 DRE into the sea. This eruption was generated from a dome collapse, like the 1996 to 1998 events, with two major phases, each phase producing large pyroclastic lobes. The cores revealed that the pyroclastic flows of the Soufriere Hills volcano mixed rapidly at the sea entrance depositing coarse, poorly sorted, fines-depleted material in proximal areas via hyper-concentrated flows, and finer, well-sorted material via turbidity currents with distance (Trofimovs et al., 2006).

2.6 Modelling Pyroclastic Flows

Modelling volcanic eruptions has become essential for volcanological studies in the past decade. Results gained from modelling volcanic eruptions give insight into the dynamics of

pyroclastic density currents, eruptive sequences, buried topography or bathymetry, eruption intensity, deposit lithologies, and cascading hazards. From numerical models to laboratory trials, various methods have been adopted by different researchers. Recent studies have helped improve our understanding of eruptions of the past, which in turn help us better prepare for potential eruptions in the future. Improving our understanding and preparation techniques has become increasingly important as the world has witnessed catastrophic events such as the 1980 Mount St. Helens eruption in the US, and the 1991 Mount Pinatubo eruption in the Philippines.

Alongside volcanic eruption and flow modelling, it is also relevant to consider experiments related to turbidity currents and plumes. Modelling turbidity currents in a laboratory can help to understand correlations between sediment size and sorting, and density current characteristics (e.g., size, behaviour).

2.6.1 Flume Experiments

One of the most common methods used to model gravity or density currents, specifically turbidity currents, is through laboratory experiments using a flume. Alongside those laboratory experiments, numerical and computational modelling can be used to support lab studies, as well as field observations. A flume tank is an artificial tank or channel, filled with water, accompanied with necessary components depending on the experiment. Example components include a slope, a supply tank holding the material for the current, a tube or pipe that feeds the material into the tank, an additional catch tank or outlet, and measuring devices. Khavasi et al. (2012) generated turbidity currents in the lab using these components, as shown in Figure 2.7.

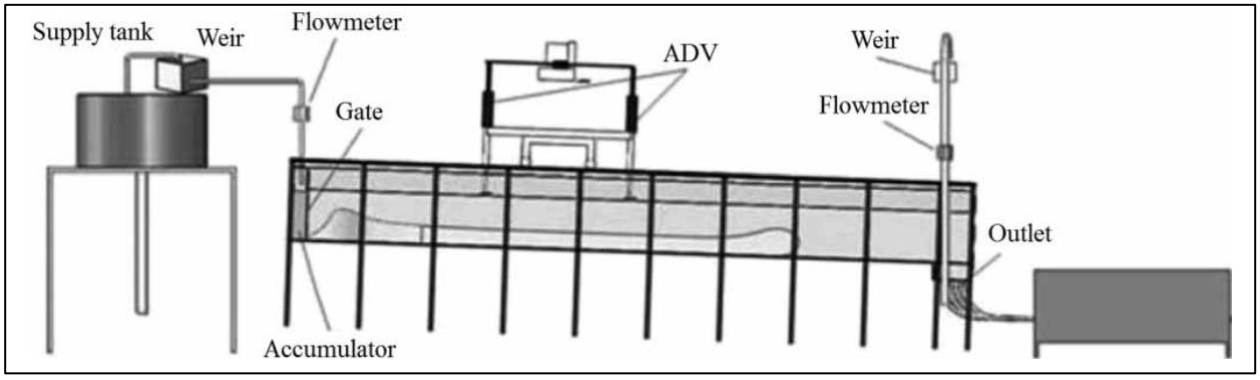

Figure 2.7 – Diagram of flume tank used for turbidity current experiments (Khavasi et al., 2012).

Other ways to feed material into a flume tank to simulate a current are through other gravity or density driven mechanisms. An example of this is using a vertical barrier, known as the 'lock gate' to separate the test material or water from the control or main water of the tank. This method can be known as a lock exchange, or dam-break flow. Shin et al. (2004) generated gravity currents in a flume using the lock exchange method. In their experiment, two fluids, one being denser than the other were separated in a flume tank using a lock gate. During the tests, the barrier was lifted, promoting the denser fluid to flow into the lighter fluid along the bottom the tank as a density current.

2.6.2 PDC simulator at Massey University

PELE (Pyroclastic flow eruption large-scale experiment) is an international eruption simulation facility located at Massey University in Palmerston North, New Zealand. PELE is used to study the dynamics of PDCs. This facility is unique as there are few experiments on pyroclastic density currents conducted at this scale. The research undertaken at the PELE facility outreaches studies conducted at other medium to large scale experiments around the world. PELE simulates pyroclastic density currents by producing a controlled gravitational collapse, simulating an eruption column collapse, consisting of hot gas and volcanic particles. This is done by transporting the volcanic material in a vertical elevator to a vertical drop of 7 m height and travelling onto a 12 m long inclined channel and dispersed onto the ground (Brosch et al., 2021). These experiments have generated PDCs with speeds ranging from 7 to 30 m s^{-1} and run out distances >35 m (Lube et al., 2015). Figure 2.8 below presents a schematic diagram of PELE.

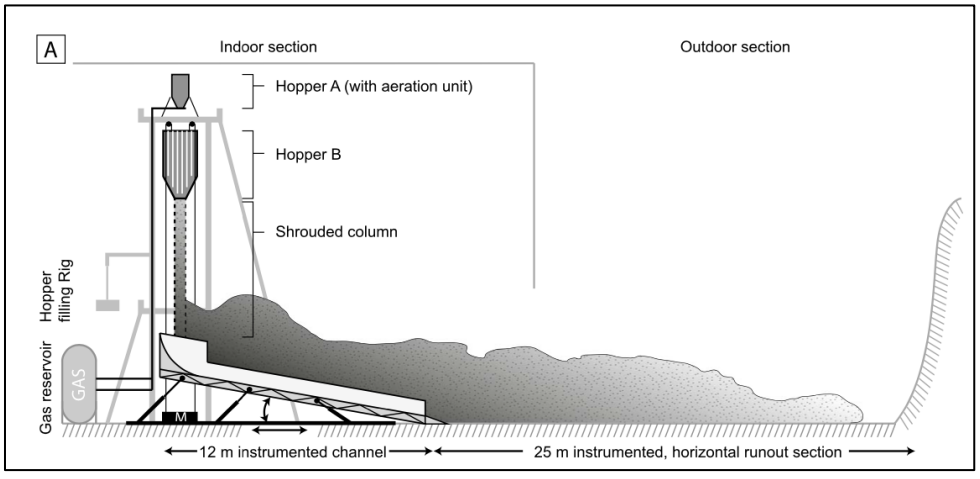

Figure 2.8 – Schematic diagram of the PELE facility used for pyroclastic flow simulations (Lube et al., 2015).

PELE can generate currents characteristic of both dilute surge-like PDCs and pyroclastic-flow like PDCs. The surge-like currents developed a thin basal layer overlain by a thick, turbulent suspension. The flow-like currents developed a thick basal layer overlain by a thinner upper ash cloud surge (Lube et al., 2015).

2.6.3 Simulating the Mount Peleé Eruption of 1902

On the 8th of May 1902, a major explosive eruption took place on Mount Peleé. This eruption produced pyroclastic density currents that killed almost 30,000 people and destroyed nearly the entire city of Saint Pierre (Gueugneau et al., 2020). This event was significant in initiating major studies on the behaviour of pyroclastic density currents. Since the event, several theories have been made about the types of currents produced from the eruption and how the dynamics of those currents were able to cause great destruction. Gueugneau et al. (2020) used the numerical model VolcFlow to simulate the pyroclastic density currents produced from the eruption. VolcFlow is geophysical modelling system used to reproduce the simulation of isothermal geophysical flows, like pyroclastic flows (Kelfoun & Vallejo Vargas, 2016). The parameters of the model were supported with data extracted from the field. The study found that a pyroclastic block-and-ash flow and associated ash-cloud surge were most likely to have been produced from the eruption, where the block-and-ash flow stayed confined to the local river valley system and the ash-cloud surge spread over a greater distance. Once the ash-cloud surge met the sea it spread laterally towards the northern plains and city of Saint Pierre. One third of the total volume of the deposit from the currents was placed in the sea, a significant amount that has not been reported before. For the block-and-ash flow, the simulation showed once the flow entered the sea it produced large lobes. This is an error in the model as the sea surface is given an elevation of 0 m which causes a break in slope allowing the material to thicken at the break (Gueugneau et al., 2020). With the VolcFlow model it is challenging to simulate the behaviour of a flow into the sea, but the main findings are that an ash-cloud surge, a typically dilute current, will flow over the sea surface and spread, as described previously in this literature review. Figure 2.9 displays the most accurate simulation of the eruption based on field deposits.

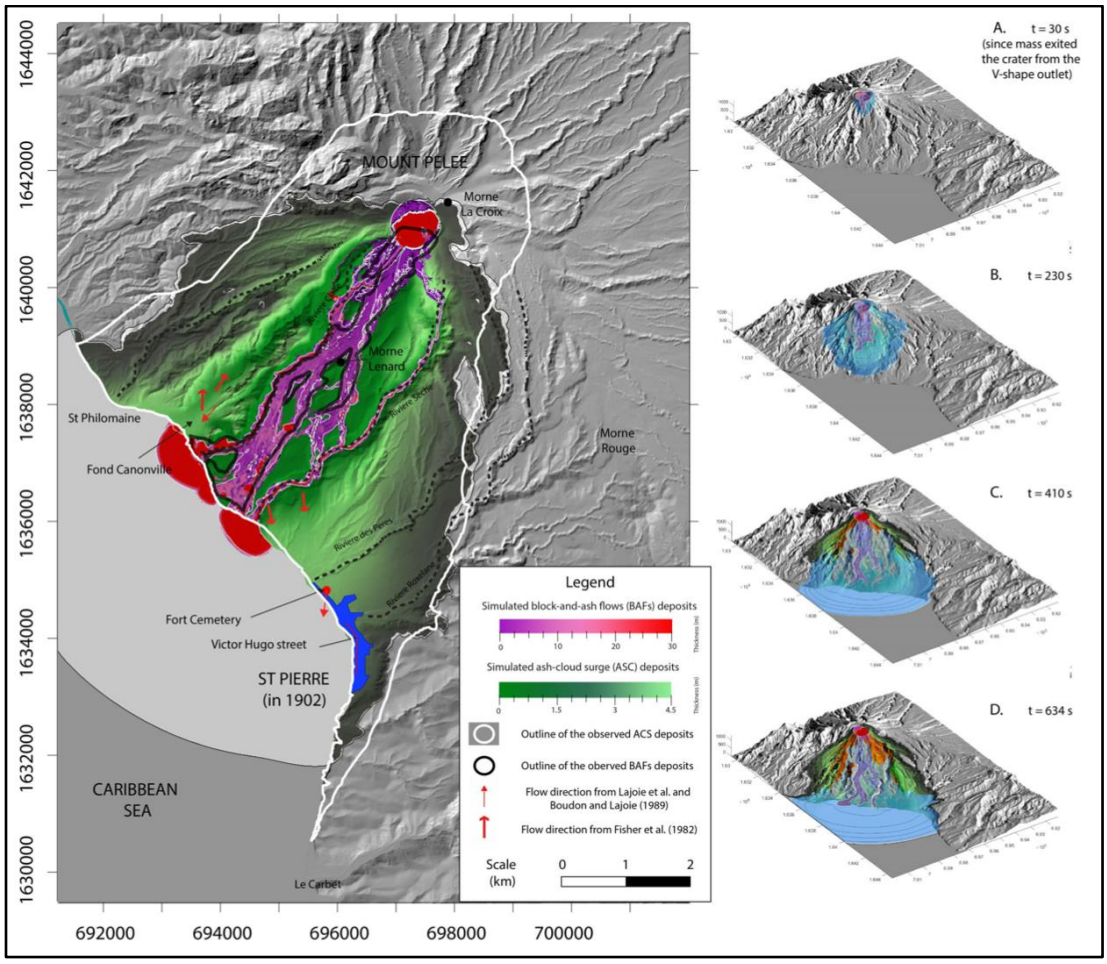

Figure 2.9 – Results of the 1902 Mount Peleé pyroclastic flow simulation produced (Gueugneau et al., 2020).

2.6.4 Simulating tsunamis generated by PDCs

PDCs produced on islands or near coastal settings have the potential to flow into the sea. When a PDC enters the sea, it is very possible for a wave to generate. A well-known and well-studied example as previously discussed is the 1883 Krakatau event, where a tsunami generated by a pyroclastic flow created more destruction than the eruption itself. Due to the energetic and dense nature of PDCs, significant water displacement or transfer of energy can occur when a flow enters the sea. Other generation mechanisms for tsunamis from PDCs include steam explosion, plume pressure, and plume shear (Watts & Waythomas, 2003). Figure 2.10 demonstrates those different mechanisms.

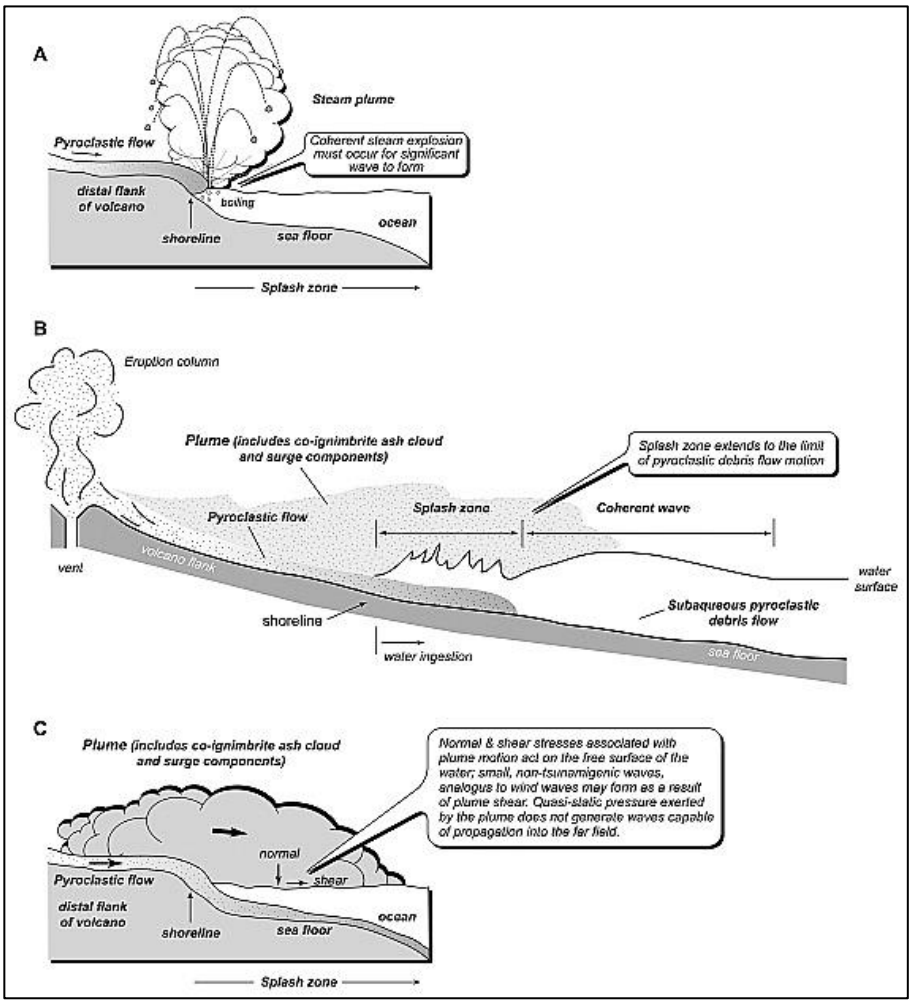

Figure 2.10 – A schematic diagram of the different mechanisms associated with pyroclastic flows entering the sea (Watts & Waythomas, 2003).

Examples of tsunamis generated by PDCs occurred during the Late Bronze Age Eruption (LBA) of Thera, Greece. Thera is an island in the Aegean Sea which is better known as the modern-day island of Santorini. The LBA eruption was a violent Plinian eruption that took place c. 3500 yrs BP. Sedimentary deposits found in proximity to the volcano have shown evidence of tsunami inundation and volcanic pumice produced from the eruption (Dominey-Howes, 2004). Novikova et al. (2011) modelled the tsunami using pyroclastic flows as the generation mechanism. The tsunami was simulated using the numerical model GEOWAVE which can simulate a variety of wavelengths with their resulting wave breaking and run-up. The pyroclastic flows were modelled as solid blocks with dimensions of width, thickness, and length, producing a bulk density which enters the water with a given density and constant depth (Novikova et al., 2011). Parameters of the pyroclastic flow were adopted from other large, comparative eruptions (e.g., Krakatau 1883, Tambora 1815) shown in Table 2.4 below.

Table 2.4 - Parameters of pyroclastic flows from adopted eruptions, notes compiled from (Novikova et al., 2011).

Eruption		**Parameters**				
Location	Date	Flow volume (km^3)	Flow velocity (ms^{-1})	Flow duration (s)	Run-out distance (km)	Mean thickness (m)
Krakatau	1883	20	150	217.2	N/A	20
Tambora	1815	80	200	257.5	N/A	80
LBA	3500 yrs BP	60	170	<500	<40	<50

The results of the study showed that tsunamis generated from 50 m thick pyroclastic flows produced tsunamis up to 29 m in height, and inundation distances from 250 to 450 m on Crete, a Greek island located ~115 km south from Thera. Thinner pyroclastic flows (~1 m) produced smaller waves around 4 m (Novikova et al., 2011).

2.7 Conclusion

It is evident that the complex event of a PDC entering the sea is not uncommon. Through historic to present day events, this complexity has occurred in several areas of the world. These events have caused significant change to the topography and bathymetry of coastal and island arc settings. The deposits produced from these events are different to typical ignimbrites as the dynamics of these flows are different than typical on-land, dry flows. Scientific understanding of PDCs entering the sea has improved with study and time but there is still much to learn. Steam explosions, heightened fragmentation, and hyper-concentrated flows can all be generated from pyroclastic flow-water interaction. Decoupling or separation of a PDC entering the sea is common, as well as a change in flow velocity, shape, and components. These unique attributes have led to other related hazards with one example being tsunamis. A better understanding of PDCs entering into sea may aid in future volcanic monitoring and prediction of changes to coastal and oceanic settings, as well as volcanic hazard management.

Chapter 3

NZ Case Studies

3.1 Introduction

This chapter explores examples of PDCs in the field at four locations: (1A) Pacific Coast Highway, Bay of Plenty [37°50'30.80"S/176°37'36.42"E], (1B) Mimiha Road, near Matata, Bay of Plenty [37º52’04.21”S/176º41’34.35”E] (2) Glenbrook Beach, Waiuku township [37º09’58.27’S/174º43’12.23’E] and, (3) Kihi Road, Hauturu west of Kawhia harbour [38°5'37.77"S/174°56'12.90"E]. Along the Pacific Coast Highway, between Pukehina and Matata there are several road cutting outcrops and coastal cliffs exhibiting the Rotoiti Ignimbrite sourced from the Okataina Volcanic Centre (OVC). The Rotoiti Ignimbrite is also presented along Mimiha Road just off the Pacific Coast Highway. Along Glenbrook Beach beside the Waiuku River inlet is an outcrop exhibiting the Ongatiti Ignimbrite sourced from the Mangakino Volcanic Centre. Along Kihi Road, near Hauturu is a road cutting that also exhibits the Ongatiti Ignimbrite. Both ignimbrites are sourced from significant pyroclastic flows, that span over a great area of land before reaching the sea. The aim of the field studies is to characterize deposits with either unique pyroclastic flow-water interaction features, or of pyroclastic flows about to the enter the sea. These case studies are to provide local context to the experimental studies in Chapter 4.

3.2 Methods

The methods used include both field observations and sample collection on site, and laboratory analysis of the samples. Data recorded during laboratory analysis have been organized into spreadsheets. Figure 3.1 below shows a location overview of the four sites visited with respect to their volcanic source.

Figure 3.1 - Map showing locations of case studies observed in the field *(Google, n.d.-d)*.

3.2.1 Site Investigation

Site visits took place on public land, therefore travel and access were within reach. At all locations, written notes were taken describing grain size, textural characteristics, components, and colour of the deposit with any notable features. Stratigraphic logs were also constructed, with support of photos and drawings using a digital camera. Approximately 2 kg samples of each unit were collected to later be studied in the lab. The tools utilized in the field included a measuring staff, a rock hammer, a hand lens, a handheld trowel, and a spade. At Site 1A (Pacific Coast Highway) the rockface was logged, noting large-scale deposit structure. At Site 1B (Mimiha Road) photographs and notes were taken about the lower 8.5 m section of the Rotoiti Ignimbrite. The location of the outcrop at Site 2 was specified by Alloway et al. (2004) as the NZ Topographic Map Reference: R12 627 465 and was revisited for this study and a stratigraphic log was constructed. At Site 2 (Glenbrook Beach) a sketch

of the Ongatiti Ignimbrite (~5.5 m) was drawn. At Site 3 (Kihi Road) photographs and notes were taken of a 7 m section of the Oparau Tephra (local name for Ongatiti Ignimbrite).

3.2.2 SEM Imaging

Scanning electron microscopy (SEM) is a technique used to study a range of materials for science. An electron microscope uses a focused beam of high-energy electrons to generate signals at the surface of a solid specimen. The signals reveal information about the texture, morphology, composition, and crystalline structure of the specimen. This information is displayed in a greyscale image with magnification ranging from 20X to 30,000X (Swamp, n.d.). The instrument utilized for this project was a HITACHI S-4700 field emission SEM, at the University of Waikato, assisted by SEM specialist, Helen Turner. The steps taken to prepare the samples and use the instrument begin with samples being were split and labelled into trays and dried in an oven at 180^{o}C overnight. The following day small portions of each sample (approximately 1/16th tsp) were scooped onto double-sided tape attached to a round stub. The sample stubs were labelled, then coated with platinum using a coating device.

Scanning electron microscopy secondary electron imaging was conducted on samples 3, 4 and 5 collected at Glenbrook Beach (Figure 3.17), as well as images for sample 1 at Site 1A (Figure 3.10). Samples 3 to 5 represent the lower portion of Ongatiti Ignimbrite Unit 1, near the contact boundary of the ignimbrite and mud horizon, as specified in the stratigraphic column seen in Figure 3.12. Sample 1 represents a Rotoiti Ignimbrite flow unit, as specified in the stratigraphic column (Figure 3.5). These samples were selected for SEM analysis to see if there were any distinctive features about the pumice and ash within this portion of the deposit. Overall grain size was observed at 35x to 40x magnification, while close images of individual particles were observed at 200x to 800x magnification, at 5kV.

3.2.3 Grainsize by Laser Diffraction Particle Size Analysis

One method for obtaining precise grain sizes and distribution of a sample is by laser diffraction particle size analysis. A Malvern Mastersizer 3000 supplied by the University of Waikato was used. Particle size analysis that uses laser diffraction allows particle measurements from 100 nm to 3500 µm to be taken at 10 kHz (ATA Scientific, n.d.). The steps taken to prepare the samples and use the instrument started with cleaning the

Mastersizer. Then approximately 1 tsp of each sample was poured into a beaker with water and mixed into a slurry. Three droplets from a pipette of 5% Calgon solution was added to the beaker to help disaggregate the sample. The mixture was then poured into a dispersion tank. The dispersion tank mixes and disaggregates the sample further. Once dispersed, a laser beam passes through the sample and the particles within the sample create a scattered light pattern. The results were presented on a display screen, showing the particle size distribution of the sample.

Samples 3 to 5 collected from the lower portion of ignimbrite Unit 1 at Site 2 and samples 10 to 11 collected from the upper portion of ignimbrite Unit 2 also at Site 2 underwent laser diffraction particle size analysis (Figure 3.1).

3.2.4 Grainsize by Dry Sieving

A much simpler physical method for obtaining grain size and distribution is by sieving. This technique uses a range of sieve pans from 32 mm to 0.0625 mm stacked on top of one another, from largest to smallest mesh aperture, allowing the sample to distribute into their corresponding grain size groups. Samples were separated and labelled in trays to dry in an oven at 180^{o}C overnight. The following day the dry samples were then brought to the sieving lab for preparation and use. Initial weights of each sample were measured on a scale. The sample was then placed into the top of the sieve pan. The pan stack was shaken by hand to help with distribution. Each pan was removed and weighed from top to bottom.

Sample 1, representing some of the lower unit, collected from Site 1A (Figure 3.1) and Sample 13 collected from the Site 2 were taken into the dry sieving lab for grain size analysis. Sample 13 represents a pumice concentration zone not found within the main outcrop observed but from another one further south of the beach. The sample was taken because it was easier to collect and more distinct. This pumice concentration zone corresponds to the same one described within the log from Site 2, Glenbrook Beach (Figure 3.1).

3.3 Rotoiti Ignimbrite along the Bay of Plenty Coast

The Rotoiti Ignimbrite, also known as the Rotoiti Breccia, is a non-welded ignimbrite that erupted from the northern sector of Haroharo volcanic complex of the Okataina volcanic

centre (OVC). The ignimbrite was produced from a caldera collapse eruption known as the Rotoiti eruption, which has been given varying dates of 45.2 ± 8.2 ka by Buhay et al. (1992), and 64 ± 4 ka by Wilson et al. (2010) and generated >100 km^3 of pyroclastic material (Cole et al., 2010). The deposit spans from Rotorua to the Bay of Plenty coastline, covering an estimated area of >850 km^2 (Schmitz & Smith, 2004). The Rotoiti Ignimbrite is one of the most voluminous ignimbrites from the most recent caldera collapse in the OVC (Flude & Storey, 2016). The majority of the Rotoiti ignimbrite deposited near source has been buried by younger lavas and pyroclastic units. Outcrops of the ignimbrite can be found northeast of the OVC and along the coast between Matata and Maketu townships. Previous work by Burt et al. (1998) subdivided the Rotoiti eruption sequence into four different units based on mineralogy: (1) predominantly biotite-free plinian-ash beds, (2) biotite-free ignimbrite, (3) biotite-bearing ignimbrite, and (4) biotite-bearing air fall. All of these units contain plagioclase, quartz, orthopyroxene, calcic amphibole, and cummingtonite (Burt et al., 1998). Figure 3.2 is a stratigraphic column assembled from four outcrops northeast of OVC described by Burt et al. (1998).

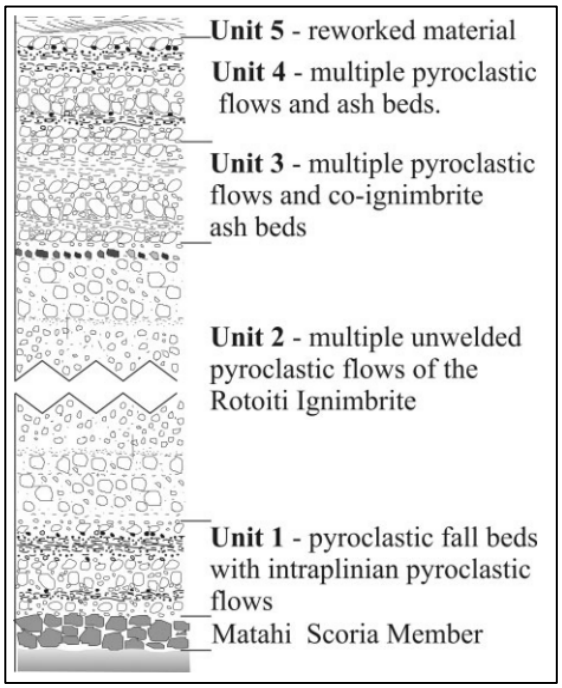

Figure 3.2 – Composite stratigraphic column of the Rotoiti Breccia (Burt et al., 1998).

3.3.1 Site 1A: Pacific Coast Highway

Several road cuttings presenting a non-welded ignimbrite facing northeast towards the sea were found along the south side of the Pacific Coast Highway between Matata and Maketu. The ignimbrite cross-section height varies along the highway from 5 to 30 m in height. The deposit was described at Stop 1A (Figure 3.3).

Figure 3.3 – Map showing locations of Site 1A and Site 1B visited for this field study *(Google, n.d.-e)*.

At Pikowai Campground, on the northern side of the Pacific Coast Highway adjacent to Site 1A, the bluffs were observed to be approximately 15 m thick (Figure 3.4).

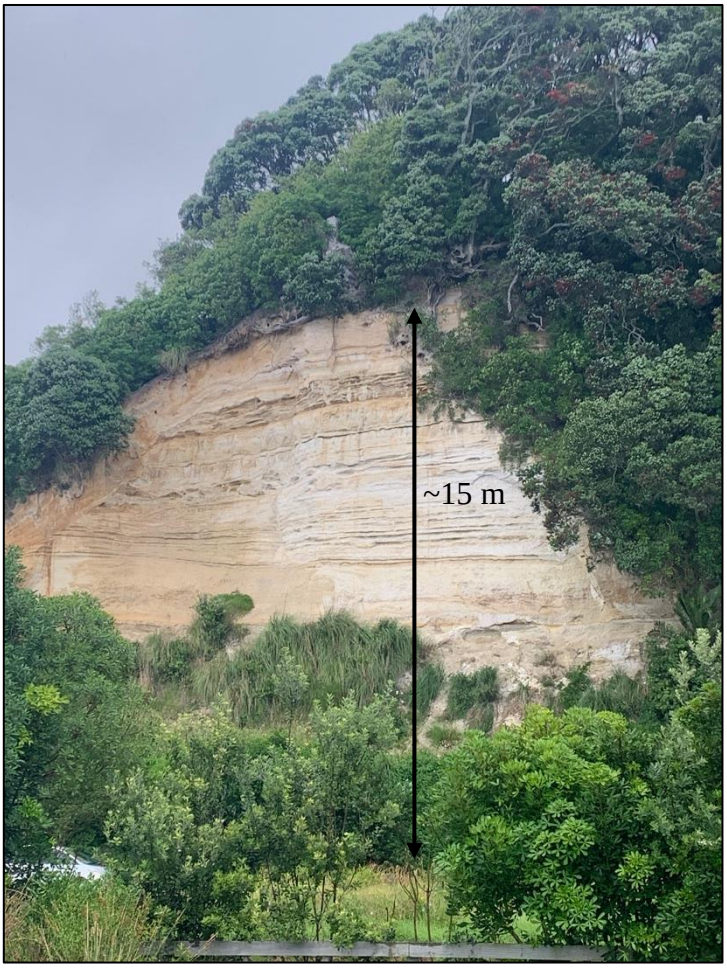

Figure 3.4 – Photographic image of a large-scale deposit of Rotoiti Ignimbrite observed from Pikowai Campground along the Pacific Coast Highway [37º51'24.11" S / 176^{0}39'56.78" E].

At Site 1A the accessible lower flow unit of the Rotoiti Ignimbrite was logged in detail in Figure 3.5.

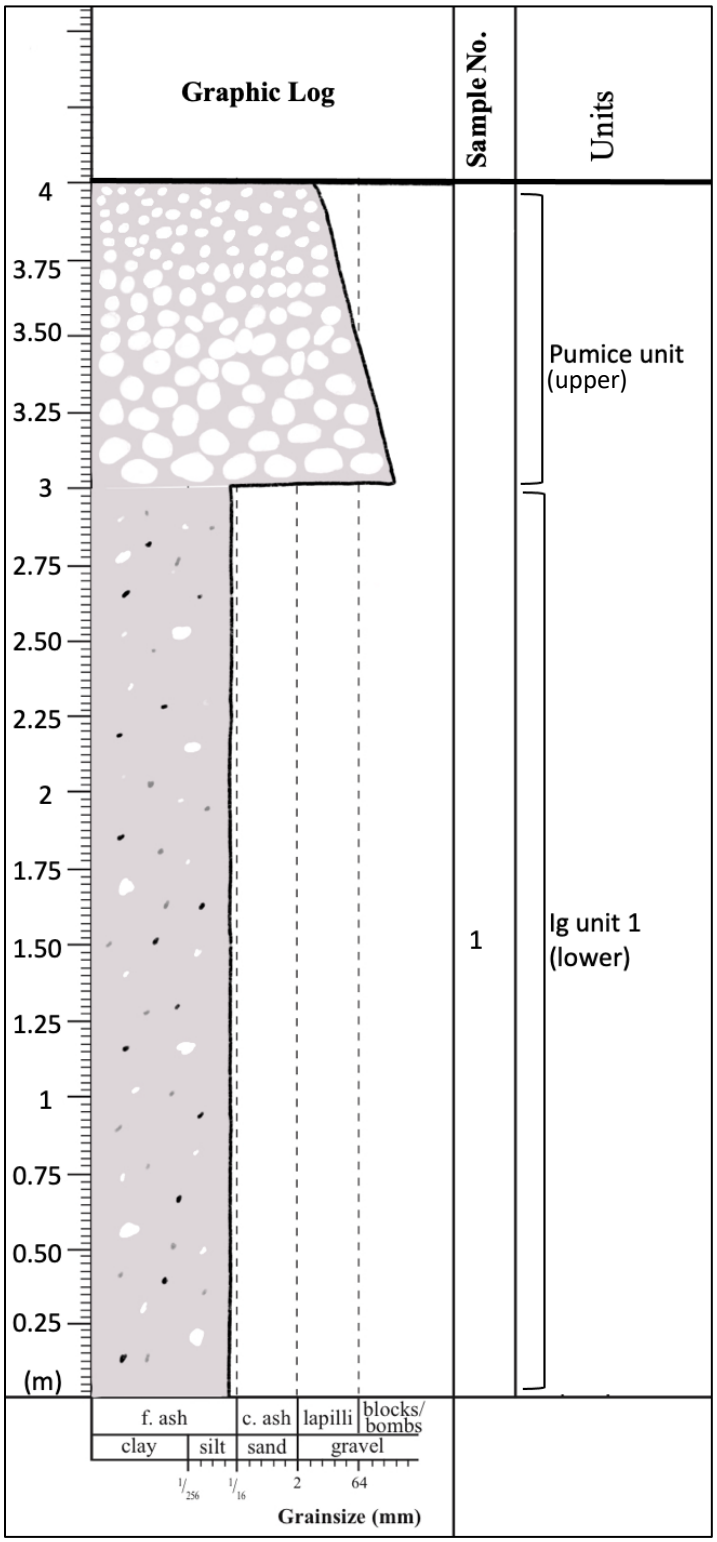

Figure 3.5 – Stratigraphic column of the lower unit of the Rotoiti ignimbrite observed at Site 1A.

Some of the lower unit, measuring from 0 to 3 m height, consisted of a nonwelded, very poorly sorted, pumice-lapilli fine ash, grey and pinkish white in colour. Visible crystals included plagioclase and biotite. Pumice clasts ranged from 0.5 to 3 cm in size with moderate

vesicularity, a sub-rounded to rounded shape, fibrous texture, and white in colour. Lithic clasts were round and ranged from 0.25 to 1 cm in size, and dark brown to black in colour. The upper zone of the lower unit (~1.5 m thick) was a very poorly sorted pumice concentration zone. These pumice clasts also were sub-rounded to rounded in shape, and ranged from 5 to 10 cm in size, exhibiting a fibrous texture, elongated vesicles and white in colour. From 5.5 m to the top of the outcrop was inaccessible and covered in vegetation. Figure 3.6 displays the main outcrop observed at Site 1.

Figure 3.6 – Photograph of the lower portion of the Rotoiti ignimbrite at Site 1A. PCZ = pumice concentration zone.

3.3.2 Site 1B: Mimiha Road

The Rotoiti ignimbrite was also observed along Mimiha Road off Pacific Coast Highway, approximately 6.5 km from Site 1A. Mimiha Road runs parallel to a small stream and gully environment. The outcrop itself is situated approximately 175 m inland from the Bay of Plenty shoreline. The outcrop was approximately 8.75 to 9 m in height. Overall, the deposit is a greyish white, non-welded ignimbrite composed of coarse coarse-ash with minor lapilli and pumice. There were significant cross-bedding features in the lower section of the unit. Within the deposit were discontinuous beds of poorly sorted angular pebble and cobble-sized white lithic clasts, while no marine-derived or shelly material was found. The amount and size of the lithic clasts increased towards sea. Figure 3.7 and Figure 3.8 shows the outcrop.

Figure 3.7 – Photograph of the entire outcrop observed at Site 1B (Mimiha Road).

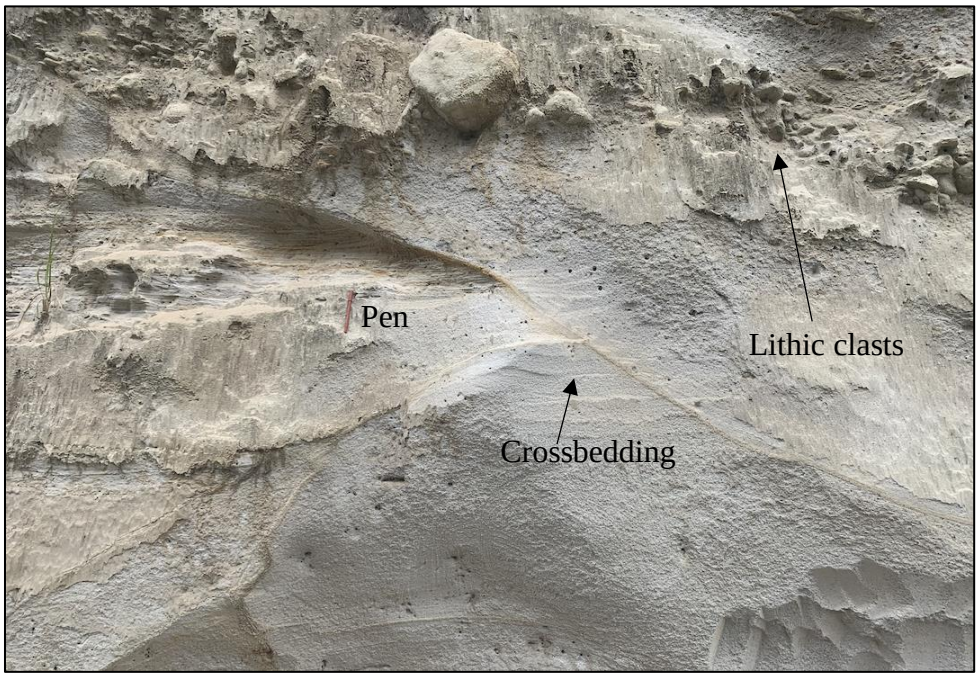

Figure 3.8 – Close up image of crossbedding within the Rotoiti Ignimbrite at Site 1B.

3.3.3 Grainsize and Textural Analysis

Grainsize statistics were calculated using Inman and Folk and Ward statistics (Folk & Ward, 1957; Inman, 1952). The mean grain size for Sample 1 from Site 1A is 0.739 mm (0.44 phi), with a median of 0.717 mm (0.48 phi). The sorting value for this sample is 2.11 phi. Figure 3.9 below presents the grain size distribution of Sample 1 collected from Site 1A, along the Pacific Coast Highway.

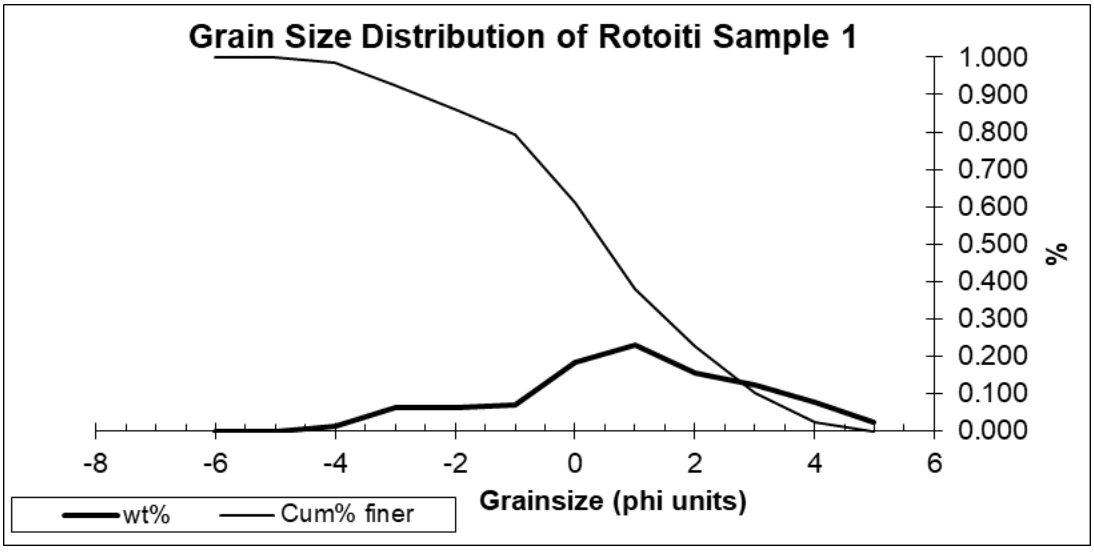

Figure 3.9 – Scatter plot of the grain size distribution of Sample 1 collected from Site 1A.

Ash particles from Sample 1 were examined by scanning electron microscopy. The ash and other particles within the sample range in size from 0.25 to 0.75 mm. Some smaller ash particles have smooth, curved surfaces, and some, probable lithics and crystals, have a blocky texture. The larger particles are predominately sub-angular with a rough surface. Figure 3.10 presents individual pumice particles. The pumice particles appear to be highly vesicular with elongated vesicles of a stretched and distorted morphology with thin walls.

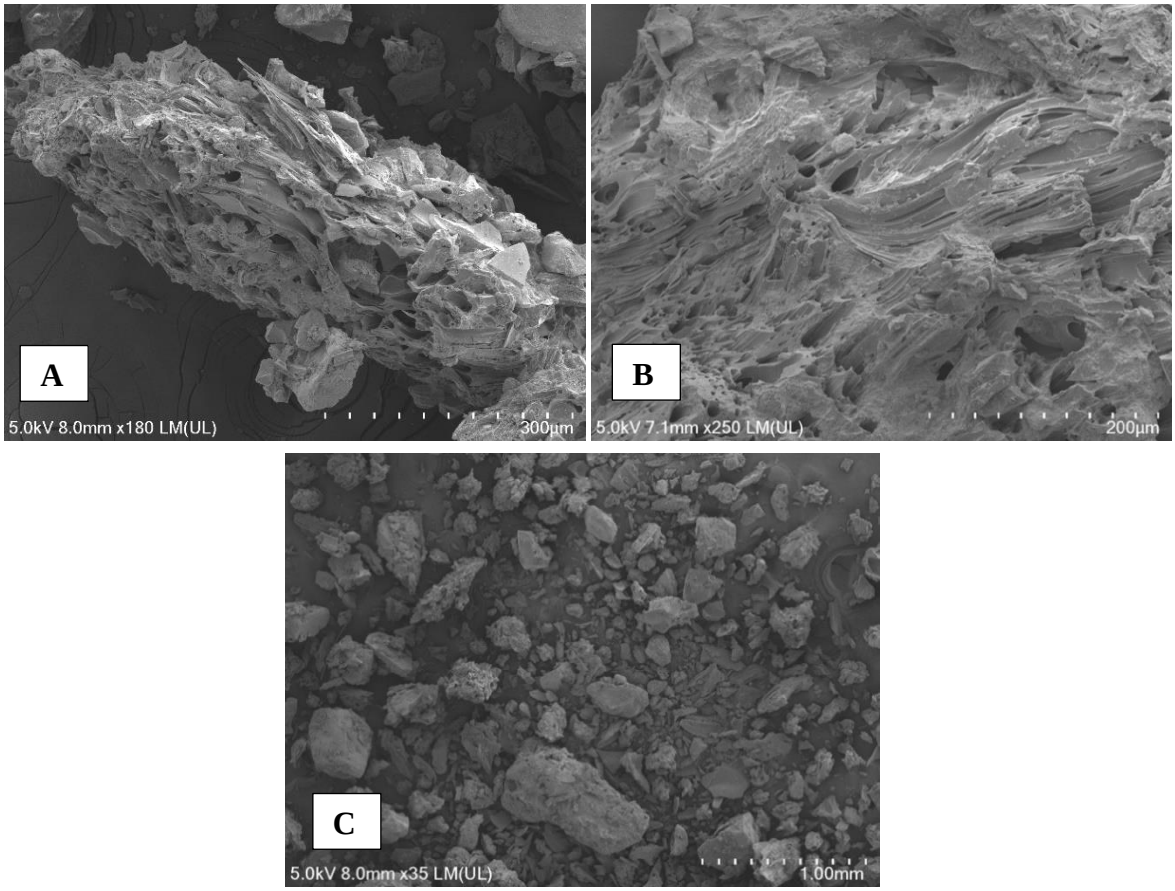

Figure 3.10 – (a) SEM image of a pumice particle from Sample 1 collected at Site 1A, (b) SEM image of pumice vesicles from Sample 1 collected at Site 1A, (c) SEM image of fine ash particles and blocky crystals from Sample 1 collected at Site 1A, including small pumice fragments and lithics.

3.4 Ongatiti Ignimbrite in the Waiuku Inlet

The Ongatiti Ignimbrite is a widespread, partially welded ignimbrite sourced from the Mangakino Volcanic Centre (Brown et al., 2004). The ignimbrite was produced from a caldera collapse eruption dated 1.21 ± 0.04 Ma, totalling a volume greater than 500 km^3 DRE (Cooper & Wilson, 2014), deeming the ignimbrite to be one of the largest, by volume, products from the Mangakino Volcanic Centre (Alloway et al., 2010). Evidence of this deposit have been found all around the Waikato region and South Auckland region. Alloway

et al. (2010) identified an outcrop of the Ongatiti Ignimbrite at Glenbrook Beach, Waiuku Township. They identified this outcrop to be a 3.8 m thick deposit with two distinct units, an upper unit, and a lower unit, with the lower unit presenting distinct flow-water interaction features. The location of the outcrop is in Figure 3.11 below.

Figure 3.11 - Map showing location of Site 2 along Glenbrook Beach (Google, n.d.-b).

3.4.1 Site 2: Glenbrook Beach

In this study, two units of the ignimbrite were also identified with both the top and bottom of the deposit bounded by mud horizons. The overall deposit is a greyish white to light grey and dark grey fine to coarse ash, with a pumice concentration zone between the lower and upper unit. The pumice concentration zone includes moderate quantities of charcoal and woody material. Figure 3.12 is a stratigraphic log and Figure 3.13 is a sketch of the Ongatiti succession observed at Site 2, respectively.

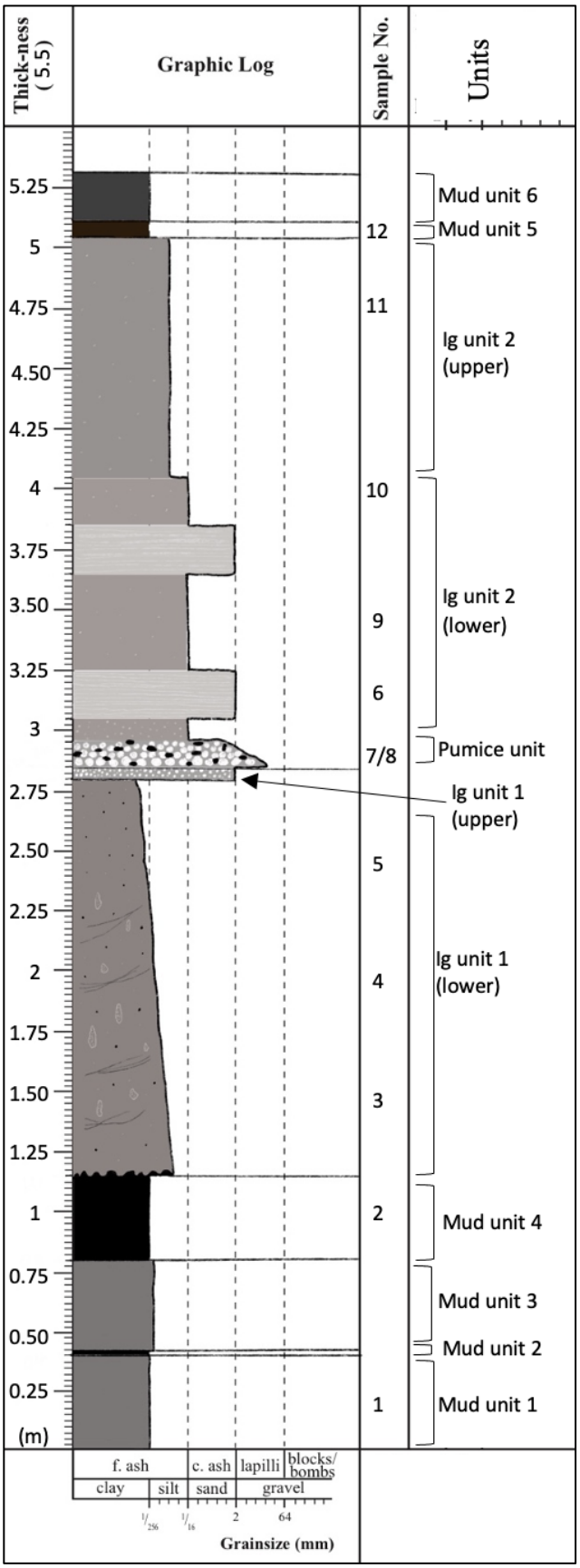

Figure 3.12 - Stratigraphic column of Ongatiti Ignimbrite showing multiple flow units and underlying and overlying sedimentary units at Site 2

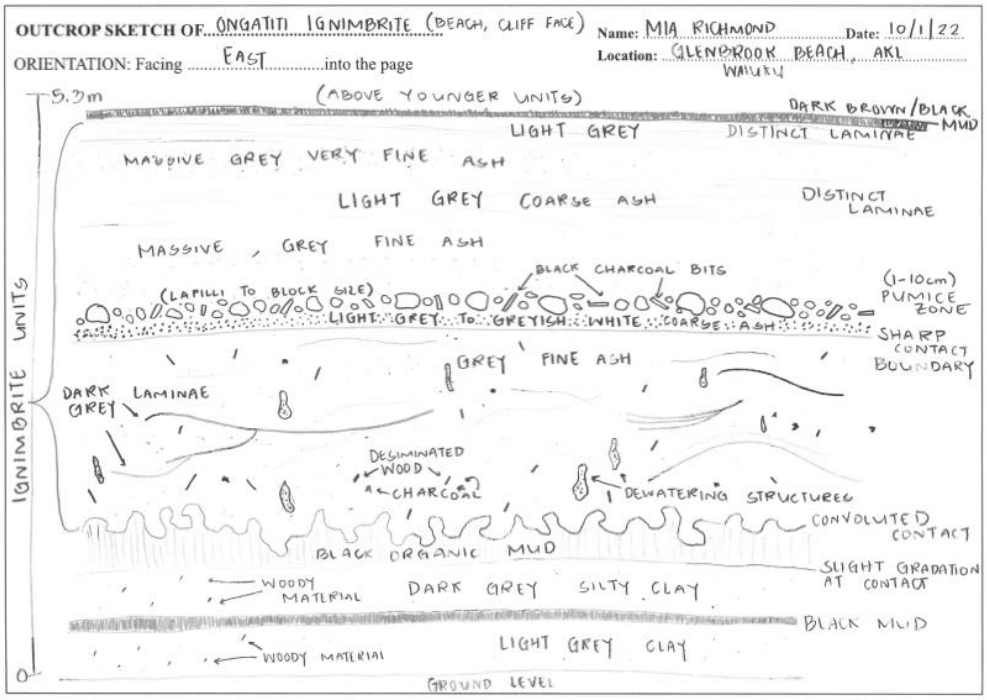

Figure 3.13 - Sketch of outcrop observed at Site 2.

A detailed description of the sequence is described here. Units underlying the ignimbrite were alternating horizons of dark grey and black organic mud including woody material.

Overlying the mud units was lower ignimbrite Unit 1. This unit was broken into a lower portion and upper portion. The lower portion of this unit was moderately sorted, composed of grey fine to coarse ash with minor decimated wood (~1 cm), minor white, round pumice (~3mm), and dark brown lithics (~1mm). The unit had thin dark grey convoluted laminae. The unit also had irregular, round, vertical domains of coarse ash described as dewatering structures. These dewatering structures decreased in size and concentration vertically within the unit. Overall ignimbrite Unit 1 was described as chaotic. The bottom contact of the unit was irregular with flame structures or load casts. Figure 3.14 below shows the bottom contact with the flame structures, the convoluted laminae, and a dewatering structure.

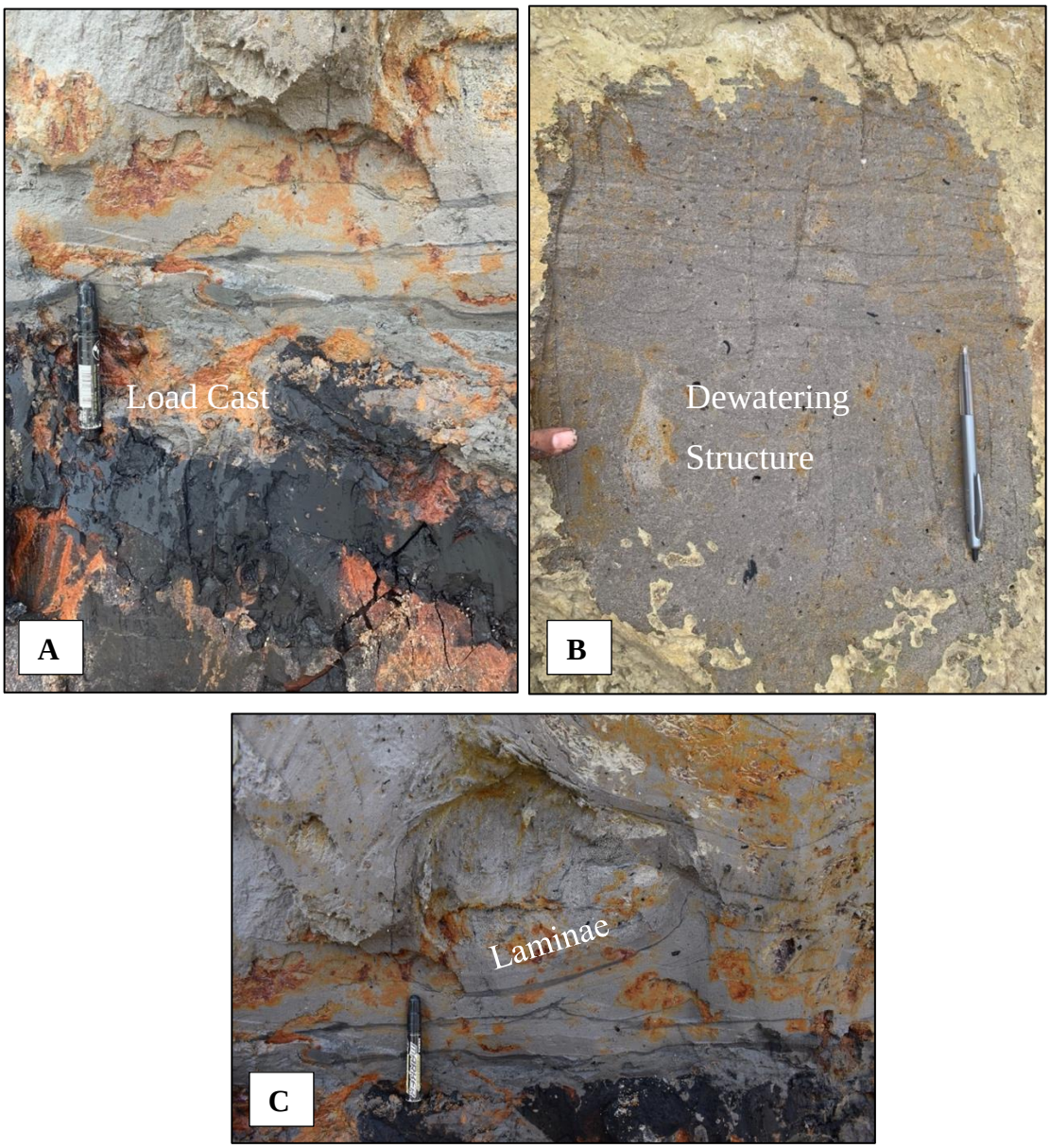

Figure 3.14 – (a) Photograph of load casts observed along the contact of mud Unit 4 and base of ignimbrite Unit 1 at Site 2, (b) Photograph of dewatering structures observed within ignimbrite Unit 1 (lower) at Site 2, (c) Photograph of convoluted laminae observed within ignimbrite Unit 1.

The upper portion of ignimbrite Unit 1 was a well sorted, greyish white, very coarse ash with a sharp top contact. Visible crystals included plagioclase and quartz. Overlying ignimbrite Unit 1 is pumice concentration zone composed of sub-rounded, white pumice lapilli to bombs, and large pieces of charcoal (~8 cm). The pumice in this zone shows a slight normal grain size grading. Figure 3.15 shows the upper portion of Unit 1 overlain by the pumice and charcoal zone.

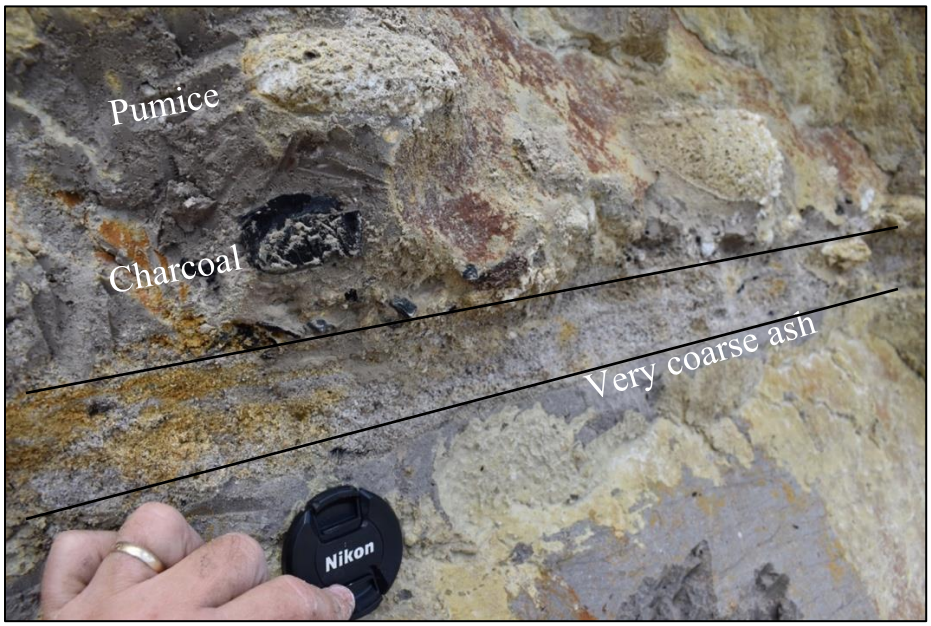

Figure 3.15 - Photograph of ignimbrite Unit 1 (upper) showing the contact between very coarse ash and pumice unit.

Overlying the pumice zone is ignimbrite Unit 2, which was also divided into a lower and upper portion. The lower portion of ignimbrite was a dark grey fine coarse ash with two alternating subunits within the unit. The subunits were light grey coarse ash with distinct lamination affected by convolution. These subunits present pulses within the flow. The upper portion of ignimbrite Unit 2 is a massive, grey, fine coarse ash. Overlying the entire ignimbrite sequence were more mud units which were dark brown and black organic rich clay. Figure 3.16 below is a photograph of the lower portion of ignimbrite Unit 2 with subunit pulses.

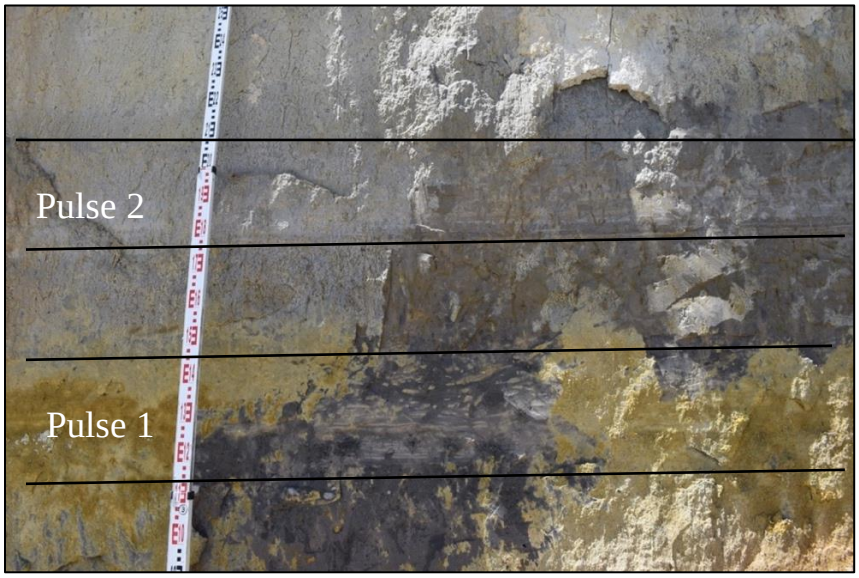

Figure 3.16 - Photograph of ignimbrite Unit 2 (lower) at Site 2.

3.4.2 Grainsize and Textural Analysis

Samples collected from the lower portion of ignimbrite Unit 1 were observed under SEM. The imaging showed irregular pumice shards, with some sub-rounded and some angular, ranging in size from 0.15 to 0.5 mm. Most pumice clasts had strong vesicularity with elongated vesicles and thick vesicle walls. The imaging also showed blocky angular particles (e.g., lithics, crystals) 0.25 mm in size. Figure 3.17 display SEM images from ignimbrite Unit 1 (lower).

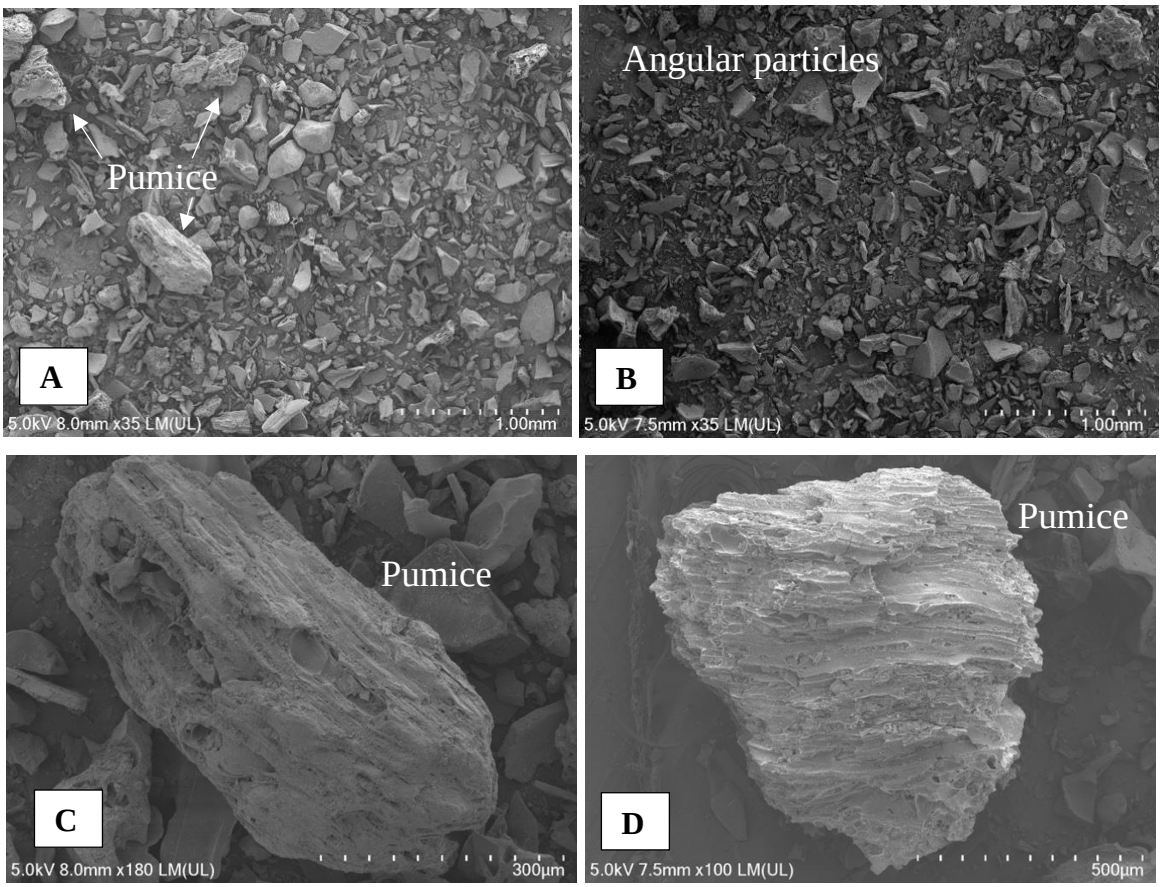

Figure 3.17 - a) SEM image of pumice particles within Sample 3 collected at Site 2, b) SEM image of angular particles (crystals, lithics) within Sample 4 collected at Site 2, c) SEM image of pumice particle within Sample 4 collected at Site 2, d) SEM image of pumice

The mean grain size for Sample 13 is 2.681 mm (-1.42 phi), with a median of 4.135 mm (-2.05 phi). The sorting value for this sample is 1.87 phi. Figure 3.18 below presents the grain distribution for Sample 13, representing the previously discussed pumice concentration zone.

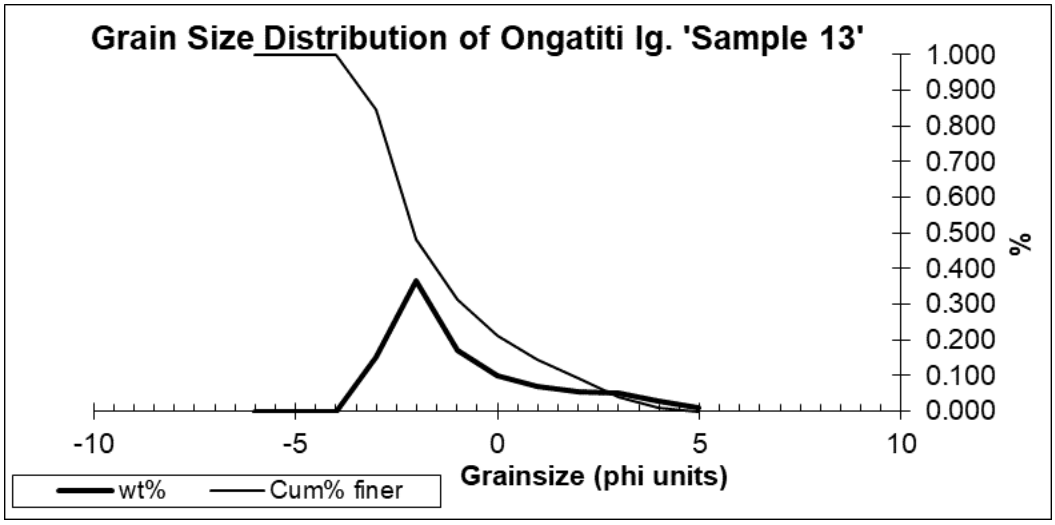

Figure 3.18 - Scatter plot of the grain size distribution of Sample 13 collected near Site 2, along Glenbrook Beach.

Grain size distribution for samples 3-5 and 10-11 from Site 2 using laser diffraction particle analysis can be found in Figure 3.19 below.

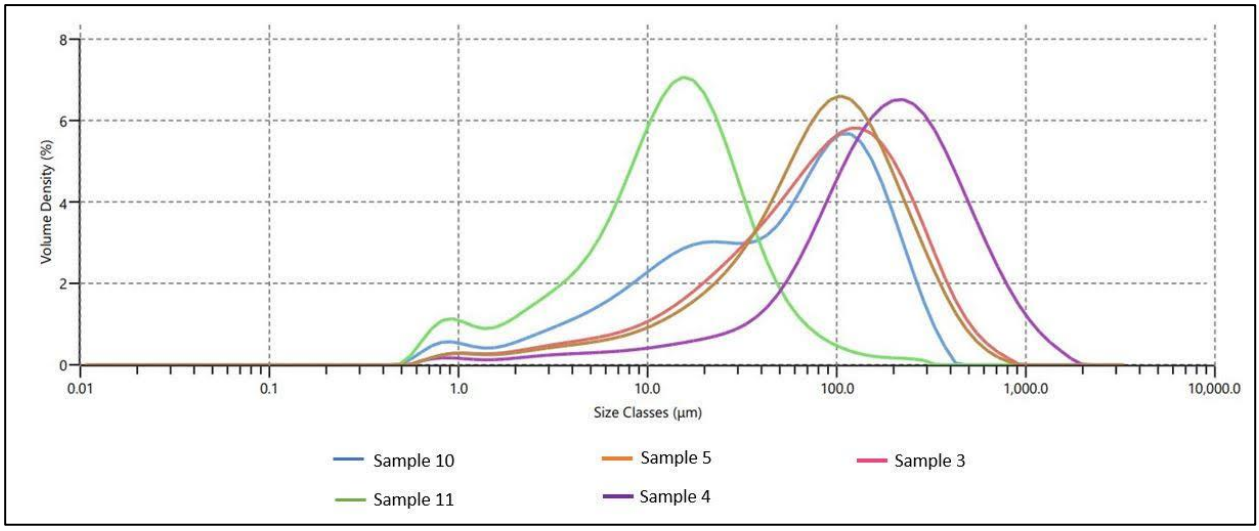

Figure 3.19 - Grain size distribution using laser diffraction particle analysis on Samples 3-5 and Samples 10-11 collected from Site 2.

Table 3.1 below displays information about each individual sample from the Mastersizer analysis. The laser diffraction data was presented in units of micrometres but has been converted to millimetres and the phi for this table.

Table 3.1 - Median, mean, and sorting values for samples 3-5 and 10-11 collected from Site 2.

Name	**Ongatiti Ignimbrite**				
	Unit 1			Unit 2	
Sample	**3**	**4**	**5**	**10**	**11**
Median (Md_ϕ)	3.52	2.41	3.54	4.2	6.22
Mean (Mz_ϕ)	3.913	2.633	3.883	4.72	6.493
Sorting ($\sigma\phi$)	2.27	1.965	2.085	2.55	1.96
Size Class	Very fine coarse ash	Medium coarse ash	Very fine coarse ash	Very fine coarse ash	Fine ash

Sample 11 presents the smallest mean grain size (0.018 mm). Sample 4 presents the largest mean grain size (0.269 mm). Overall, the samples from ignimbrite Unit 1 are finer than ignimbrite Unit 2. Sample 10 has the highest sorting value, and Sample 4 the lowest.

3.5 Ongatiti Ignimbrite in Kawhia

As previously mentioned, the Ongatiti Ignimbrite is a very voluminous ignimbrite spread over a great area in North Island, New Zealand. Another outcrop for this ignimbrite was observed along Kihi Road, Hauturu, inland of Kawhia Harbour. This outcrop was also studied by Yousef Zadeh (2020). Kawhia Harbour is a large natural inlet located on the west coast. Kawhia harbour feeds into the Tasman Sea like the Waiuku Inlet at Glenbrook Beach, but in contrast is much closer (approximately half the distance) from its volcanic source, the Mangakino Volcanic Centre. The Ongatiti ignimbrite within in the Kawhia area is also known as the Oparau tephra. Figure 3.20 shows the exact location of Site 3.

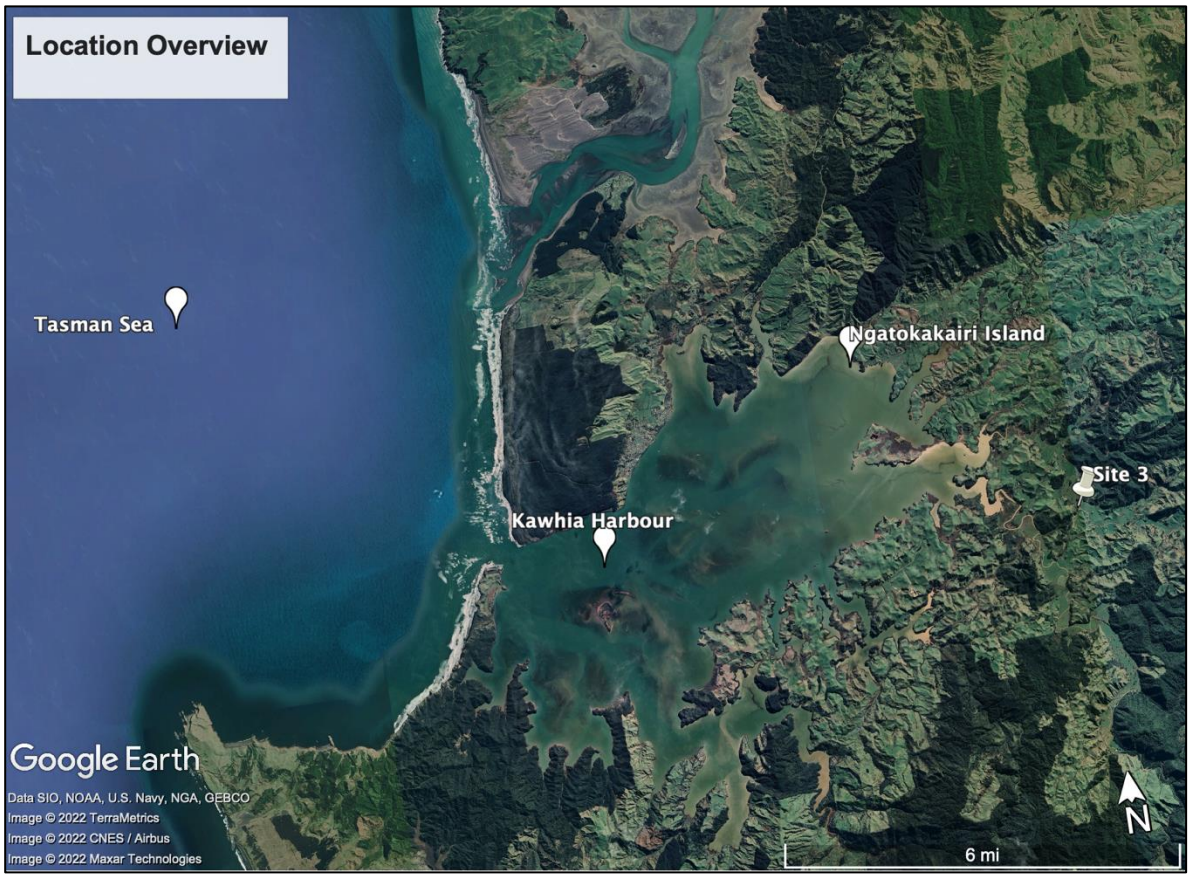

Figure 3.20 - Map showing location of Site 3 ***(Google, n.d.-c)*****.**

The overall outcrop presented one ignimbrite flow unit approximately 7 m in height with no observable lower boundary. The ignimbrite had a greyish white to greyish yellowish white colour and was a non-welded medium coarse ash to lapilli with abundant lithics and pumice. The volcanic particles were clayey in texture and crumbly. The upper portion of the outcrop was highly weathered and red in colour at the surface. Crystals of quartz and plagioclase were observed with the naked eye. The ignimbrite was massive and showed no complexities or evidence of flow-water interaction. The location of the outcrop is situated approximately 3 km east of the edge of the coastal inlet. Figure 3.21 presents photographs of the outcrop. Extensive deposits extend westward onto Ngatokakairi Island in Kawhia Harbour.

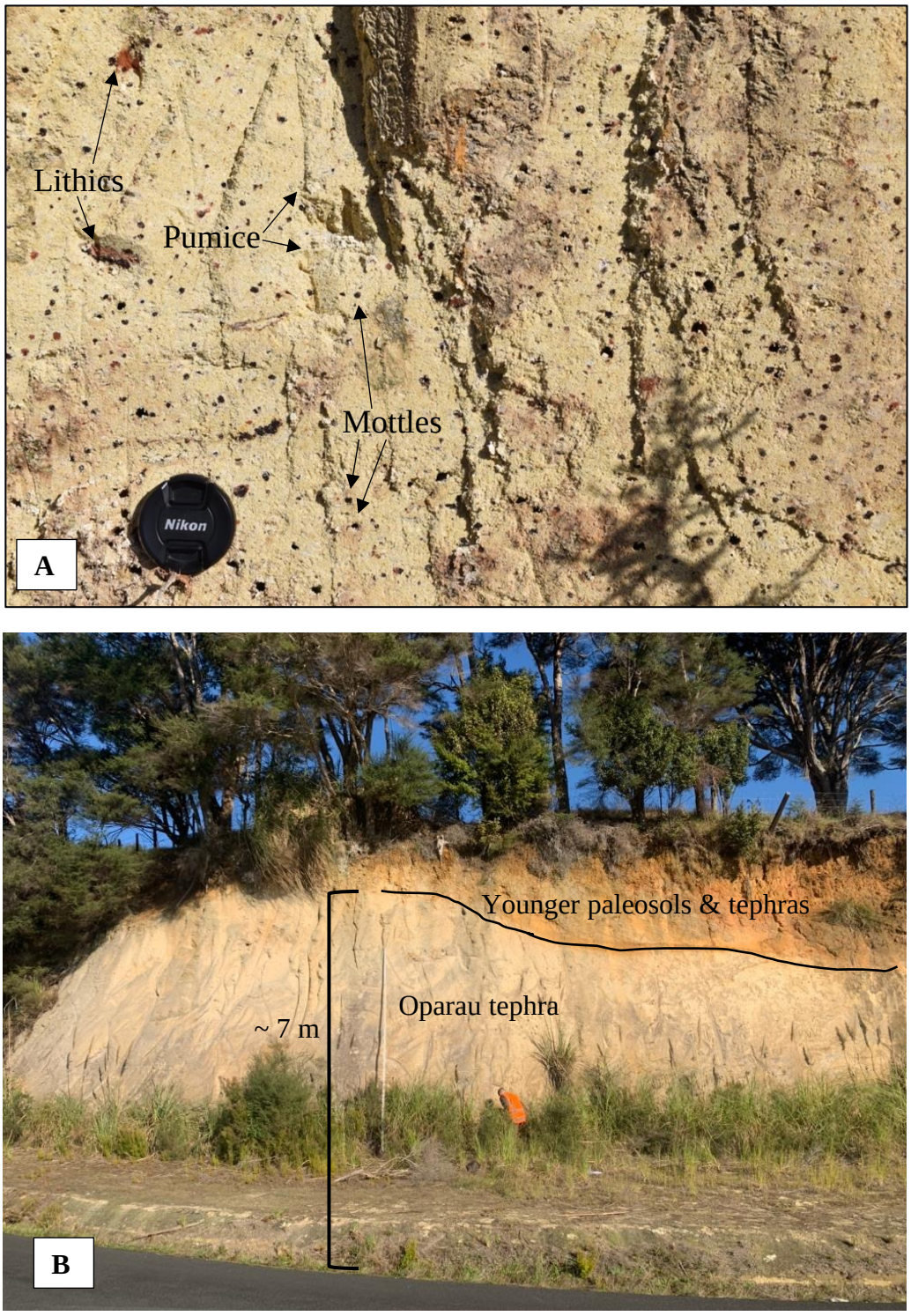

Figure 3.21 - a) Photograph of pumice, lithics, and mottle components within the Ongatiti unit observed at Site 3, b) Photograph of large-scale deposits of the Ongatiti Ignimbrite at Site 3.

Sample 20 was collected from Site 3 at about 1.2 m height. Figure 3.22 below displays the grain size distribution of this unit. The mean grain size for this sample is 4.868 mm (-2.28 phi), with a median of 8.729 mm (-3.13 phi). The sorting value for this sample is 2.65 phi.

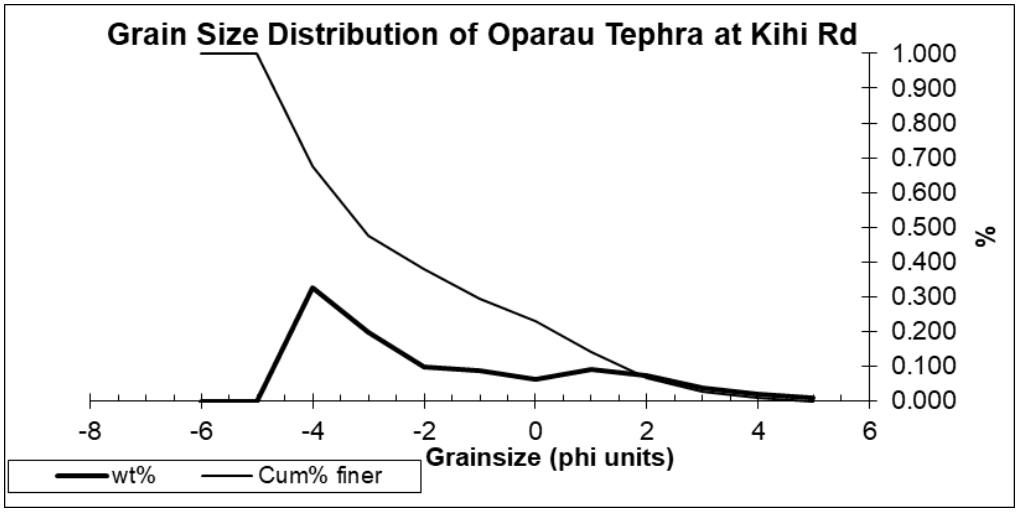

Figure 3.22 - Scatter plot of the grain size distribution of Sample 20 collected near Site 3.

3.6 Conclusion

The deposit at Site 1A was a massive, non-welded vesicular pumice-lapilli fine ash ignimbrite, overlain by a pumice concentration zone. At Site 2A on Mimiha Road, the ignimbrite deposit had cross-bedding and interbedded lithic clast concentration zones throughout the deposit.

The deposit at Site 2, Glenbrook Beach, presents two distinct flow units composed of medium to very fine coarse ash for Unit 1, and very fine coarse to fine ash for Unit 2. Unit 1, the lower unit, had flame structures, dewatering structures, and thin beds of convoluted laminae. Unit 2, the upper unit, had a basal pumice concentration zone and distinct layering representing two different pulses. All throughout the deposit were pieces of charcoal, with largest pieces being in the basal pumice zone of Unit 2. No marine or shelly material was observed within the deposit.

The deposit at Site 3, off Kihi Rd, Hauturu, presented a massive, non-welded, medium coarse ash to lapilli with abundant lithics and pumice, an ignimbrite in a subaerial environment. The location of the outcrop is approximately 1.5 km from the nearest water inlet of Kawhia Harbour. At this outcrop there were no unique features or indications of water interaction.

Chapter 4

Experimental Studies

4.1 Introduction

The aim of this chapter is to explore the behaviour and depositional processes of sediment gravity flows composed of pyroclastic material travelling into water. This was achieved through several experiments taking place in the laboratory at the University of Waikato, using a flume tank and pyroclastic material collected from the field. The purpose of the experiment relates to the phenomena of pyroclastic flows entering the sea. This has been done to simulate the volcanism of the Bay of Plenty region in a lab setting. The previously reviewed OVC includes the northmost caldera within the TVZ, with the northeast edge of the centre sitting approximately 20 km from the Bay of Plenty coastline. Volcanism within the OVC has taken place over the last 625,000 years, yielding numerous explosive eruptions, two of which were major caldera collapse events producing voluminous ignimbrite deposits (Matahina and Rotoiti eruptions) (Cole et al., 2014). Both ignimbrites can be found along the Bay of Plenty coastline, where the Rotoiti ignimbrite was studied within this area in Chapter 3 of this thesis.

4.2 Methods

The methods used in this chapter are based on flume experiments, where pyroclastic ash material was transported or placed into the tank to interact with water as a flow. Two different release mechanisms were used for this experiment to help propagate a flow. The first release mechanism was a gravity driven mechanism composed of transporting ash material down a vertical PVC pipe. The PVC pipe is 78.5 cm long with a diameter of 9 cm. A slit was cut 18 cm from the top of the pipe and a thin cardboard insert was cut and made to slide into the slit. The purpose of the insert was to hold the material at the top of pipe, and when pulled create a constant, instantaneous collapse of ash. The insert was 23 cm long, 9 cm wide, and 0.5 cm thick. The second release mechanism was a lock-exchange flow, also known as a dam-break flow, where the ash was placed in a dry, dammed section at the top of the slope. The dam was then lifted allowing the ash to travel down slope into the water within the tank. For the

dam-break flow mechanism, two thin inserts were constructed out of cardboard to create a dammed section. The inserts were 25 cm long, 10 cm wide, and 0.2 cm thick.

As previously discussed, pyroclastic density currents are large, hot flows that travel at great velocities. Simulating a flow in a laboratory setting that is analogous to a pyroclastic flow in real time is challenging. On the basis of the Rotoiti ignimbrite, the numerous flow units associated with this eruption produced >100 km^3 of ignimbrite deposit with at least 10 km^3 of those flow units deposited into the sea. A scale of 1:20 000 for flow volume has been adopted for this experiment where 500 mL (0.0005 m^3) of pyroclastic ash released into the flume will represent a flow unit of approximate 10 km^3 in the field. In terms of velocity, the flow of a pyroclastic density current in the field is dependent on the energy and generation mechanism of the eruption. Again, typical speeds of pyroclastic density currents range in the order of tens to hundreds of kilometres per hour which is untestable in a lab. Therefore, relevant generation mechanisms were chosen to help maintain a reasonable experiment. The described release mechanisms include gravity and density driven processes to apply energy to the flow. The material was heated at 180^{o}C in an oven overnight to ensure the material was dry when released into the flume. Additional heating was not applied to the material due to constrains of the flume and facilities. With that, high or extreme temperature factors typically associated with pyroclastic density currents were not applied to this experiment. A Panasonic 90x zoom hybrid camcorder, supplied by the University of Waikato, was used to capture videographic and photographic images of the flows.

4.2.1 Flume

The experiment runs were undertaken using a wave-maker flume tank supplied by the University of Waikato. The wave-maker section and paddle were not used for this experiment. The tank was 3.1 m long, 10 cm wide, and 33 cm deep, and was filled with room-temperature fresh water to depths ranging from 6 to 7 cm for each experiment. An aluminium sheet ramp was used to model the slope into the water. A diagram of the tank is provided in Figure 4.1 below. Figure 4.2 and Figure 4.3 show the tank with the two different release mechanisms.

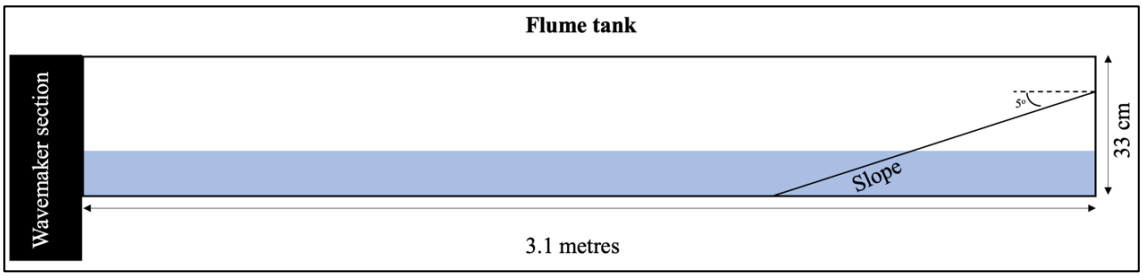

Figure 4.1 – Diagram of wavemaker flume tank used for the experiments.

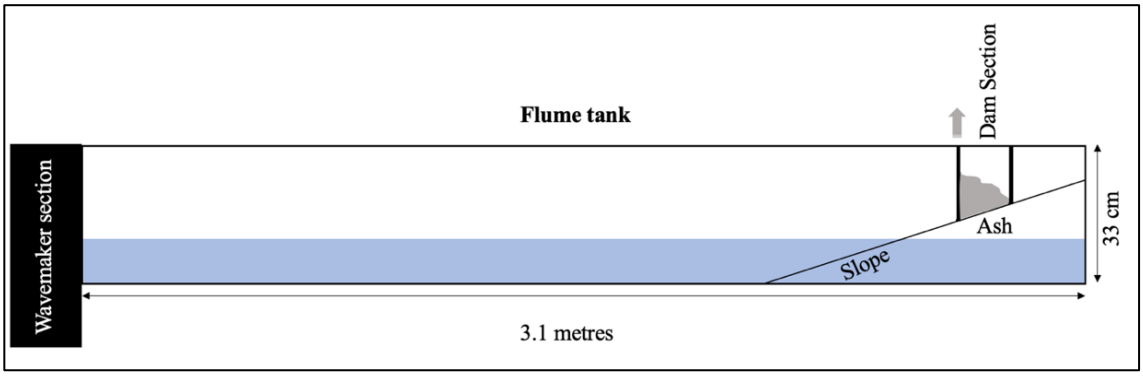

Figure 4.2 – Diagram of the flume tank with the dam insert used for the dam-break flow experiments.

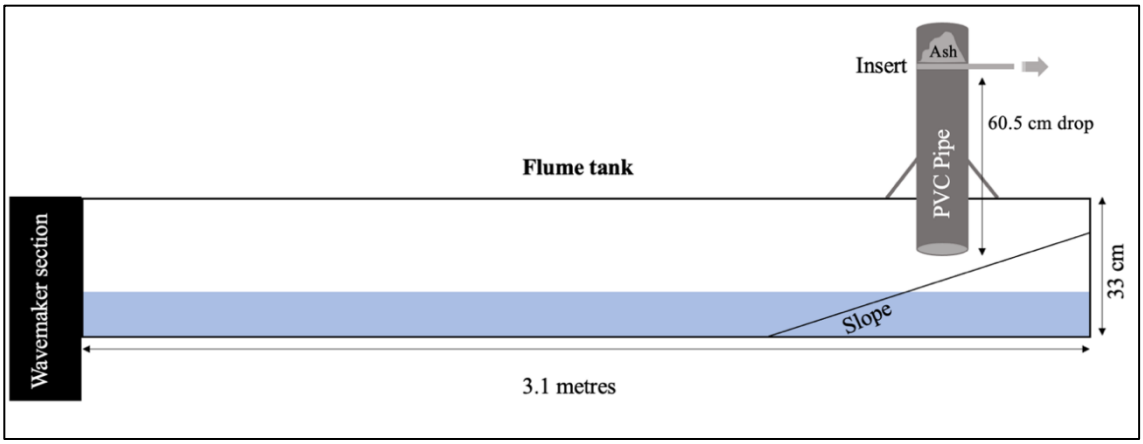

Figure 4.3 – Diagram of the flume tank with the PVC column used for the ash collapse experiments.

In preparation for the experiment, the flume tank was emptied of water and existing sediments. The tank was then scrubbed clean and re-filled with water. Rulers were placed at different positions along the flume to aid in taking measurements. Plain white boards were placed along the back of the flume to help better observe the runs. After each run, any floating particles were removed from the tank and all glass above water was wiped clean. Finer sediments that were suspended after each run were left overnight to settle. For every run the water was clear and free of any suspended and/or floating sediments. Before each run the material was weighed, the temperature of the water and ash were taken using a thermometer, and both the water height and thickness of the sand at the bed were measured using a ruler.

During each run, heights and distances were measured using a marker and ruler. Time measurements were made by playing back recordings from the camcorder. All measurements were recorded in a notebook which were later transferred to a spreadsheet. Basic statistics (mean, median, minimum, maximum) of each run were expressed. Velocity (mm/s) of each run were calculated by distance (mm) over time (seconds) measurements. Scatter plots of runout distance versus time were also created using the recorded measurements.

4.3 Desktop Analysis of the Bay of Plenty Coastline

The OVC occupies a large area. The caldera encompasses the Haroharo and Tarawera mountains, significant lakes like Lake Tarawera, Rotomahana, Okataina, and Blue Lake, parts of Lake Rotoiti, Rotoehu, and Rotoma, and numerous stream systems associated with those lakes. Overall, the geomorphology of the volcanic centre itself is quite complex with a range of topographic highs and lows. Northeast of the caldera, heading towards the Bay of Plenty coastline between Pukehina and Matata townships, there are no significant lakes or geological obstructions or features. The distance between the centre of the volcano (present day Rotoiti Forest) and the coastline is approximately 31.5 km with a very low gradient slope of less than 0.5^{o}. From the coast into the sea, the slope remains relatively flat. Within this area of the Bay of Plenty sea there are no significant bathymetrical obstructions or features (Bay of Plenty Regional Council, n.d.). Table 4.1 below displays the distances and depths of the bay, using data collected from the Bay of Plenty contours and bathymetry map provided by the Bay of Plenty Regional Council. A cross-section line of the approximate area for the basis of this experiment is provided in Figure 4.4 below.

Table 4.1 - Table displaying the depths, distances, and slopes within the Bay of Plenty Northeast of Mimiha Road using data provided by the Bay of Plenty Regional Council.

From Mimiha Road to 70 metres depth								
Depth (m)	10	20	30	40	50	51	61	71
Distance (m)	1100	1500	4500	1900	2000	2700	4300	2100
Slope (degrees)	0.52	0.76	0.38	1.21	1.43	1.08	0.81	1.94

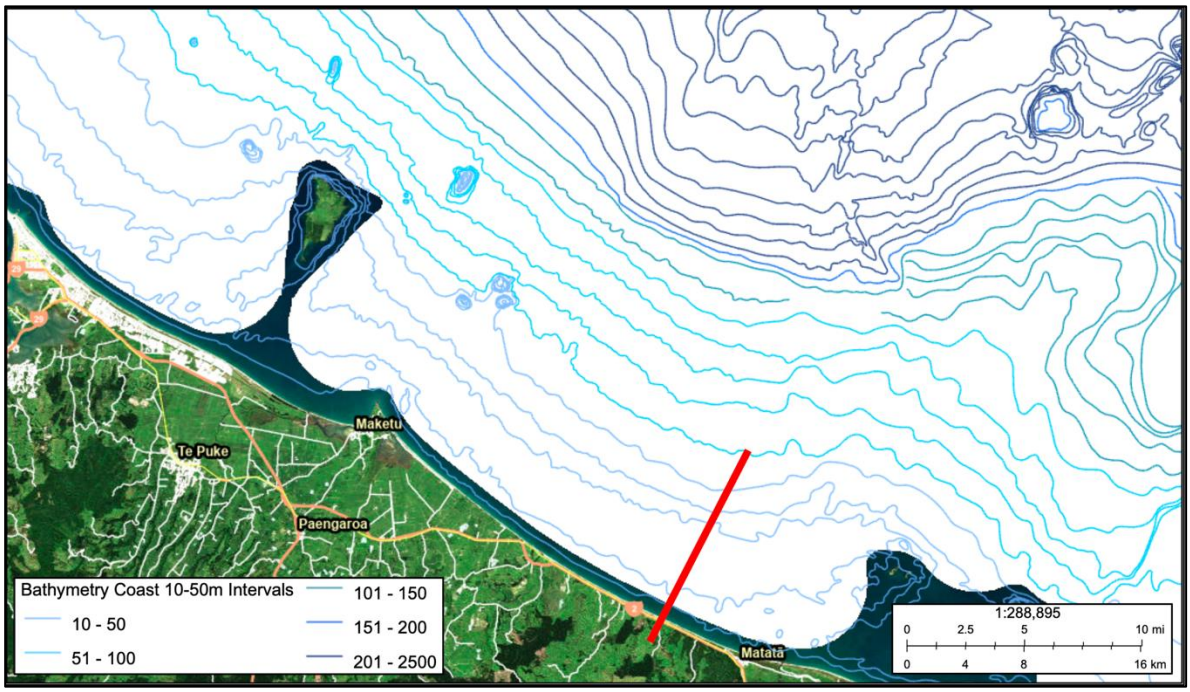

Figure 4.4 - Map of approximate cross-section area used for experimental basis (birds eye view) (Bay of Plenty Regional Council, n.d.).

In general, the geology and bathymetry northeast of the OVC allows for sizable pyroclastic flows to travel into the sea, taking note that this course was previously taken by the Rotoiti ignimbrite which forms a large fan of rhyolitic pyroclastic flow deposits (>850 km^2) from the OVC to the Bay of Plenty coastline (Cole et al., 2010).

4.4 Column Collapse Experiment

With consideration of information derived from the desktop analysis of the OVC/Bay of Plenty region, the methods and parameters for the main experiment were established. To best represent the Bay of Plenty coast for this study, a low slope (~5^o) and shallow water heights were chosen. The vertical PVC pipe was set for all runs to best represent a vertical collapse of ash in an eruption. The key focuses of the experiment are (1) underwater current height, length, shape, and velocity, (2) overflow cloud height, length, shape, and velocity, (3) deposit thickness and patterns, and (4) wave action. Three runs were carried out using the column collapse mechanism with the PVC pipe.

4.4.1 Column Collapse Results

Run 1.1 was carried out using 700 mL of Sample 1 collected from Site 1A (very poorly sorted, pumice-lapilli fine ash, refer to Figure 3.1). The temperature of the ash was 25.5^{o}C.

The water height was 6.5 cm and 21.2°C. The material forming the bed of the tank was a 1.3 cm thick layer of moderately sorted, medium to coarse sand. The sand bed was overall a flat bed, with very minor undulations (<3 mm change). Upon release, a large portion of the ash was emplaced on the dry slope, with the rest of the material emplaced in the water. The impact of the pyroclastic ash with the water line created a wave of height ~2 cm. Upon emplacement, the larger lapilli sized clasts settled quickly, creating a wedge (~3 cm thick) of coarse material at the base of the slope. The remaining finer ash formed an underwater current which travelled away from the slope along the bed of the tank. As the flow travelled with distance, it decreased in height. Alongside a decrease in size, the shape of the current travelled as a turbulent flow with a bulbous head, but eventually transitioned into a smooth laminar flow before ceasing completely at ~110.3 cm distance. The velocity of flow also decreased with distance, with initial speeds of 3.5 cm/s to end speeds of 0.65 cm/s. After the flow ceased, the fine ash material slowly settled on the sand bed. A very fine layer of this ash material was observed a few minutes after the flow. The ash layer ranged in thickness from 3 mm to <1 mm. Alongside the underwater current was a dilute short-lived ash cloud which travelled very quickly over the surface of the water. Within 2 seconds of the column collapse, the cloud exceeded the height of the tank travelling ~25 cm/s. Figures 4.5 and 4.6 present the current and cloud for Run 1.1.

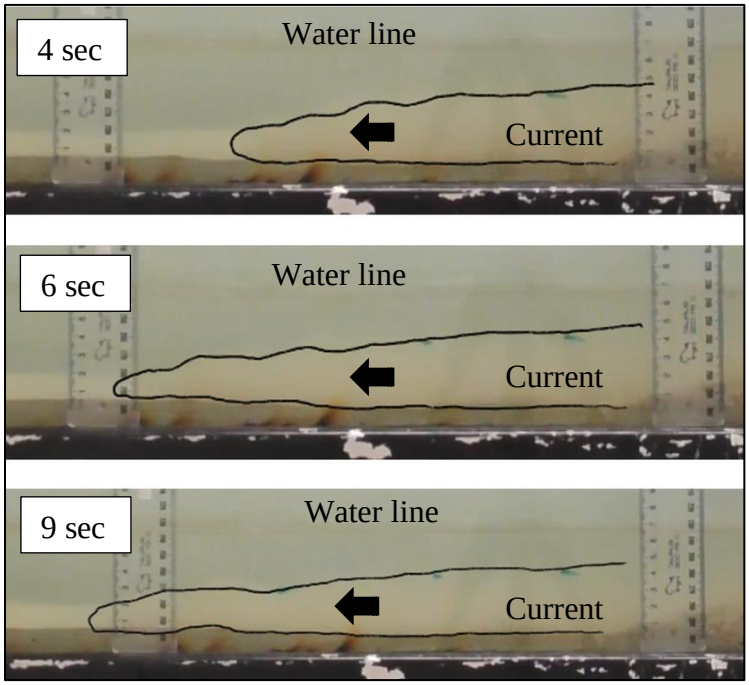

Figure 4.5 –Timeseries images of the underwater current produced during experimental Run 1.1.

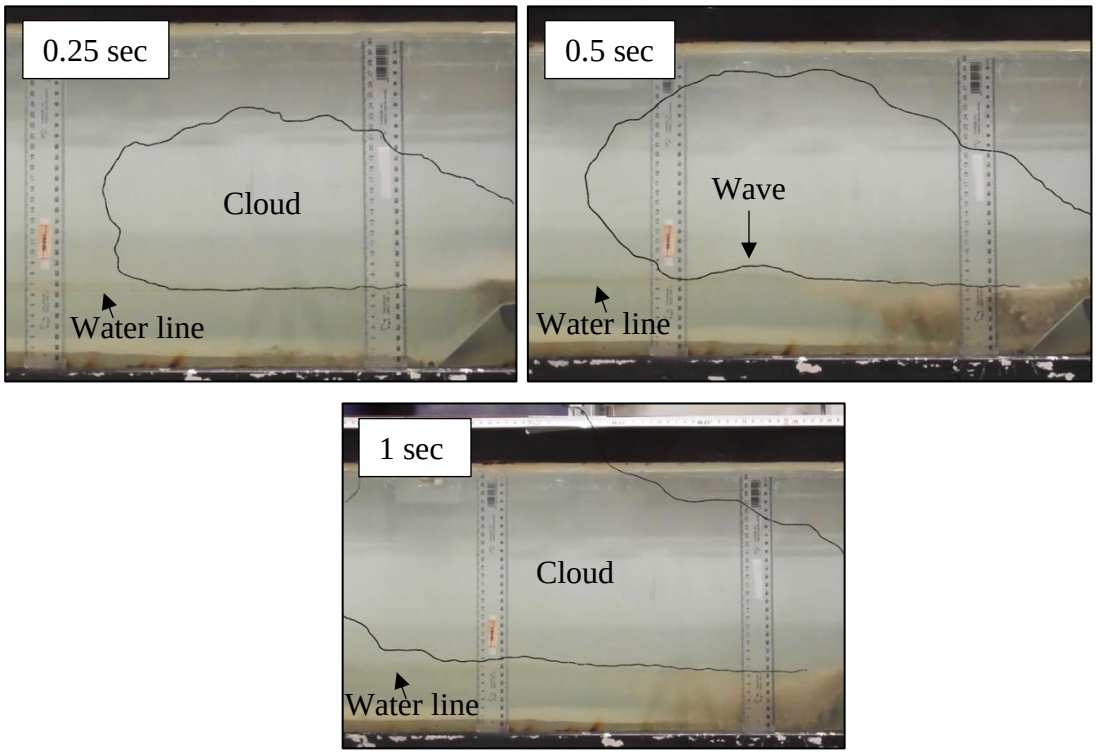

Figure 4.6 - Timeseries images of the cloud produced during experimental Run 1.1.

Run 1.2 was carried out using 300 mL of Sample 1 again. The temperature of the ash was 32.2ºC. The water height was 6.5 cm and 21ºC. The material at the bed of the tank was 1.6 cm thick. Upon release, again a large portion of the ash was emplaced on the dry slope, with the larger lapilli clasts settling first and the finer ash producing a flow underwater. Similar trends were observed for this run, which with time and distance, were the size and shape of the flow decreased and changed from turbulent to laminar. Initial speeds were around 20 cm/s and 0.86 cm/s near the end of flow. The coarse material wedge created at the base of the slope for this run was ~1.3 cm thick. The thin layer composed of fine ash ranged 0.75 mm to <0.25 mm thick. The height of the wave created from this run was ~1 cm. The flow from run 2 completely ceased at ~990 cm distance. Run 1.2 also produced a dilute ash cloud over the surface of the water, which travelled ~20 cm/s. Figure 4.7 and Figure 4.8 below presents images of the current and associated cloud from run 1.2.

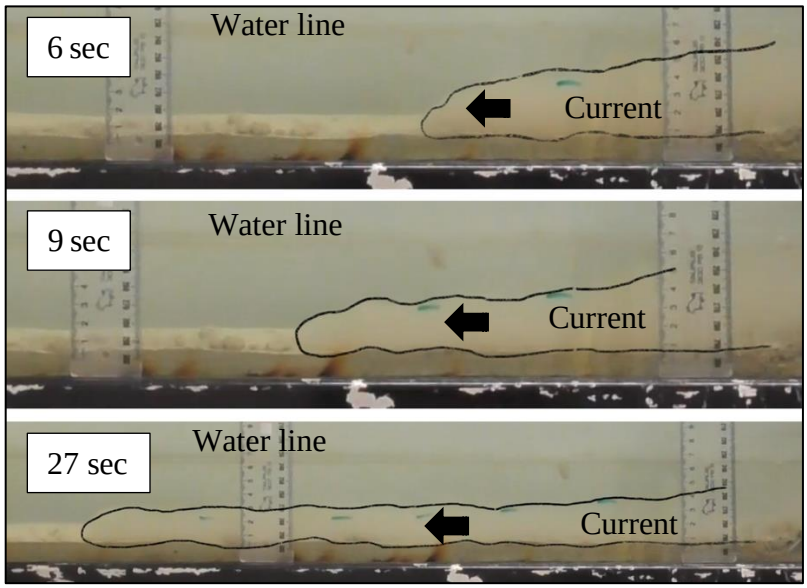

Figure 4.7 –Timeseries images of the underwater current produced during experimental Run 1.2.

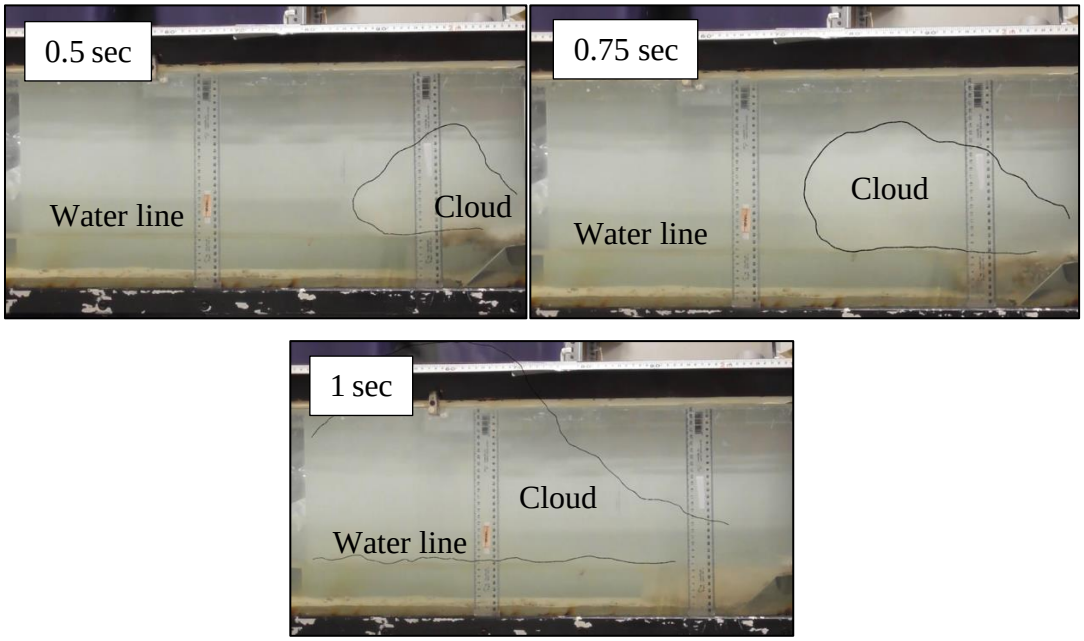

Figure 4.8 – Timeseries images of the cloud produced during experimental Run 1.2.

Run 1.3 was carried out using 500 mL of Sample 1. The temperature of the ash was 33.3^{o}C. The water height was 6.5 cm and 23^{o}C. The material at the bed of the tank was 1.9 cm thick. Upon release, most of the material ended up on the slope, with larger clasts settling first and the finer ash producing a current. Overall speeds of Run 1.3 were less than those of Runs 1 and 2. The wave height for Run 1.3 was ~0.6 cm. Figure 4.9 below shows time versus runout distance for all three underwater currents from Runs 1.1 to 1.3. Table 4.2 displays some basic statistics for the underwater currents from Runs 1.1 to 1.3.

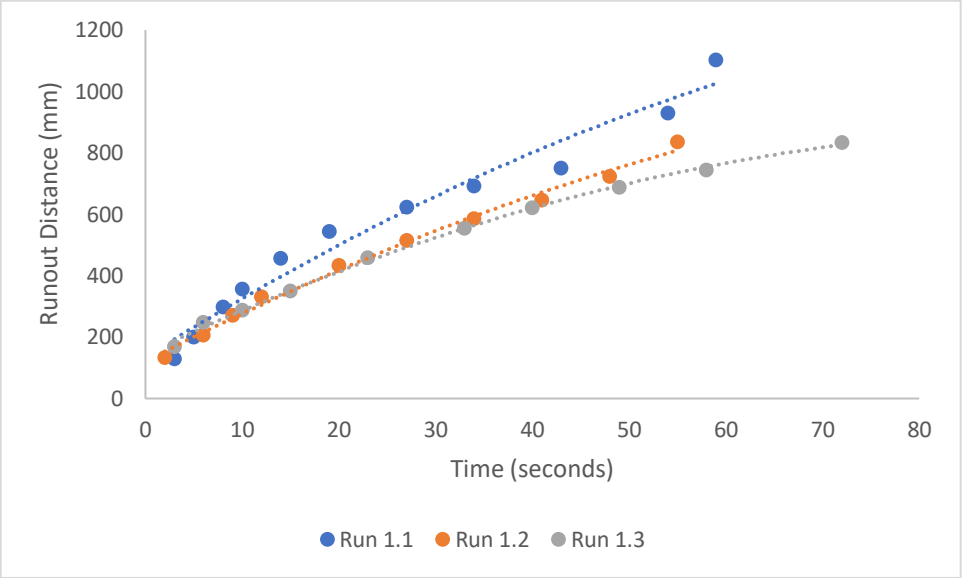

Figure 4.9 – Graph of current length versus current height for underwater currents from Runs 1.1 to 1.3.

Table 4.2 - Descriptive statistics of all the three underwater currents from runs 1.1 to 1.3.

Basic Statistics Table						
	Run 1.1		Run 1.2		Run 1.3	
	Height (cm)	Velocity (cm/s)	Height (cm)	Velocity (cm/s)	Height (cm)	Velocity (cm/s)
Mean	2.00	2.36	1.87	1.97	1.92	1.58
Median	1.60	2.53	1.80	1.44	1.90	0.97
Minimum	0.60	0.63	1.00	0.86	0.70	0.62
Maximum	3.80	4.33	3.00	6.65	3.10	5.60
Count	11	11	11	11	11	11

4.5 Dam Break Experiment

For the dam-break flow method, similar conditions to the previous experiments were set. The slope (~5^{o}) remained in the tank, shallow water heights remained, and a moderately sorted layer of sand sat at the bed of the tank. The only difference from the previous experiment, besides the release mechanism for these experiments, was the material. For these experiments, Samples 3 to 5 from Site 2 (fine coarse ash, Glenbrook Beach) were used. This material is finer and better sorted than the material of the previous experiment. Fine ash was used because gravity was not the main driving force for this mechanism, so emplacement differences based on grain sizes were not tested. The key measurements and observation for this mechanism remain (1) current height, length, shape, and velocity, (2) cloud height, length, shape, and velocity, (3) deposit thickness and patterns, and (4) wave action. Two runs were carried out using the dam-break flow mechanism.

4.5.1 Dam Break Results

Run 2.1 was carried out using 900 mL of fine to medium coarse ash from Samples 3 to 5. The temperature of the ash was 33.8°C. The water was 6.5 cm and 19.9°C. The sand at the bed of the tank was 17 mm thick, composed of moderately sorted sand and thin layers of ash from the Sample 1 runs. When the front insert was lifted, the ash quickly escaped the dammed section travelling into the water, creating a flow. Initial heights of the flow were 27 to 24 mm. At the base of the slope a thick wedge (~38 cm) developed, mainly composed of the larger grains (medium coarse ash). The flow moved quite slowly, with an average velocity of 1.27 cm/s. A small wave was produced from the impact of the ash, the wave height from run 2.1 was 0.6 cm. The flow ceased completely at 74 cm distance. No observable ash-cloud was produced for this run. Figure 4.10 presents the current for Run 2.1.

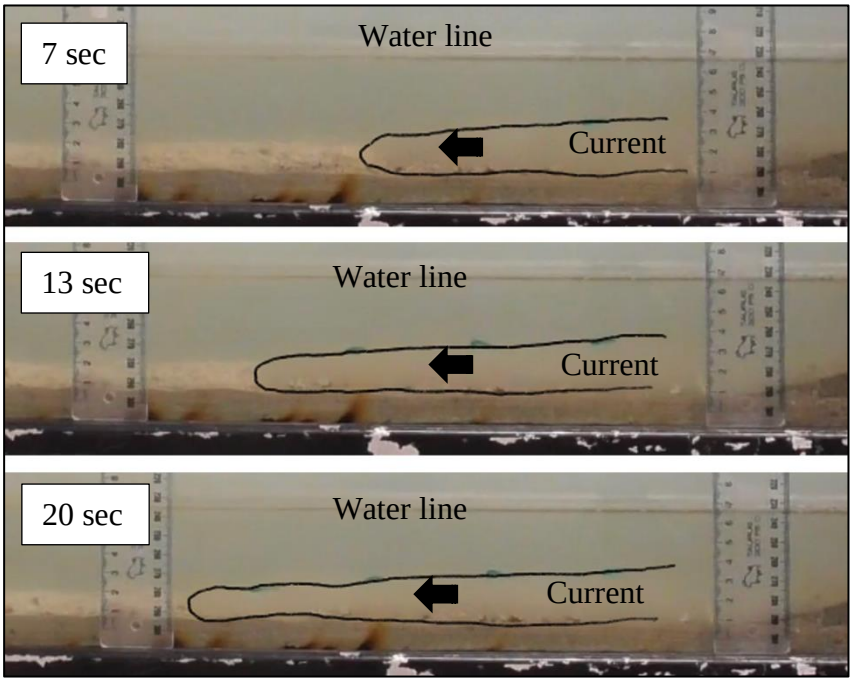

Figure 4.10 – Timeseries images of the current produced during experimental Run 2.1.

Run 2.2 was carried out using 600 mL of the same material. The temperature of the ash was 31.5°C. The water height was 6.5 cm and 13.2°C. Sand bed conditions were the poorly sorted coarse sand and layers of fine ash and lapilli components from the previous runs. The wave height for run 2.2 was 0.4 cm. A small and very dilute ash-cloud was produced for this run. This ash cloud travelled at ~1.4 cm/s and had heights ranging from 13 to 9 cm. Figure 4.11 below is an image of the cloud for run 2.2. Both underwater currents (Run 2.1 and 2.2) left behind a very thin layer of ash <0.25 mm thick. Figure 4.12 shows the time versus runout

distance for underwaters current produced for Runs 2.1 and 2.2. Table 4.3 displays the basic statistics from Runs 2.1 and 2.2.

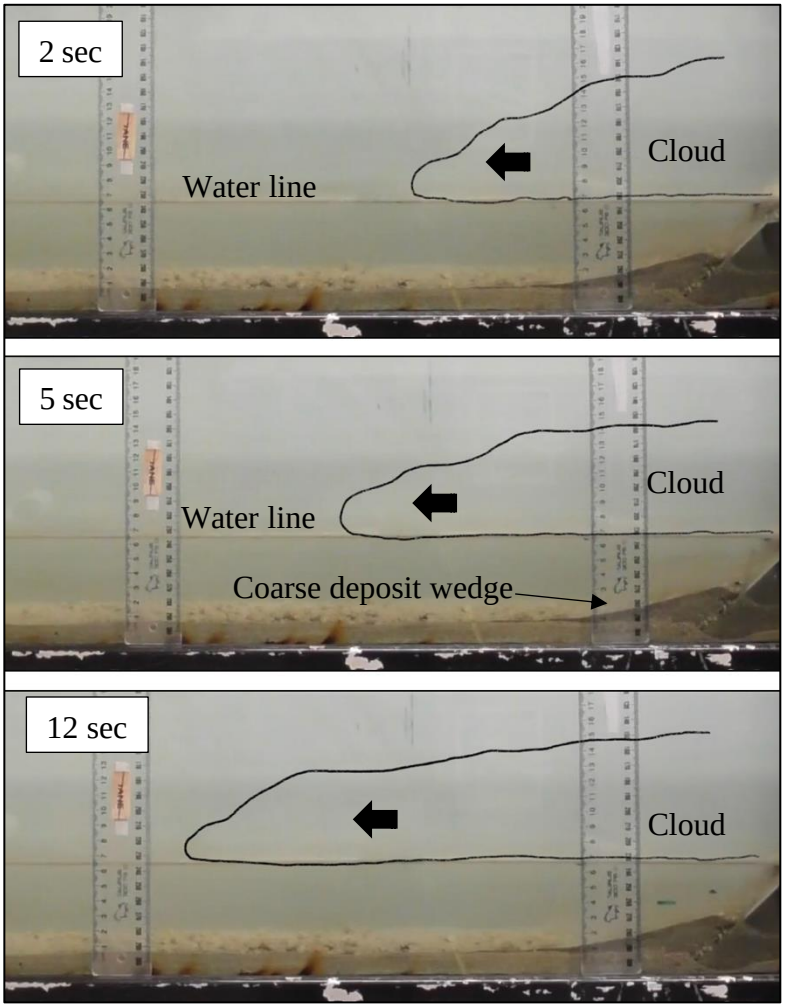

Figure 4.11 – Timeseries images of the cloud produced during experimental Run 2.2

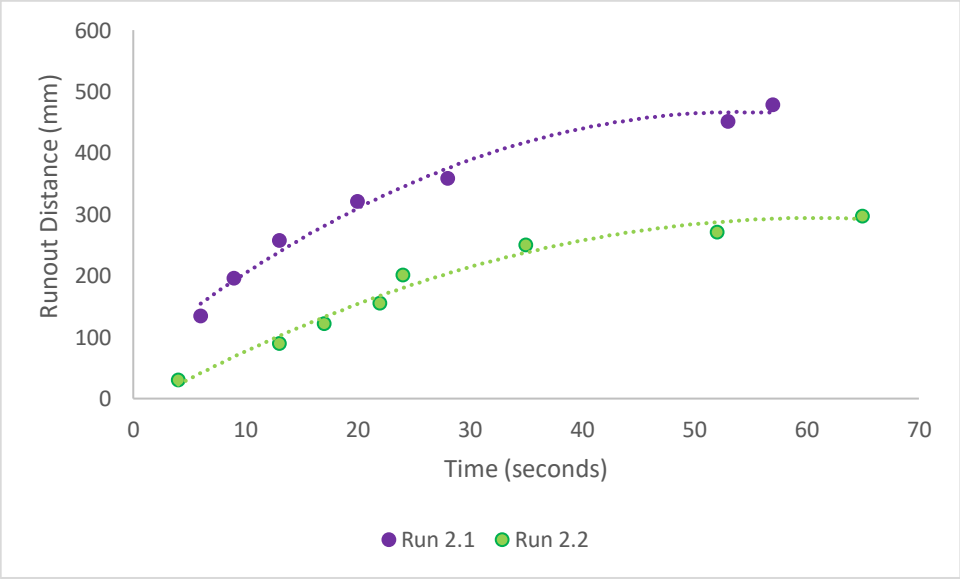

Figure 4.12 - Graph of current length versus current height for underwater currents from Runs 2.1-2.2

Table 4.3 - Descriptive statistics of the two underwater currents from runs 2.1 and 2.2

Basic Statistics Table				
	Run 2.1		Run 2.2	
	Height (cm)	Velocity (cm/s)	Height (cm)	Velocity (cm/s)
Mean	1.68	1.27	1.54	0.75
Median	1.65	1.22	1.50	0.67
Minimum	0.70	0.37	1.10	0.12
Maximum	2.70	2.25	1.90	2.30
Count	7	7	8	8

For all runs (column collapse and dam-break) more than 50% of the material did not travel into the water and remained predominately dry on the slope. Figure 4.13 below presents this representation.

Figure 4.13 – Photograph of ash remaining on slope above the water line during experiment

4.6 Obstruction Run

An additional run, Run 3.1, was carried with an obstruction in place. This obstruction was placed midway (~27.5 cm length) within the tank. The obstruction was a 44 mm pebble stone. The purpose of this run was to observe how the underwater current would behave with an obstruction in place. The conditions of the tank remained the same as the previous runs (~5^{o} slope, shallow freshwater, sand bed, and dried pyroclastic ash material).

Run 3.2 was carried out using 350 mL of Sample 1 and the column collapse mechanism. The water height was 66 mm and with an 18 mm thick medium to coarse sized sand bed with scattered lapilli clast from the previous runs, as well as the obstruction. Upon release, an underwater current and surface ash-cloud were produced. A wave was also produced with a wave height of 1.2 cm. The cloud with this run was like those in Runs 1.1-1.3, with a velocity of ~30 cm/s and heights that exceeded the height of the tank (>35 cm). To start, the underwater current travelled quickly with a velocity of 2.5 cm/s. When the current met the obstruction, it immediately decreased in height and speed, transitioning from 2.1 cm height to 0.8 cm, and speeds from 1.5 cm/s to 0.18 cm/s. The current moved around the sides of the rock and continued only a short distance before ceasing completely at ~114 cm distance. Figure 4.14 below displays an image of the material moving around the rock. Figure 4.15 displays the current before and after contact with the obstruction.

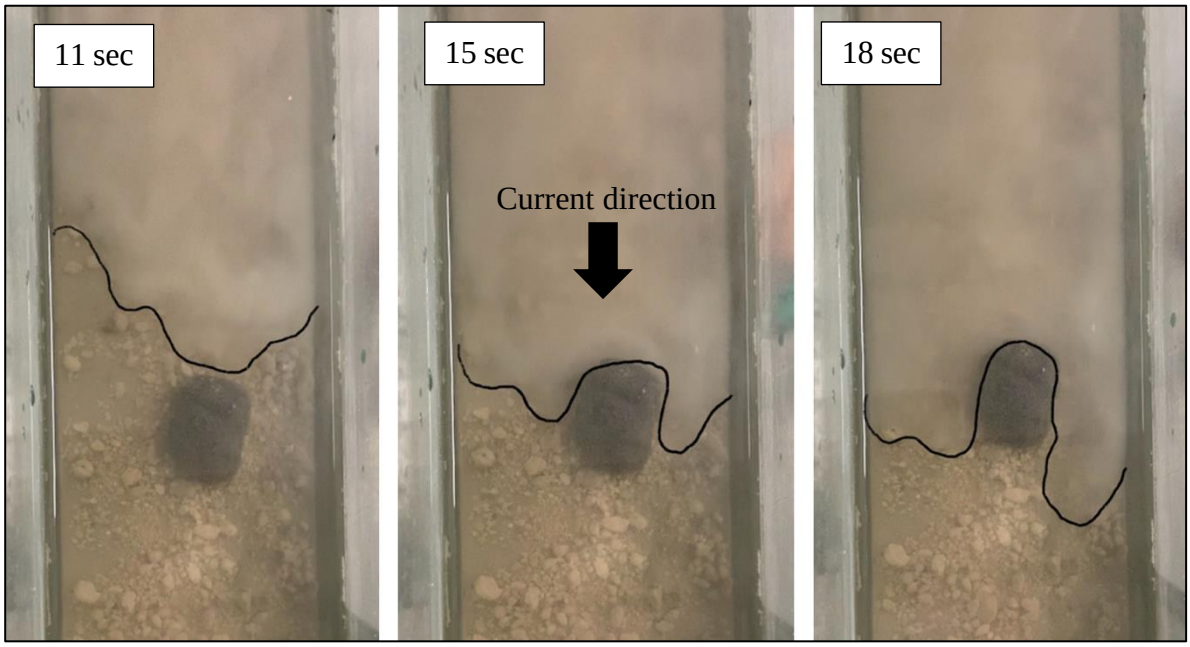

Figure 4.14 – Timeseries images of the underwater moving around an obstruction in experimental Run 3.1 (birds eye view).

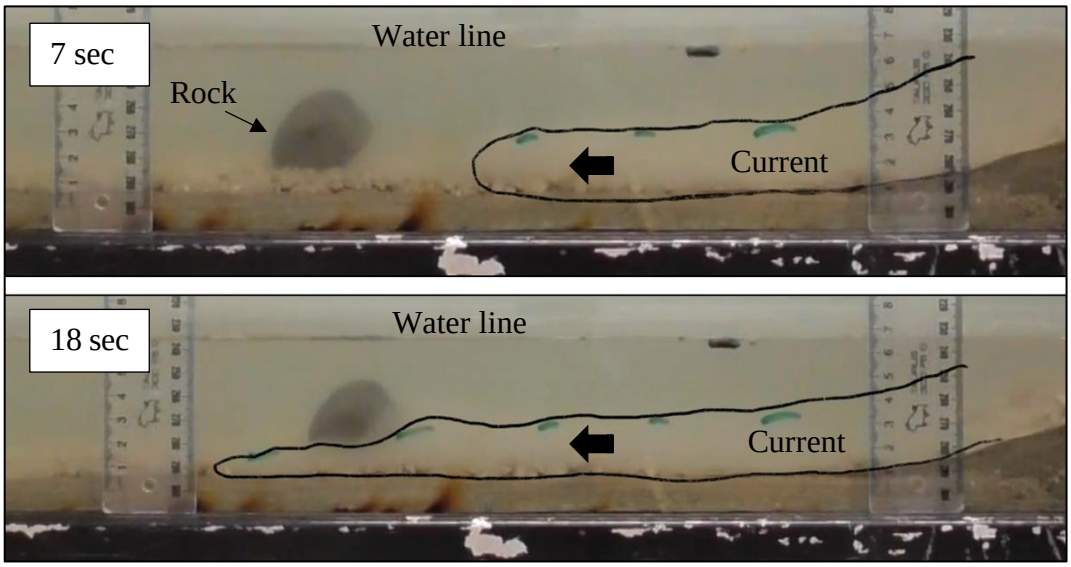

Figure 4.15 – Timeseries of the underwater current moving past an obstruction in experimental Run 3.1 (side view).

At the end of the experiment, all thin layers deposited by each run could be distinguished. Figure 4.16 below presents the layers deposited by the experimental runs.

Figure 4.16 – Photograph of layers deposited by all six experimental runs.

4.7 Conclusion

Underwater currents and associated clouds produced using the column collapse mechanism (Runs 1.1 to 1.3) were larger, faster, and longer-lived than the currents produced using the dam-break mechanism. Run 1.1 that used the greatest volume of pyroclastic ash material produced the tallest and longest current. The currents and associated cloud produced using the dam-break mechanism (Runs 2.1 and 2.2) were shorter height, had slower velocities, and were shorter-lived. Overall, all flows emplaced a small wedge of material at the base of the slope predominantly composed of the largest grains from each sample. Run 3.1 demonstrated

that when a current comes into a contact with an obstruction, the current will decrease in speed and size.

Chapter 5

Discussion

5.1 Introduction

As previously discussed, PDCs can be commonly broken up into two main types, dilute turbulent pyroclastic surges and concentrated pyroclastic flows, where surges typically override flows. This is evident in field and experimental studies. In case studies, flow units in the field present lithologies with coarser material at the base of the flow with finer material and low-density pumice clasts at the top. In experimental cases, simulations of PDCs show a concentrated flow transporting the denser material with an overriding dilute ash cloud. Results collected from both field and experimental studies of this research have been in accordance with this principle.

PDCs entering the sea introduce complexities to this natural process in various ways. Varying characteristics about individual PDCs (e.g., temperature, volume, velocity, sorting) can prompt different process behaviours. Topographical and bathymetrical variations can also prompt different behaviours. These complex behaviours result in unique flow-water interaction features within deposits. Chapter 5 is a discussion on the key findings from the field and laboratory studies. Interpretations about the processes associated with flows entering the sea will be explored, as well as connections between field and lab results.

5.2 Case Studies

5.2.1 Flows Approaching the Sea

Two of the four case study sites, those being the Rotoiti Breccia at Site 1A and the Oparau Tephra at Site 4, displayed typical ignimbrite deposits with no evident flow-water interaction features. Site 1A, along Pacific Coast Highway, presented large scale flow units with a lower portion described as a non-welded, very poorly sorted pumice-lapilli fine ash unit of a greyish pinkish colour, overlain by a pumice concentration zone. This description is in accordance with characteristics described by Schmitz and Smith (2004). Their work categorized the entire Rotoiti tephra formation, with Unit 2, the largest unit, representing multiple non-

welded flows consisting of poorly sorted pumice, lithics, and crystals in fine ash of a pink colour. Furthermore, a majority the pumice clasts are found in various concentration layers signalling the top of each flow unit. These flows are found less than 100 m from the Bay of Plenty shoreline.

Site 4, in Hauturu, presented a non-welded medium coarse ash to lapilli of a greyish yellowish white colour. Similar descriptions about the Oparau tephra have been described by Pain (2012), as a white, sandy clay tephra with weathered clasts.

These two cases present unconsolidated flows approaching sea environments. Cas and Wright (1991) have discussed the potential behaviours of such flows with a shallow angle towards the sea. These interpretations are based on several case studies, one being the Rotoehu ash (Cas & Wright, 1991). This interpretation showed that upon initial interaction of the flow with the sea, an explosive event will occur due to steam generated from the heat from the flow boiling the surface of the water causing fragmentation and a dispersion of ash into the air. This explosive event will also cause mixing of the water and pyroclastic material generating a water-supported flow transporting pyroclastic debris down slope under the sea. Alongside the underwater current is a potential surge or low concentration overflow that travels over the surface of the water. Another interpretation described was a slowing pyroclastic flow which deposits a lot of material on land before entering the sea. Once entering the sea, the flow splits into a low concentration overflow and a hot, water supported mass flow. This second interpretation is reflective of the deposit at Site 4, while the first interpretation is reflective of the deposit at Site 1A. A schematic diagram of these interpretations is shown in Figure 5.1.

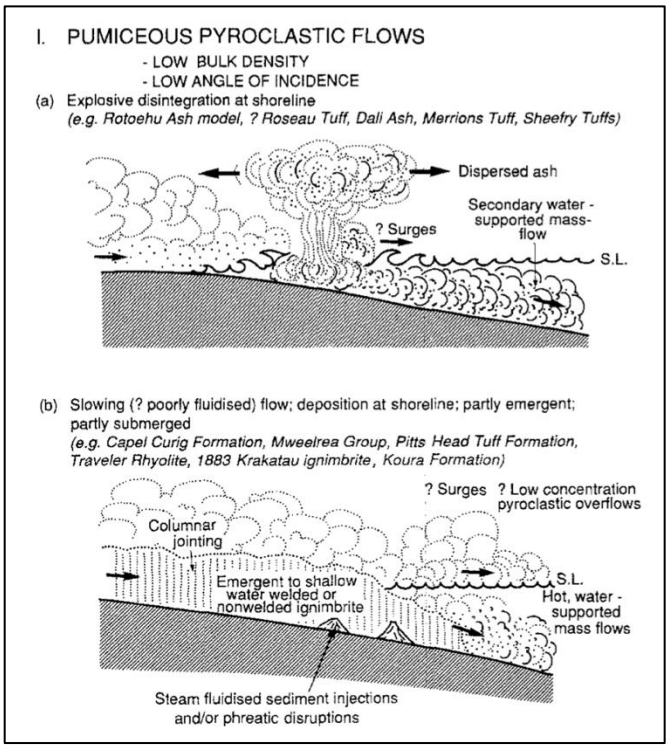

Figure 5.1 – Schematic diagram of pyroclastic flows entering the sea at a low angle of incidence (Cas & Wright, 1991).

5.2.2 Flows Entering the Sea

At Site 2, Glenbrook Beach, there is evidence of distinct features within an outcrop of the Ongatiti Ignimbrite that flow-water interaction occurred at this location. One of those distinct features were load structures along the bottom boundary of the lower flow unit. Load structures (e.g., load casts and flame structures) are soft sediment deformation structures that are produced when there is a density loading difference between two layers of sediment during a water-saturated or liquified state. Typically, shortly after deposition, a dense sediment layer sinks into an underlying less dense sediment layer creating antiforms and synforms along the contact between the two layers (e.g., Tinterri et al., 2016). For the case at Glenbrook Beach, as the pyroclastic flow travelled towards sea depositing material on the existing wet, mud layer the denser pyroclastic material slumped into the mud creating the load structures observed within the outcrop. Figure 5.2 below shows a sketch of typical load structures described by Tinterri et al. (2016). This figure can be compared to load cast structures observed at Glenbrook beach (Figure 2.1).

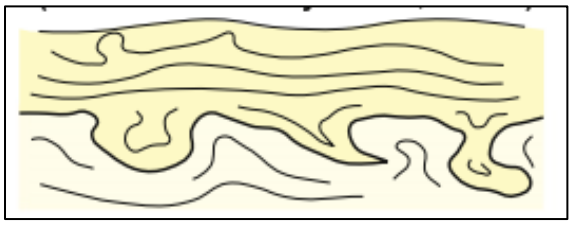

Figure 5.2 – Sketch of load structures described by (Tinterri et al., 2016)

Another distinct feature observed at Site 2 was convoluted laminae. Convoluted laminations are another example of soft sediment deformation produced within a liquefied sediment by shear stress from the flow (Gladstone et al., 2018). The convoluted laminations observed at Site 2 were mainly horizontal laminae with shallow folds that thin and thicken. Some of the laminae were breached upwards indicating water escape. The laminations were darker in colour and predominantly found within the lower half of Unit 1 near the load cast structures. It is a commonality that these soft sediment deformations are found amongst one another.

The third distinct feature observed at Site 2 were dewatering structures, which are another type of soft sediment deformation produced in liquified sediments. Dewatering structures are commonly known as water escape structures, examples include breached laminae, sand volcanoes, and fluid escape pipes (Gladstone et al., 2018). The dewatering structures at Site 2 were mainly oriented upwards in a rain drop shape composed of coarse grains and light in colour. The shape and orientation of the structure is due to the pore spaces within the flow infill with water from the bottom causing it to flow upwards creating those pockets of upward facing water escape structures.

All the deformations discussed typically occur together with silt to sand sized material and are developed during or shortly after deposition of the host unit or bed. Moreover, most commonly the host units are deposited at high, near-instantaneous rates and are poorly sorted (Lowe, 1975). The structures observed at Site 2 indicate that there was interaction between the pyroclastic flow and water, probably at the coastline. The black organic mud underlying the ignimbrite also indicate that the environment of deposition was an anoxic marginal marine environment (e.g., lagoon).

At Site 1B on Mimiha Rd, prominent cross lamination structures and interbedded layers of coarse lithic clasts were observed. These distinct features are evidence of complex deposition mechanisms. Cross lamination structures within a pyroclastic density current deposit indicate that the current was dominated by turbulence, either through a dilute surge or a fluid-supported flow. When turbulence dominates, particle movement and deposition is dynamic and inconsistent. The interbedded layers of coarse material are from lags within the current which eventually transition into laminar beds of finer material. This mechanism is known as 'granular jamming' (Douillet et al., 2019). The interbedded layer of coarse lithic clats observed at Mimiha Road are a result of granular jamming. The cross lamination structure, or cross-bedding features, observed at Mimiha Road are a result of a flow dominated by turbulence.

5.3 Experimental Studies

The experimental studies undertaken for this research demonstrated several distinctions about pyroclastic ash-laden flows travelling into water. The main findings are (1) a density current entering the water will segregate into an underwater flow and a dilute cloud overflow that travels over the surface of the water, where the dilute cloud has a shorter runout than the underwater flow, (2) flows entering the water will generate a wave with speeds that exceed that of the flow, (3) the greater the flow volume the greater the flow height, length, and deposition thickness, (4) the greater the flow velocity the longer the run out, and (5) obstacles in the path of a flow will reduce the flow height, length, and speed. Additionally, the simulated column collapse technique was a suitable generation mechanism for producing a small-scale pyroclastic flow into water.

Almost all runs demonstrated the segregation of a dry flow into a concentrated underwater flow and an overriding dilute cloud. This process has been noted during past pyroclastic eruptions, with the 1883 Krakatau eruption as an example. This eruption produced pyroclastic flows that segregated into two main components at the shoreline, (1) a dense basal component, and (2) a dilute overflow. The dense component sunk due to density differences travelling as a subaqueous pyroclastic flow depositing material along the seabed (Mandeville et al., 1996). This desegregation process was observed by victims on the coast of Sumatra. As for experimental studies, Freundt, (2002) concluded that flows separated into two

portions, (1) a low concentration surge cloud that travels over the water, and (2) a high concentration flow that penetrates the water and travels downslope. Moreover, the coarse material of the flow deposits on the bed and the remaining finer material travels as a turbidity current down the tank.

Alongside the desegregation process, all runs triggered a wave or waves that travelled ahead of both the flow and cloud. The waves were generated by the flow displacing the water level. Waves that would be a tsunami at the real scale, have also been noted during past pyroclastic eruptions. Examples of tsunamis generated by pyroclastic flows include the 1883 Krakatau eruption, the 1994 Rabaul eruption, and the more recent 2003 Montserrat eruption (Paris, 2015). Experiments carried out by Freundt (2002) showed that a wave will be generated from a pyroclastic flow entering the sea if the bulk density of the flow is close to that of the water.

Runs 1.1 to 1.3 demonstrated that the flow with the greatest volume produced an underwater current with the greatest height and length. The greater flow volume also deposited the most amount of material over a greater distance then those of a lower volume. This is due to density differences between the flow and the water. Runs 2.1 and 2.2, using the dam break flow mechanism, demonstrated that the lower the velocity the shorter runout distance. The dam-break mechanism did not generate fast flows due to there being less of an effect from gravity whereas the column collapse mechanism created a greater velocity due to the greater height from which the material was released from. Run 3.1 demonstrated that obstacles in the path of a flow reduce the flow height and speed significantly. This is a result of friction acting on the flow, where the obstacles resist and nearly stop the flow entirely. The obstacle used for the experiment was a substantial size relative to the height of flow. The instance of an obstacle affecting a flow has occurred for turbidity currents and subaerial pyroclastic flows before (e.g., Asghari Pari et al., 2010, Legros & Kelfoun, 2000). The extent of the friction force is dependent on the size, surface area, and surface roughness of the obstacle relative to the flow. In many cases subaerial pyroclastic flows will destroy obstacles in their path like trees and infrastructure but may only damage or alter significant obstructions like rock formations and hills. All runs that generated a cloud, particularly runs 1.1 to 1.3, demonstrated that those clouds are shorter-lived than their associated flows. This is due to those overriding clouds having a lower particle concentration than those of the flows (e.g., Breard & Lube, 2017). The fine ash material that makes up the cloud is more easily able to

disperse and end within a shorter amount of time. This is because the surrounding medium for the dilute cloud is air, which is less dense than the particles, while the current is travelling through water which is denser than air.

5.4 Connecting Field Observations to Experimental Studies

Stop 1A along Pacific Coast Highway represented a significant portion of flow that did not reach the coastline. This portion of flow units represent the portion of ash material that did not travel into the water during the experiment (refer to Figure 4.13).

As for the ash material that did enter the water during the experiment, thin layers deposited by each run could be observed. These deposits reflect deposits observed at Site 1B Mimiha Road, and Site 2 Glenbrook Beach which presented parts of flow that were underwater and had flow-water interaction structures. Since the layers of the experimental deposits were less than 3 mm thick, specific structures within each run layer could not be seen. These layers mainly represent the main flow that travelled underwater. Since the ash particles within the dilute cloud took overnight to settle, deposits left behind were indistinguishable from the main underwater flow. To better reflect the deposits at Site 1B and Site 2, a larger scale experiment that creates thicker deposits could help to identify experimental flow-water structures within the layers. These layers reflect those deposits observed at Site 1B and Site 2 (Figure 4.16).

As for the obstacle experimental run, this instance is analogous of any obstructions in the ocean, particularly near the coast, that could affect a PDC entering the sea. One example of this in relation to case studies, are small oceanic hills situated about 8 km and 14 km out from Maketu township (Figure 3.3). Another example are the small islands within Kawhia Harbour (Figure 3.20). The harbour inlet is a very dynamic area with shallow shelfs and deep channels that squeeze towards the harbour inlet opening. A PDC entering this space would cover the shallows and infill the channels with pyroclastic material, but travel around islands and highs. The obstacle within the experimental run reflects any bathymetrical high to which an underwater PDC would travel around. Furthermore, these obstructions would slow the flow and decrease the height of the flow. To best reflect islands in the experiment, an obstruction that exceeds the water level of the flume could be used.

5.5 Cascading Hazards

Cascading hazards are two or more natural hazards that are triggered by the same event, occurring around the same time (Auckland Council, 2014). Potential cascading hazards associated with pyroclastic flows entering the sea include tsunamis, submarine slides, further turbidity currents and the pyroclastic flows themselves. The likelihood of all these hazards occurring at once is low, but the potential damage they could cause is high, therefore awareness is necessary. In regard to this research, tsunamis are generated from the sudden displacement of pyroclastic flows entering the water, submarine slides are formed from slope failure due to stress applied by the load of a pyroclastic flow depositing material along the seabed (Scarselli, 2020) and turbidity currents are created alongside slope failures where the loosened sediment mixes with the water and travels as a dense current down slope (NOAA, 2021). Spaces that can be affected by tsunamis are nearby coasts including coastal environments and ecosystems, infrastructure, and people. Submarine slides and turbidity currents can affect the surrounding bathymetry, submarine ecosystems, and submarine infrastructure (e.g., pipelines, cables). Due to the scale and nature of the experiment undertaken for this thesis the only cascading effect that was observed while simulating a flow into water was a wave.

In terms of these cascading hazards occurring around New Zealand, in particularly in the areas related to the case studies, several conclusions can be made. For the Bay of Plenty area, a PDC entering the sea could generate a tsunami which could affect several coastal towns and islands. The area covered and extent of damage would depend on the magnitude of the PDC and associated tsunami, but risk would be moderate. Potential nearby spaces include, Moutohora Island, Motiti Island, Whaakari/White Island, Maketu township, and Whakatane township. As for the west coast, Kawhia Harbour there are also islands within the inlet and coastal townships around the inlet that are at risk. Further north, Glenbrook Beach is situated on the south end of Manukau Harbour. A PDC entering the water at that location could send a wave across the harbour towards the densely populated areas of Mangere, New Lynn, and the Auckland Airport which are situated on the north and west ends of the harbour. As for submarine slides and turbidity currents, there are no immediate noteworthy slopes for significant slips or slides in these areas, therefore risk is low.

5.6 Limitations

One limitation of the case study portion of this thesis was not investigating enough outcrops with flow-water structures, in particularly deposits that overlie marine-derived sediments with shelly or other organic material. Another limitation of the case study portion of this thesis was lack of marine corps. Core samples of pyroclastic deposits presently in the marine environment could give some insight about the processes that occur below sea level as the flow travels under water and not just at the coastline. Core samples should be taken somewhere between 2.5 to 5 km out from shore and the cores would need to be tens to hundreds of metres deep due to PDC deposits being buried by more recent marine sediments.

A limitation of the experimental portion of this thesis was the size of the experiment. The flume used for this experiment was 10 cm wide therefore friction along boundaries could have played a role in how the flow behaved, and the length of the flume (~3 m) allowed the wave to reflect off the end of the tank and travel back up effecting secondary waves. Another limitation was that heat was not applied to the material. During real pyroclastic flow events extreme temperatures play a major role on the behaviour of the flow and the way the flow interacts with water (e.g., steam explosions). Those processes promoted by heat were not able to be tested. Another limitation are the release mechanisms. Both release points had to be placed close to the water line as both mechanisms did not have adequate energy to propagate a flow that could travel a long distance over the slope before entering the water. This is not representative of a real-life event where PDCs travel a long distance over land before reaching the coastline.

5.7 Further Research

One recommendation for future work around case studies within New Zealand is further investigation around the Kawhia area and the west coast in general for outcrops of the Oparau Tephra. A potential site is Ngatokakairi Island that sits within the Kawhia Harbour inlet. This island extrudes the inlet presenting the same greyish white to greyish yellowish white ignimbrite representative of the Oparau Tephra. A closer look at this outcrop and its bottom contact could reveal evidence of flow-water interaction considering its location to the sea. Another recommendation is to develop the petrography of the deposits further to assess the

role of grain shape characteristics in controlling the flow and if marine-derived sediments have been entrained.

A recommendation for future work around the experimental study is using a larger flume. A wider and longer tank would allow one to observe the full three-dimensional extent of the wave and underwater flow. Another recommendation is using a generation mechanism that applies energy to material greater than the effect of gravity and to provide a continuous supply of flowing material to the water. This would allow the material to be released at higher point on the slope since it will have the ability to travel. A greater energy source could come from either a higher column collapse point or a pump that pushes the material downslope.

Chapter 6

Conclusion

PDCs entering the sea is a unique event with dynamic processes different than those of subaerial PDCs. PDC behaviour will vary depending on the characteristics of the flow itself and the conditions of the area (e.g., coastal environment, topography, bathymetry, obstructions). Since PDC are substantially hot, the initial interaction with water will produce a steam explosion causing significant fragmentation of the pyroclasts. Due to the volume and density of flows, the emplacement of material will cause sudden water displacement producing a wave or waves (tsunamis). Wave heights will depend on the extent of displacement. Upon sea entrance, the PDC will segregate into two distinct features, (1) a dense water-supported flow that travels along the seabed interacting with the submarine environment, depositing an unsorted mix of pyroclastic material, and (2) a dilute cloud that travels along the surface of the water transporting fine particles. Some high-volume, low-density clasts will float (e.g., pumice, decimated wood) remaining separate from those two features. The dense underwater flow behaviour will depend on the volume of the flow, where greater volume flows will have a greater height and runout. Deposit thickness will decrease with distance, as well as the size of the clasts within the material. The dilute cloud will behave similarly to pyroclastic surges, where they have a low particle concentration and are dominated by turbulence. Over time, those fine particles from the cloud disperse and settle to the sea surface and sink into water leaving no significant deposition. The main deposit left by the dense flow will present unique flow-water structures like load casts and convoluted laminae. The deposit will also present interbedded layers or with components of the underlying sediments that indicate the existing environment at the time of the pyroclastic flow event, like the wood and mud material at Glenbrook Beach and the lithic clasts at Mimiha Road.

Simulations of PDCs in the laboratory have reflected aspects of pre-historic PDC deposits entering the sea around New Zealand. The Rotoiti Ignimbrite on Mimiha Road, Bay of Plenty and the Ongatiti Ignimbrite at Glenbrook Beach show flow-water interaction structures, were

scaled down as thin layers deposited by underwater currents produced in the small-scale flume experiment. The Rotoiti Ignimbrite along Pacific Coast Highway and the Ongatiti Ignimbrite in Kawhia present typical subaerial ignimbrites that have approached but not yet reached the sea are reflected as portions of ash material that were deposited on the ramp above the water line in the experiments.

Obstacles or obstructions can affect PDCs entering the sea by reducing their speed and height. Potential obstructions in the New Zealand context are oceanic hills and islands in the Bay of Plenty and on the west coast.

PDCs that enter the sea can cause potential cascading hazards, being tsunamis, submarine slips and turbidity currents. A better understanding of these events and their behaviours will aid future natural hazard risk and management. Simulating PDCs in general comes with many challenges and limitations due to their extreme characteristics. Conditions of an experiment that would best simulate a flow into sea would need to account for high temperatures, voluminous material, great speeds, and runouts, and wave action and sea currents. Further research involving thorough investigations of new deposits and conducting more large-scale experiments are recommended.

References

Agustan, Kimata, F., Pamitro, Y. E., & Abidin, H. Z. (2012). Understanding the 2007-2008 eruption of Anak Krakatau Volcano by combining remote sensing technique and seismic data. *IJAEO*, *14*(1), 73–82. https://doi.org/10.1016/J.JAG.2011.08.011

Alloway, B., Westgate, J., Pillans, B., Pearce, N., Newnham, R., Byrami, M., & Aarburg, S. (2010). Stratigraphy, age and correlation of middle Pleistocene silicic tephras in the Auckland region, New Zealand: A prolific distal record of Taupo Volcanic Zone volcanism. *Http://Dx.Doi.Org/10.1080/00288306.2004.9515070*, *47*(3), 447–479. https://doi.org/10.1080/00288306.2004.9515070

Anastasakis, G., & Pe-Piper, G. (2006). An 18 m thick volcaniclastic interval in Pantelleria Trough, Sicily Channel, deposited from a large gravitative flow during the Green Tuff eruption. *Marine Geology*, *231*(1–4), 201–219. https://doi.org/10.1016/J.MARGEO.2006.06.005

Asghari Pari, S. A., Kashefipour, S., Ghomeshi, M., & Bajestan, M. (2010). *Effects of obstacle heights on controlling turbidity currents with different concentrations and discharges*. Journal of Food Agriculture and Environment. https://www.researchgate.net/publication/265267949_Effects_of_obstacle_heights_on_controlling_turbidity_currents_with_different_concentrations_and_discharges

ATA Scientific. (n.d.). *Malvern Mastersizer 3000*. Retrieved December 4, 2022, from https://www.atascientific.com.au/products/malvern-mastersizer-3000/

Auckland Council. (2014). *Natural Hazard Risk Communications Toolbox*.

Bay of Plenty Regional Council. (n.d.). *Contours and Bathymetry Bay of Plenty*. Retrieved December 4, 2022, from https://gis.boprc.govt.nz/BayMaps/?appid=1a67c7dd0cc64c28b9b35241d3478a6f

Bemmels, J. B., Haddrath, O., Colbourne, R. M., Robertson, H. A., & Weir, J. T. (2022). Legacy of supervolcanic eruptions on population genetic structure of brown kiwi. *Current Biology*, *32*(15), 3389-3397.e8. https://doi.org/10.1016/J.CUB.2022.05.064

Breard, E. C. P., & Lube, G. (2017). Inside pyroclastic density currents – uncovering the enigmatic flow structure and transport behaviour in large-scale experiments. *Earth and Planetary Science Letters*, *458*, 22–36. https://doi.org/10.1016/J.EPSL.2016.10.016

Brosch, E., Lube, G., Cerminara, M., Esposti-Ongaro, T., Breard, E. C. P., Dufek, J., Sovilla, B., & Fullard, L. (2021). Destructiveness of pyroclastic surges controlled by turbulent fluctuations. *Nature Communications 2021 12:1*, *12*(1), 1–12. https://doi.org/10.1038/s41467-021-27517-9

Brown, S. J. A., Smith, R. T., Brown, S. J. A., & Smith, R. T. (2004). Crystallisation history and crustal inheritance in a large silicic magma system: ²⁰⁶Pb/

²³⁸U ion probe dating of zircons from the 1.2 Ma Ongatiti ignimbrite, Taupo Volcanic Zone. *JVGR*, *135*(3), 247–257. https://doi.org/10.1016/J.JVOLGEORES.2004.03.004

Browne, B. L., & Gardner, J. E. (2005). *Transport and deposition of pyroclastic*. *67*, 469–489. https://doi.org/10.1007/s00445-004-0390-6

Buhay, W. M., Clifford, P. M., & Schwarcz, H. P. (1992). ESR dating of the Rotoiti Breccia in the Taupo volcanic zone, New Zealand. *Quaternary Science Reviews*, *11*(1–2), 267–271. https://doi.org/10.1016/0277-3791(92)90072-G

Burt, R. M., Brown, S. J. A., Cole, J. W., Shelley, D., & Waight, T. E. (1998). Glass-bearing plutonic fragments from ignimbrites of the Okataina caldera complex, Taupo Volcanic Zone, New Zealand: remnants of a partially molten intrusion associated with preceding eruptions. *Journal of Volcanology and Geothermal Research*, *84*(3–4), 209–237. https://doi.org/10.1016/S0377-0273(98)00039-0

Carey, S., Sigurdsson, H., Mandeville, C., & Bronto, S. (1996). Pyroclastic flows and surges over water: an example from the 1883 Krakatau eruption. *Bulletin of Volcanology 1996 57:7*, *57*(7), 493–511. https://doi.org/10.1007/BF00304435

Cas, R. A., & Wright, J. V. (1991). Subaqueous pyroclastic flows and ignimbrites: an assessment. *Bulletin of Volcanology 1991 53:5*, *53*(5), 357–380. https://doi.org/10.1007/BF00280227

Cole, J. W., Deering, C. D., Burt, R. M., Sewell, S., Shane, P. A. R., & Matthews, N. E. (2014). Okataina Volcanic Centre, Taupo Volcanic Zone, New Zealand: A review of volcanism and synchronous pluton development in an active, dominantly silicic caldera system. *Earth-Science Reviews*, *128*, 1–17. https://doi.org/10.1016/J.EARSCIREV.2013.10.008

Cole, J. W., Spinks, K. D., Deering, C. D., Nairn, I. A., & Leonard, G. S. (2010). Volcanic and structural evolution of the Okataina Volcanic Centre; dominantly silicic volcanism associated with the Taupo Rift, New Zealand. *Journal of Volcanology and Geothermal Research*, *190*(1–2), 123–135. https://doi.org/10.1016/J.JVOLGEORES.2009.08.011

Cooper, G. F., & Wilson, C. J. N. (2014). Development, mobilisation and eruption of a large crystal-rich rhyolite: The Ongatiti ignimbrite, New Zealand. *Lithos*, *198–199*(1), 38–57. https://doi.org/10.1016/J.LITHOS.2014.03.014

Dominey-Howes, D. (2004). A re-analysis of the Late Bronze Age eruption and tsunami of Santorini, Greece, and the implications for the volcano–tsunami hazard. *Journal of Volcanology and Geothermal Research*, *130*(1–2), 107–132. https://doi.org/10.1016/S0377-0273(03)00284-1

Douillet, G. A., Bernard, B., Bouysson, M., Chaffaut, Q., Dingwell, D. B., Gegg, L., Hoelscher, I., Kueppers, U., Mato, C., Ritz, V. A., Schlunegger, F., & Witting, P. (2019). Pyroclastic dune bedforms: macroscale structures and lateral variations. Examples from the 2006 pyroclastic currents at Tungurahua (Ecuador). *Sedimentology*, *66*(5), 1531–

1559. https://doi.org/10.1111/SED.12542

Flude, S., & Storey, M. (2016). 40Ar/39Ar age of the Rotoiti Breccia and Rotoehu Ash, Okataina Volcanic Complex, New Zealand, and identification of heterogeneously distributed excess 40Ar in supercooled crystals. *Quaternary Geochronology*, *33*, 13–23. https://doi.org/10.1016/j.quageo.2016.01.002

Folk, R. L., & Ward, W. C. (1957). Brazos River bar [Texas]; a study in the significance of grain size parameters. *Journal of Sedimentary Research*, *27*(1), 3–26. https://doi.org/10.1306/74D70646-2B21-11D7-8648000102C1865D

Freundt, A. (2002). Entrance of hot pyroclastic flows into the sea: experimental observations. *Bulletin of Volcanology 2003 65:2*, *65*(2), 144–164. https://doi.org/10.1007/S00445-002-0250-1

Gladstone, C., McClelland, H. L. O., Woodcock, N. H., Pritchard, D., & Hunt, J. E. (2018). The formation of convolute lamination in mud-rich turbidites. *Sedimentology*, *65*(5), 1800–1825. https://doi.org/10.1111/SED.12447

GNS Science. (n.d.). *Kermadec arc and the Taupō Volcanic Zone*. Retrieved December 4, 2022, from https://www.gns.cri.nz/our-science/land-and-marine-geoscience/our-plate-boundary/kermadec-arc-and-taupo-volcanic-zone/

Google. (n.d.-a). *Location of the Tar River and White River deltas in Montserrat* . Retrieved December 4, 2022, from https://earth.google.com/web/search/Montserrat/@16.74853756,-62.19260258,435.00182313a,35640.69095307d,35y,0.00000029h,0t,0r/data=CigiJgokCdHa188ZvUFAEfavZVGoOzVAGag6RuBCWU3AIUQvy_CW0VfA

Google. (n.d.-b). *Map Showing Location of Site 2 Along Glenbrook Beach* . Retrieved December 4, 2022, from https://earth.google.com/web/search/Waiuku/@-37.17400041,174.70280486,1.60232983a,6795.16630436d,35y,0h,0t,0r/data=CigiJgokCQZcwWPO00LAEYwyKX6t-kLAGVTE7hjGIWZAIfUwdZuECGZA

Google. (n.d.-c). *Map Showing Location of Site 3*. Retrieved December 4, 2022, from https://earth.google.com/web/@-38.07351311,174.82034396,-3.60010168a,35807.06064229d,35y,0h,0t,0r

Google. (n.d.-d). *Map showing locations of case studies observed in the field* . Retrieved December 4, 2022, from https://earth.google.com/web/@-37.77930994,175.38573996,111.96978446a,282842.86228459d,35y,0h,0t,0r

Google. (n.d.-e). *Map showing locations of Site 1A and Site 1B visited for this field stud*. Retrieved December 4, 2022, from https://earth.google.com/web/@-37.80723328,176.66080961,-7.1833275a,53440.68800432d,35y,0h,0t,0r

Gueugneau, V., Kelfoun, K., Charbonnier, S., Germa, A., & Carazzo, G. (2020). Dynamics and Impacts of the May 8th, 1902 Pyroclastic Current at Mount Pelée (Martinique): New Insights From Numerical Modeling. *Frontiers in Earth Science*, *8*, 279.

https://doi.org/10.3389/FEART.2020.00279/BIBTEX

Hage, S., Cartigny, M. J. B., Sumner, E. J., Clare, M. A., Hughes Clarke, J. E., Talling, P. J., Lintern, D. G., Simmons, S. M., Silva Jacinto, R., Vellinga, A. J., Allin, J. R., Azpiroz-Zabala, M., Gales, J. A., Hizzett, J. L., Hunt, J. E., Mozzato, A., Parsons, D. R., Pope, E. L., Stacey, C. D., … Watts, C. (2019). Direct Monitoring Reveals Initiation of Turbidity Currents From Extremely Dilute River Plumes. *Geophysical Research Letters*, *46*(20), 11310–11320. https://doi.org/10.1029/2019GL084526

Hart, K., Carey, S., Sigurdsson, H., Sparks, R. S. J., & Robertson, R. E. A. (2004). Discharge of pyroclastic flows into the sea during the 1996-1998 eruptions of the Soufrière Hills volcano, Montserrat. *Bulletin of Volcanology*, *66*(7), 599–614. https://doi.org/10.1007/S00445-004-0342-1/FIGURES/12

Hopkins, J. L., Lowe, D. J., & Horrocks, J. L. (2021). Tephrochronology in Aotearoa New Zealand. *Https://Doi.Org/10.1080/00288306.2021.1908368*, *64*(2–3), 153–200. https://doi.org/10.1080/00288306.2021.1908368

Inman, D. L. (1952). Measures for describing the size distribution of sediments. *Journal of Sedimentary Research*, *22*(3), 125–145. https://doi.org/10.1306/D42694DB-2B26-11D7-8648000102C1865D

Kelfoun, K., & Vallejo Vargas, S. (2016). VolcFlow capabilities and potential development for the simulation of lava flows. *Geological Society Special Publication*, *426*(1), 337–343. https://doi.org/10.1144/SP426.8

Khavasi, E., Afshin, H., & Firoozabadi, B. (2012). Effect of selected parameters on the depositional behaviour of turbidity currents. *Http://Dx.Doi.Org/10.1080/00221686.2011.641763*, *50*(1), 60–69. https://doi.org/10.1080/00221686.2011.641763

Kirkman, J. H. (2012). Mineralogy of the Kauroa Ash Formation of south-west and west Waikato, North Island, New Zealand. *Http://Dx.Doi.Org/10.1080/00288306.1980.10424196*, *23*(1), 113–120. https://doi.org/10.1080/00288306.1980.10424196

Krippner, S. J. P., Briggs, R. M., Wilson, C. J. N., & Cole, J. W. (2010). Petrography and geochemistry of lithic fragments in ignimbrites from the Mangakino Volcanic Centre: Implications for the composition of the subvolcanic crust in western Taupo Volcanic Zone, New Zealand. *Http://Dx.Doi.Org/10.1080/00288306.1998.9514803*, *41*(2), 187–199. https://doi.org/10.1080/00288306.1998.9514803

Legros, F., & Kelfoun, K. (2000). On the ability of pyroclastic flows to scale topographic obstacles. *Journal of Volcanology and Geothermal Research*, *98*(1–4), 235–241. https://doi.org/10.1016/S0377-0273(99)00184-5

Lowe, D. R. (1975). Water escape structures in coarse-grained sediments. *Sedimentology*, *22*(2), 157–204. https://doi.org/10.1111/J.1365-3091.1975.TB00290.X

Lube, G., Breard, E. C. P., Cronin, S. J., & Jones, J. (2015). Synthesizing large-scale pyroclastic flows: Experimental design, scaling, and first results from PELE. *Journal of Geophysical Research: Solid Earth*, *120*(3), 1487–1502. https://doi.org/10.1002/2014JB011666

Maeno, F., & Taniguchi, H. (2007). Spatiotemporal evolution of a marine caldera-forming eruption, generating a low-aspect ratio pyroclastic flow, 7.3 ka, Kikai caldera, Japan: Implication from near-vent eruptive deposits. *Journal of Volcanology and Geothermal Research*, *167*(1–4), 212–238. https://doi.org/10.1016/J.JVOLGEORES.2007.05.003

Mandeville, C. W., Carey, S., & Sigurdsson, H. (1996). Sedimentology of the Krakatau 1883 submarine pyroclastic deposits. *Bulletin of Volcanology 1996 57:7*, *57*(7), 512–529. https://doi.org/10.1007/BF00304436

Manville, V., & Wilson, C. J. N. (2010). The 26.5 ka Oruanui eruption, New Zealand: A review of the roles of volcanism and climate in the post-eruptive sedimentary response. *Http://Dx.Doi.Org/10.1080/00288306.2004.9515074*, *47*(3), 525–547. https://doi.org/10.1080/00288306.2004.9515074

Nairn, I. A. (1981). *Some Studies of the Geology, Volcanic History, and Geothermal Resources of the Okataina Volcanic Centre, Taupo Volcanic Zone, New Zealand*. http://researcharchive.vuw.ac.nz/handle/10063/774

Nairn, I. A. (2012). Rotoehu ash and the Rotoiti Breccia Formation, Taupo Volcanic zone, New Zealand. *Http://Dx.Doi.Org/10.1080/00288306.1972.10421958*, *15*(2), 251–261. https://doi.org/10.1080/00288306.1972.10421958

NOAA. (2021). *What is a turbidity current?* https://oceanservice.noaa.gov/facts/turbidity.html

Novikova, T., Papadopoulos, G. A., & McCoy, F. W. (2011). Modelling of tsunami generated by the giant Late Bronze Age eruption of Thera, South Aegean Sea, Greece. *Geophysical Journal International*, *186*(2), 665–680. https://doi.org/10.1111/J.1365-246X.2011.05062.X

Palladino, D. M. (2017). Simply pyroclastic currents. *Bulletin of Volcanology 2017 79:7*, *79*(7), 1–5. https://doi.org/10.1007/S00445-017-1139-3

Paris, R. (2015). Source mechanisms of volcanic tsunamis. *Philosophical Transactions of the Royal Society A: Mathematical, Physical and Engineering Sciences*, *373*(2053). https://doi.org/10.1098/RSTA.2014.0380

Pierson, T. C. (2005). Distinguishing between debris flows and floods from field evidence in small watersheds. *Fact Sheet*. https://doi.org/10.3133/FS20043142

Scarselli, N. (2020). Submarine landslides – architecture, controlling factors and environments. A summary. *Regional Geology and Tectonics: Volume 1: Principles of Geologic Analysis*, 417–439. https://doi.org/10.1016/B978-0-444-64134-2.00015-8

Schmitz, M. D., & Smith, I. E. M. (2004). The Petrology of the Rotoiti Eruption Sequence, Taupo Volcanic Zone: an Example of Fractionation and Mixing in a Rhyolitic System. *Journal of Petrology*, *45*(10), 2045–2066. https://doi.org/10.1093/PETROLOGY/EGH047

Schneider, J. L., Le Ruyet, A., Chanier, F., Buret, C., Ferrière, J., Proust, J. N., & Rosseel, J. B. (2001). Primary or secondary distal volcaniclastic turbidites: how to make the distinction? An example from the Miocene of New Zealand (Mahia Peninsula, North Island). *Sedimentary Geology*, *145*(1–2), 1–22. https://doi.org/10.1016/S0037-0738(01)00108-7

Shane, P., Black, T., Eggins, S., & Westgate, J. (1998). Late Miocene marine tephra beds: recorders of rhyolitic volcanism in North Island, New Zealand. *Http://Www.Royalsociety.Org.Nz/Publications/Journals/Nzjg/1998/016*. https://researchspace.auckland.ac.nz/handle/2292/4858

Smithsonian Institution. (2022, November 1). *Global Volcanism Program, 2022. [Database] Volcanoes of the World (v. 5.0.0; 1 Nov 2022). Distributed by Smithsonian Institution, compiled by Venzke, E. https://doi.org/10.5479/si.GVP.VOTW5*. https://doi.org/10.5479/si.GVP.VOTW5-2022.5.0

Swamp, S. (n.d.). *Scanning Electron Microscopy (SEM)*. Retrieved December 4, 2022, from https://serc.carleton.edu/research_education/geochemsheets/techniques/SEM.html

Tinterri, R., Muzzi Magalhaes, P., Tagliaferri, A., & Cunha, R. S. (2016). Convolute laminations and load structures in turbidites as indicators of flow reflections and decelerations against bounding slopes. Examples from the Marnoso-arenacea Formation (northern Italy) and Annot Sandstones (south eastern France). *Sedimentary Geology*, *344*, 382–407. https://doi.org/10.1016/J.SEDGEO.2016.01.023

Trofimovs, J., Amy, L., Boudon, G., Deplus, C., Doyle, E., Fournier, N., Hart, M. B., Komorowski, J. C., Le Friant, A., Lock, E. J., Pudsey, C., Ryan, G., Sparks, R. S. J., & Talling, P. J. (2006). Submarine pyroclastic deposits formed at the Soufrière Hills volcano, Montserrat (1995–2003): What happens when pyroclastic flows enter the ocean? *Geology*, *34*(7), 549–552. https://doi.org/10.1130/G22424.1

USGS. (2019). *Volcano Hazards Program Glossary - ignimbrite*. https://volcanoes.usgs.gov/vsc/glossary/ignimbrite.html

Walker, G. P. L. (1979). A volcanic ash generated by explosions where ignimbrite entered the sea. *Nature 1979 281:5733*, *281*(5733), 642–646. https://doi.org/10.1038/281642a0

Watts, P., & Waythomas, C. F. (2003). Theoretical analysis of tsunami generation by pyroclastic flows. *Journal of Geophysical Research: Solid Earth*, *108*(B12), 2563. https://doi.org/10.1029/2002JB002265

Wilson, C. J. N., Houghton, B. F., Lanphere, M. A., & Weaver, S. D. (2010). A new radiometric age estimate for the Rotoehu Ash from Mayor Island volcano, New Zealand. *Http://Dx.Doi.Org/10.1080/00288306.1992.9514530*, *35*(3), 371–374.

https://doi.org/10.1080/00288306.1992.9514530

Wohletz, K. H., & Sheridan, M. F. (1979). *A model of pyroclastic surge*. 177–194. https://doi.org/10.1130/SPE180-P177

Woods, A. W. (2009). Turbulent Plumes in Nature. *Https://Doi.Org/10.1146/Annurev-Fluid-121108-145430*, *42*, 391–412. https://doi.org/10.1146/ANNUREV-FLUID-121108-145430

Yousef Zadeh, E. (2020). *Eruption and emplacement of the 1.3-Ma Ongatiti Ignimbrite, New Zealand: Regional pathways, particle processes, and pumice evolution associated with a large-volume pyroclastic flow deposit*. https://researchcommons.waikato.ac.nz/handle/10289/14063

Appendices

Appendix 1:

Dry Sieving

Dry Sieving Graph							
Location	Pacific Coast Highway						
Deposit	Rotoiti Ignimbrite						
Sample	Sample 1						
phi interval:	1						
mm	phi	Cum. Wt. (g)	Wt. (g)	Wt. Percent (%)	Cum.Wt. Percent (%)	Mode	
64	-6	0.00	0	0.000	100.00%		
32	-5	0.00	0	0.000	100.00%		
16	-4	2.94	2.94	0.014	98.60%		
8	-3	15.95	13.01	0.062	92.39%		
4	-2	29.14	13.19	0.063	86.09%		
2	-1	43.49	14.35	0.068	79.24%		
1	0	81.61	38.12	0.182	61.05%		
0.5	1	129.86	48.25	0.230	38.02%	mode at	0.5
0.25	2	162.32	32.46	0.155	22.53%		
0.125	3	188.43	26.11	0.125	10.07%		
0.0625	4	204.53	16.1	0.077	2.39%		
0.0313	5	209.53	5	0.024	0.00%		
Sum		209.53	209.53	1.000			

Statistics	mm	phi
Inman Stats (1952)		
Median diameter (Md_f)	0.717	0.48
Graphic St. Dev. (s_f)	2.11	
Folk & Ward Stats (1957)		
Graphic Mean (Mz)	0.739	0.44
Inclusive Graphic St. Dev. (f_I)	2.13	

Dry Sieving Graph							
Location	Glenbrook Beach						
Deposit	Ongatiti Ignimbrite						
Sample	Sample 13						
phi interval:	1						
mm	phi	Cum. Wt. (g)	Wt. (g)	Wt. Percent (%)	Cum.Wt. Percent (%)	Mode	
64	-6	0.00	0	0.000	100.00%		
32	-5	0.00	0	0.000	100.00%		
16	-4	0.00	0	0.000	100.00%		
8	-3	25.64	25.64	0.153	84.70%		
4	-2	86.75	61.11	0.365	48.25%	mode at	-2.5
2	-1	115.19	28.44	0.170	31.28%		
1	0	132.02	16.83	0.100	21.24%		
0.5	1	143.59	11.57	0.069	14.34%		
0.25	2	152.41	8.82	0.053	9.08%		
0.125	3	161.05	8.64	0.052	3.93%		
0.0625	4	166.02	4.97	0.030	0.96%		
0.0313	5	167.63	1.61	0.010	0.00%		
Sum		167.63	167.63	1.000			

Statistics	mm	phi
Inman Stats (1952)		
Median diameter (Md_f)	17.965	-4.17
Graphic St. Dev. (s_f)	2.38	
Folk & Ward Stats (1957)		
Graphic Mean (Mz)	5.811	-2.54
Inclusive Graphic St. Dev. (f_I)	2.15	

Dry Sieving Graph							
Location	Kihi Road						
Deposit	Ongatiti Ignimbrite/Oparau Tephra						
Sample	Sample 20						
phi interval:	1						
mm	phi	Cum. Wt. (g)	Wt. (g)	Wt. Percent (%)	Cum.Wt. Percent (%)	Mode	
64	-6	0.00	0	0.000	100.00%		
32	-5	0.00	0	0.000	100.00%		
16	-4	108.54	108.54	0.326	67.41%	mode at	-4.5
8	-3	174.85	66.31	0.199	47.49%		
4	-2	206.96	32.11	0.096	37.85%		
2	-1	235.58	28.62	0.086	29.26%		
1	0	256.21	20.63	0.062	23.06%		
0.5	1	286.18	29.97	0.090	14.06%	mode at	0.5
0.25	2	310.79	24.61	0.074	6.67%		
0.125	3	323.87	13.08	0.039	2.74%		
0.0625	4	330.09	6.22	0.000	0.88%		
0.0313	5	333.01	2.92	0.009	0.00%		
Sum		333.01	333.01	1.000			

Statistics	mm	phi
Inman Stats (1952)		
Median diameter (Md_f)	8.729	-3.13
Graphic St. Dev. (s_f)	2.65	
Folk & Ward Stats (1957)		
Graphic Mean (Mz)	4.868	-2.28
Inclusive Graphic St. Dev. (f_I)	2.43	

Appendix 2:

Laser Particle Diffraction Analysis

Particle Laser Diffraction					
Location	Glenbrook Beach				
Deposit	Ongatiti Ignimbrite				
(mm)					
Sample #	3	4	5	10	11
dv 10	0.012	0.038	0.014	0.005	0.003
dv 90	0.279	0.580	0.255	0.185	0.039
dv 50	0.087	0.188	0.086	0.054	0.013
average	0.126	0.269	0.118	0.082	0.018
phi					
Sample #	3	4	5	10	11
dv 10	6.380	4.710	6.140	7.530	8.590
dv 90	1.840	0.780	1.970	2.430	4.670
median	3.520	2.410	3.540	4.200	6.220
average	2.980	1.890	3.080	3.608	5.790
graphic mean (Mz)	3.913	2.633	3.883	4.720	6.493
sorting value	2.270	1.965	2.085	2.550	1.960

Appendix 3:

Desktop Analysis for Slope

Bay of Plenty Slope Calculations for Experimental Basis								
Location	BOP coastline Maketu to Matata Section / Mimiha Road							
Volcanic Centre	Okataina Volcanic Centre, Haroharo vent zone (present day Rotoiti Forest)							
Deposit	Rotoiti Ignimbrite >50 km^3 pyroclastic flow on land, estimated >10 km^3 into sea							
From OVC to the BOP Coastline								
	OVC	**Coastline**						
Elevation (m asl)	110	5						
Distance (m)		31500						
Distance (km)		31.5						
Slope (degrees)		0.19						
From Mimiha Road coastline to 70 metres depth								
Depth (m)	10	20	30	40	50	51	61	71
Distance (m)	1100	1500	4500	1900	2000	2700	4300	2100
Distance (cumm) (m)	32600	34100	38600	40500	42500	45200	49500	51600
Distance (cumm) (km)	32.6	34.1	38.6	40.5	42.5	45.2	49.5	51.6
Slope (degrees)	0.52	0.76	0.38	1.21	1.43	1.08	0.81	1.94
Slope (cumm) (degrees)	0.52	0.44	0.24	0.25	0.26	0.21	0.19	0.20

Appendix 4:

Experimental Raw Data

Flume Experiment				
Preparation Notes				
	length	width	depth	height
Flume Tank Dimensions (mm)	3100	330	100	650
	length	diameter		
PVC Pipe Dimensions (mm)	785	90		
	length	width	depth	
PVC Insert Dimensions (mm)	230	90	5	
	length	width	depth	
Dam Insert Dimensions (mm)	250	100	2	
Slope (degrees)	5			

Run 1.1						
Current	Height (mm)	Length (mm)	Time (sec)	Length (cumm)	Time (cumm)	Velocity (mm/s)
Collapse			<1			
1	38	130	3	130	3	43.3
2	37	70	2	200	5	35.0
3	25	98	3	298	8	32.7
4	23	58	2	356	10	29.0
5	14	101	4	457	14	25.3
6	14	87	5	544	19	17.4
7	17	80	8	624	27	10.0
8	15	69	7	693	34	9.9
9	11	57	9	750	43	6.3
10	6	180	11	930	54	16.4
End		173	5	1103	59	34.6
Cloud						
1	290	70	<1			
2	350	60	1			
3	>400	45	2			
						period t=1/f
Wave	75	400	<1			
Ash Layer						
1	3					
2	1					
3	1					
rest	<1					
Freshwater	65					
Temp	22.1					
Sand	13					
	medium to coarse sand					
Ash	700 mL Sample 1 Rotoiti					
Temp	25.5					

Run 1.2						
Current	Height (mm)	Length (mm)	Time (sec)	Length (cumm)	Time (cumm)	Velocity (mm/s)
Collapse			<1			
1	30	133	2	133	2	66.5
2	29	73	4	206	6	18.3
3	22	64	3	270	9	21.3
4	18	61	3	331	12	20.3
5	19	103	8	434	20	12.9
6	18	80	7	514	27	11.4
7	14	72	7	586	34	10.3
8	15	60	7	646	41	8.6
9	12	77	7	723	48	11.0
10	10	112	7	835	55	16.0
End		155		990		
Cloud						
1	220	90	<1			
2	285	70	<1			
3	>400	50	1			
Wave	70	400	1			
Ash Layer						
1	0.75					
2	0.5					
3	0.25					
rest	<0.25					
Ash Wedge	28	260				
Freshwater	65					
Temp	21					
Sand	16					
	medium to coarse sand					
Ash	300 mL Sample 1 Rotoiti					
Temp	32.2					

Run 1.3						
Current	Height (mm)	Length (mm)	Time (sec)	Length (cumm)	Time (cumm)	Velocity (mm/s)
Collapse			<1			
1	31	168	3	168	3	56.0
2	25	81	3	249	6	27.0
3	24	39	4	288	10	9.8
4	20	63	5	351	15	12.6
5	19	107	8	458	23	13.4
6	13	96	10	554	33	9.6
7	19	67	7	621	40	9.6
8	17	67	9	688	49	7.4
9	17	56	9	744	58	6.2
10	7	90	14	834	72	6.4
End				979		
Cloud						
1	200	90	<1			
2	300	70	1			
3	>400	50	1			
Wave	68	400	1			
Ash Layer						
1	0.5					
2	0.5					
3	0.25					
rest	<0.25					
Ash Wedge	27	180				
Freshwater	65					
Temp	23					
Sand	19					
	medium to coarse sand with lapilli/pebbles					
Ash	500 mL Sample 1 Rotoiti					
Temp	33.3					

Run 2.1						
Current	Height (mm)	Length (mm)	Time (sec)	Length (cumm)	Time (cumm)	Veloctiy (mm/s)
1	27	135	6	135	6	22.5
2	24	62	3	197	9	20.7
3	20	61	4	258	13	15.3
4	13	64	7	322	20	9.1
5	10	37	8	359	28	4.6
6	7	93	25	452	53	3.7
End				479	57	
Wave	68	400	2			
Ash Layer						
1	<0.25					
Ash Wedge	38	70				
Freshwater	65					
Temp	19.9					
Sand	17					
	medium to coarse sand with lapilli/pebbles					
Ash	900 mL Sample 3-5 Ongatiti					
Temp	33.8					

Run 2.2						
Current	Height (mm)	Length (mm)	Time (sec)	Length (cumm)	Time (cumm)	Velocity (mm/s)
1	19	31	4	31	4	7.8
2	19	59	9	90	13	6.6
3	18	32	4	122	17	8.0
4	13	34	5	156	22	6.8
5	15	46	2	202	24	23.0
6	13	49	11	251	35	4.5
7	11	21	17	272	52	1.2
End		26	13	298	65	2.0
Cloud						
1	130	90	2			
2	110	70	5			14
3	90	65	12			5.42
Wave	67	400	1			
Ash Layer						
1	<0.25					
Freshwater	65					
Temp	13.2					
Sand	17					
	medium to coarse sand with lapilli/pebbles					
Ash	600 mL Sample 3-5 Ongatiti					
Temp	31.5					

Run 3.1						
Current	Height (mm)	Length (mm)	Time (sec)	Length (cumm)	Time (cumm)	Velocity (mm/s)
Collapse			<1			
1	26	119	3	119	3	39.7
2	24	49	2	168	5	24.5
3	21	45	2	213	7	22.5
4	8	62	4	275	11	15.5
5	6	61	7	336	18	8.7
End	4	114	62	450	80	1.8
Cloud						
1	230	990	<1			
2	270	70	1			
3	>350	45	1			
Wave	72	400	1			
Ash Layer						
1	0.5					
2	0.5					
3	0.25					
rest	<0.25					
Ash Wedge	7	15				
Freshwater	66					
Temp	17					
Sand	18					
	medium to coarse sand with lapilli/pebbles					
Ash	350 mL Sample 1 Rotoiti					
Temp	30					